NASA Technical Memorandum 100459

Atomic Oxygen Effects Measurements for Shuttle Missions STS-8 and 41-G

Volume II

Compiled by James T. Visentine

FOREWORD

A variety of materials was exposed in the Orbiter cargo bay on Space Shuttle flights STS-8 and 41-G (STS-17) to develop a fundamental understanding of the deleterious effects which result from space flight exposure of thin, organic films, advanced composites, and metallized surfaces to atomic oxygen, the principal constituent of the low Earth orbit environment. These materials included polyimide films, fluorocarbons, polyurethanes, silicones, siloxanes, epoxies, carbon fibers and graphites, infrared optical materials, metallized optical films, Kevlar coverings, fiberglass fabric, and high-temperature reflective coatings. Effects measured post-flight included mass loss (surface recession), surface morphology changes, reflectance losses, chemical composition changes, and decreases in optical density of the metallized films.

To provide for controlled exposure during both missions, approximately 300 material specimens provided by the participating organizations (NASA, Canada, British Aerospace, TRW, Aerospace Corporation, Washington University and the University of Alabama) were exposed on an across-the-bay structure during STS-8 by flying the Orbiter with its payload bay into the velocity vector for 40 hours at an altitude of 222 km (120 nmi). During STS 41-G, material specimens attached to the lower arm boom of the Shuttle remote manipulator system were oriented toward the direction of flight for 34 hours at an altitude of 272 km. Given the differences in exposure time and solar activity conditions -- which influence the atomic oxygen number density in the neutral atmosphere -- that arose from different flight dates (September 1983 and October 1984), atomic oxygen fluences for STS-8 and 41-G were determined to be 3.5×10^{20} and 3.0×10^{20} atoms/cm^2, respectively. These exposures, in turn, produced surface recessions of 0.4 and 0.3 mil for highly reactive materials, such as the polyimide films, which ranged from 0.5 to 2.0 mils in thickness during both STS missions.

The results of these exposures together with the post-flight measurements are reviewed and summarized in 9 reports found in Volume I and 5 reports in Volume II of this technical memorandum. The reports were issued by the participating NASA centers and U. S. aerospace corporations, the Government of Canada, and university research centers.

James T. Visentine, Compiler
NASA Lyndon B. Johnson Space Center
Houston, Texas

ACKNOWLEDGMENT

Changes to the STS flight manifest during late 1983 provided an opportunity for the NASA materials science community to conduct an atomic oxygen effects experiment during the eighth Space Shuttle mission. This experiment was designed, developed, assembled, and integrated into the Orbiter within a 12-week period prior to flight, with special consideration given to flight safety, materials selection, and the post-flight analysis capabilities that were made available by the participating NASA Centers. Approximately 300 specimens were prepared by the participating organizations and analyzed prior to flight. After the mission was completed, these samples were returned to the co-investigators, who then completed their analyses and prepared these post-flight reports. We extend our special thanks to the following persons who contributed immensely to the successful completion of this experiment, and to their co-authors whose names are found in their respective documents: Dr. Lubert Leger of JSC, who served as principal investigator; Ms. Ann Whitaker and Ms. Sally Little of MSFC; Messrs. Wayne Slemp and George Sykes of the Langley Research Center; Dr. Bruce Banks and Mr. Mike Mirtich of the Lewis Research Center; Dr. John Park, Dr. Ted Gull, and Mr. Jack Triolo of GSFC; Drs. Ranty Liang and Dave Brinza of JPL; Drs. Wayne Stuckey and Graham Arnold of Aerospace Corporation; and Dr. John Gregory of the University of Alabama, Huntsville. Special recognition is also extended to Dr. Dave Zimcik of the Government of Canada, who later participated in the STS-41G experiment.

James T. Visentine

Contents

STS-8 MISSION SUMMARY - CHALLENGER

August 30 - September 5, 1983

COMMANDER:	**Richard H. Truly**
PILOT:	**Daniel C. Brandenstein**
MISSION SPECIALIST:	**Guion S. Bluford, Jr.**
MISSION SPECIALIST:	**Dale A. Gardner**
MISSION SPECIALIST:	**William E. Thornton**
MISSION DURATION:	**6 days, 1 hour, 9 minutes, 32 seconds**
MILES TRAVELED:	**2,184,983 nautical miles (2,514,478 statute miles)**
ORBITS OF EARTH:	**97**

First night launch and night landing

Challenger carried INSAT-1B, payload flight test article (PFTA), 2 Getaway Special canisters, and included the STS-8 (EOIM-2) atomic oxygen effects experiment

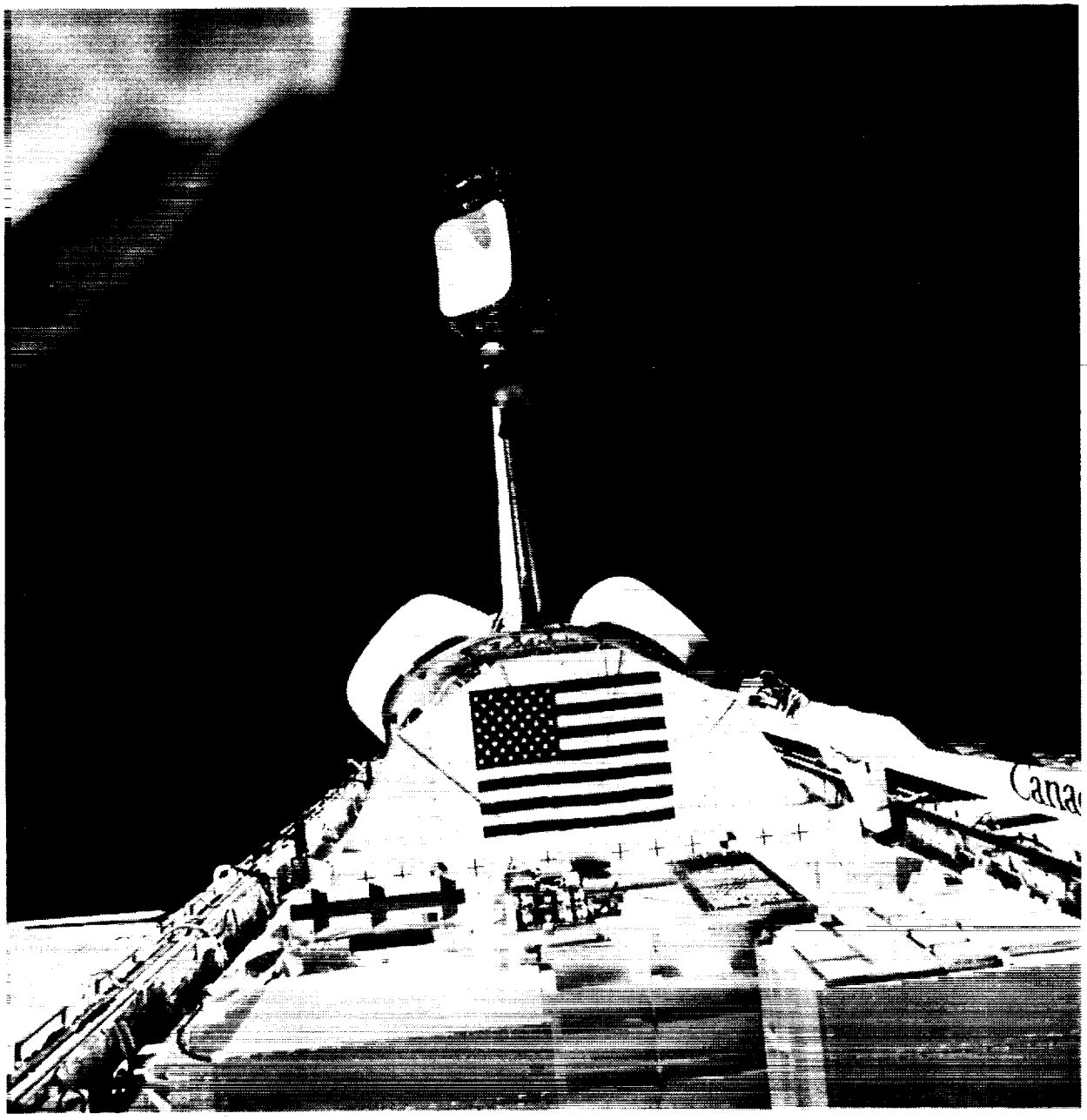

STS-8 Atomic Oxygen Effects Experiment. The STS-8 material science exposure trays are shown in the foreground during INSAT 1-B deployment (August 31, 1983).

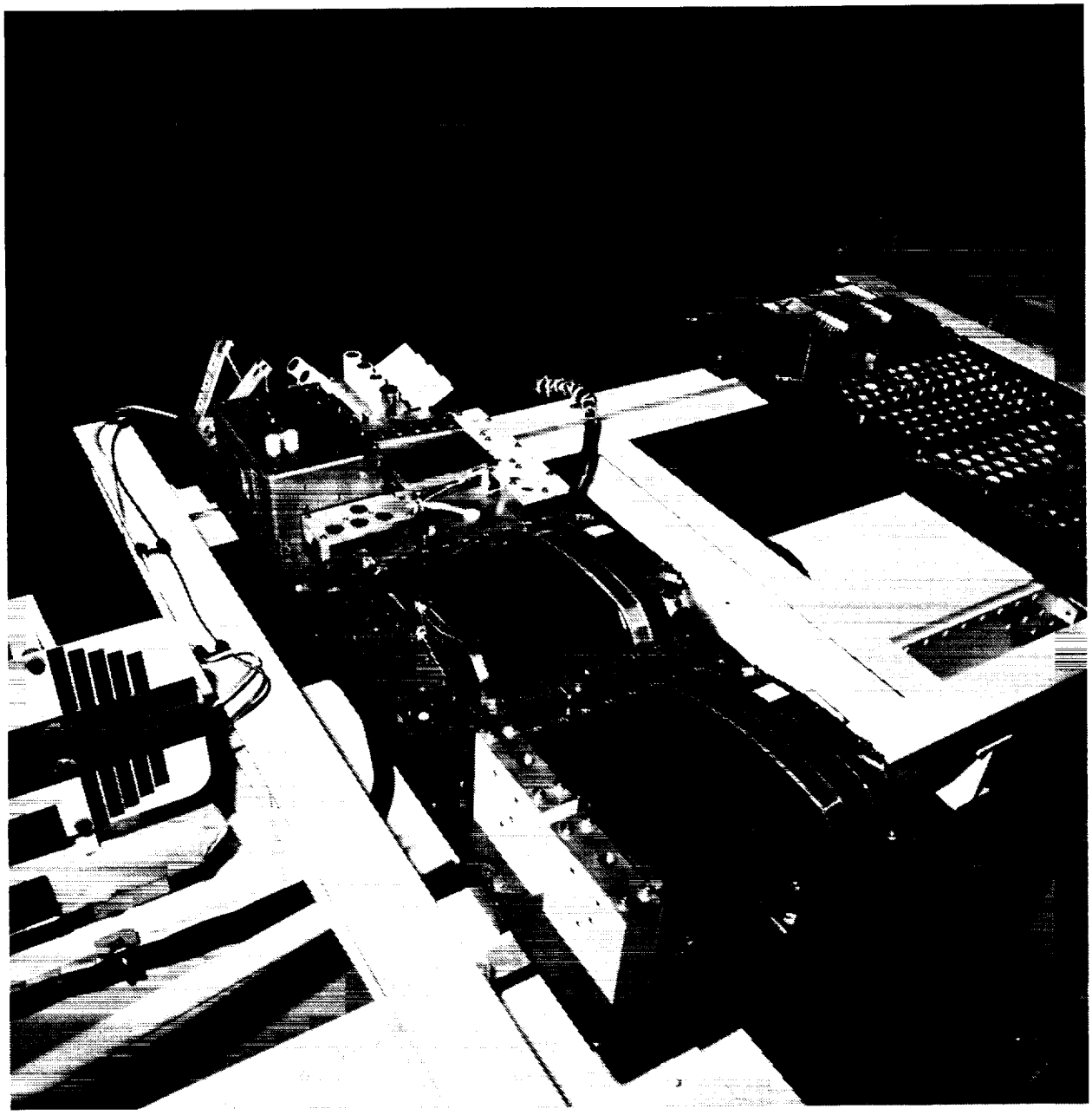

Closeup view of the STS-8 Atomic Oxygen Effects Experiment. The active and passive experiment trays are located on the left and right sides of the DFI pallet structure, respectively. These trays included approximately 300 material specimens, which were provided by the NASA Centers and aerospace contractors.

STS-8 POST-FLIGHT REPORT

The Atomic Oxygen Interaction Experiment (DSO 0301) conducted during STS-8 was successfully completed during the mission timeline. This experiment consisted of material specimens installed within passive exposure trays attached to an across-the-bay structure (DFI pallet) and active experiments to assess the effects of temperature, solar ultraviolet radiation, and charged particles (ions and electrons) on material interaction rates with atomic oxygen, the principal constituent of the LEO environment. These experiments were initiated during Flight Day 3 at 08:30 hours MET, and were concluded on Flight Day 5 at 1900 hours MET. A combination of three separate exposures (3/08:30-3/20:10; 4/07:30-4/19:30; and 5/00:55-5/19:00) resulted in a total exposure of 41.75 hours, which was accomplished by flying the Orbiter with its payload bay into the velocity vector. This attitude produced direct impingment of the oxygen atoms onto the material specimens. The flight specimens were exposed to an average atomic oxygen flux of 1.9×10^{15} atoms/S-cm^2, which produced a fluence of 2.9×10^{20} atoms/cm^2. This fluence, combined with fluences obtained during non-EOIM exposure periods during the time the Orbiter was oriented in different flight attitudes, produced a total fluence of 3.5×10^{20} atoms/cm^2.

Material specimens are being analyzed, and preliminary results indicate additional exposure will be required during future Space Shuttle flights to evaluate protective coating techniques and to further analyze atomic oxygen interactions with surfaces in more detail.

Submitted to the NSTS Integration Office, September 8, 1983.

41-G (STS-17) MISSION SUMMARY - CHALLENGER

October 5 - 13, 1984

COMMANDER:	**Robert Crippen**
PILOT:	**Jon McBride**
MISSION SPECIALIST:	**David Leestma**
MISSION SPECIALIST:	**Sally K. Ride**
MISSION SPECIALIST:	**Kathryn Sullivan**
PAYLOAD SPECIALIST:	**Paul Scully-Power**
PAYLOAD SPECIALIST:	**Marc Garneau**
MISSION DURATION:	**8 days, 5 hours, 24 minutes, 32 seconds**
MILES TRAVELED:	**2,984,397 nautical miles (3,434,684 statute miles)**
INCLINATION:	**57°**
ORBITS OF EARTH:	**132**

Extravehicular Activity (EVA):	Kathryn Sullivan and David Leestma
EVA Duration:	3 hr, 29 min

Challenger carried 4 payloads, 8 Getaway Special canisters, 4 middeck experiments and included the Canadian ACOMEX Atomic Oxygen Effects Experiment

Exposure of material samples on the Shuttle RMS, during the STS 41-G flight.

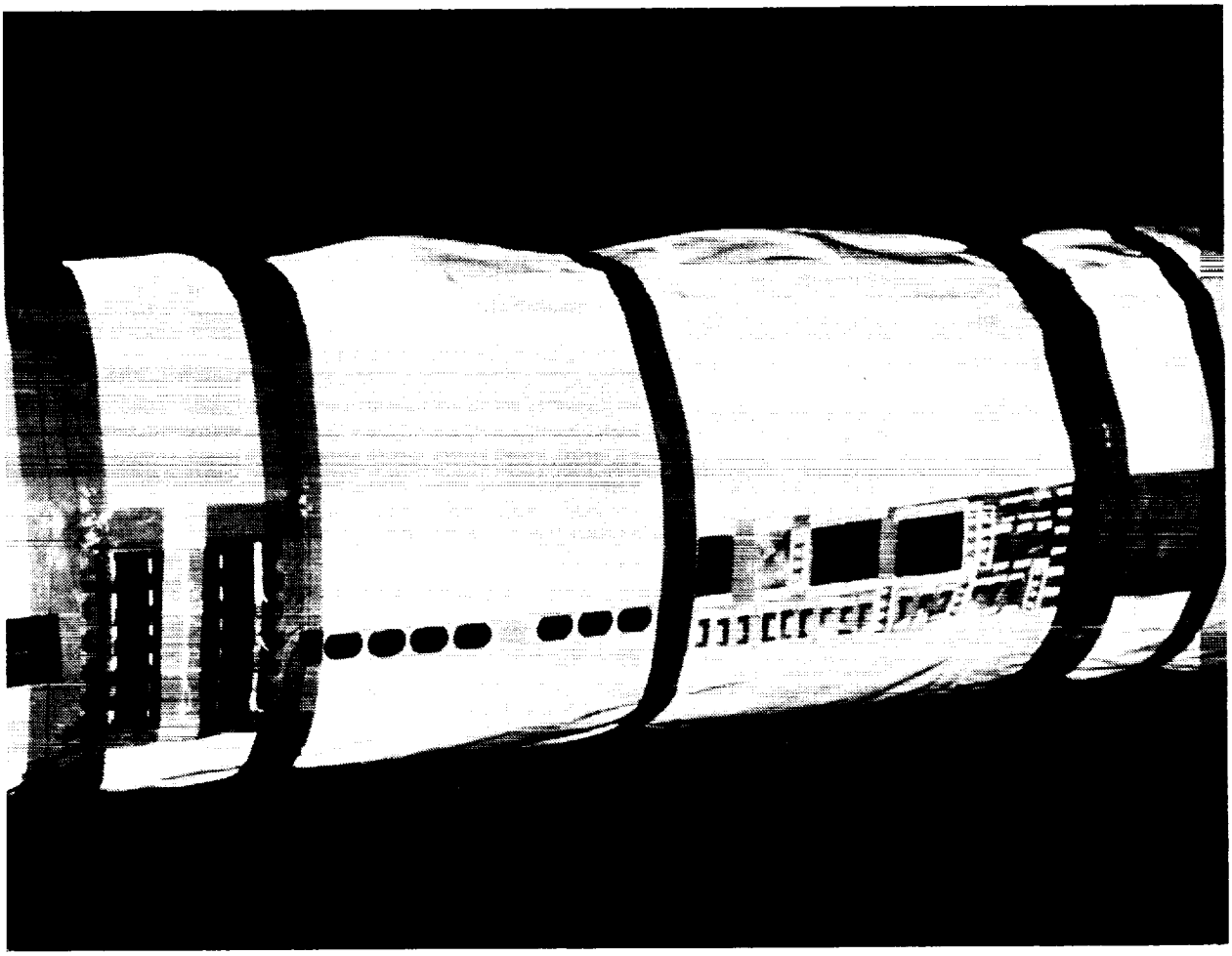

Closeup view of the STS 41-G material specimens, shown tape-attached to the thermal blanket. Nylon cord tethers used to secure the exposure trays are visible underneath the circumferential bands of Kapton tape.

STS 41-G POST-FLIGHT REPORT

The Atomic Oxygen Interaction Experiment (DSO 0308) conducted during STS 41-G was successfully completed per the mission timeline. This experiment consisted of material specimens and subassembly components provided by MSFC and Canada's Communication Research Center taped-attached (see figure 1) to the RMS to expose space telescope solar cells and coated discs (MSFC experiment) and composite specimens of different configurations of graphite and Kevlar (Acomex Experiment) to the ambient density environment. These experiments were initiated on Flight Day 3 at 2200 hours GMT and completed during Flight Day 5 at 15:22 hours GMT, for a total exposure period of 34.08 hours. Specimens were exposed to an atomic oxygen flux of 2.0×10^{15} atoms/cm^2 sec, which produced a total fluence of 2.45×10^{20} atoms/cm^2.

At other times during the mission, the RMS was positioned to observe ice buildup on the Orbiter side water dump valve during venting operations. This activity was performed for about 30 minutes twice daily and resulted in non-normal (oblique) impingement of oxygen atoms onto the material specimens. Given these exposure conditions, the total fluence (normal and oblique) experienced during the STS 41-G exposure period is estimated to be 3.0×10^{20} atoms/cm^2.

Material specimens are being analyzed, and preliminary results indicate additional exposure will be required during future Space Shuttle flights to evaluate protective coating techniques and further analyze atomic oxygen interactions with surfaces in more detail.

Submitted to the NSTS Integration Office,
October 21, 1984

ACRONYMS

AES	auger electron spectroscopy
BRDF	bidirectional reflection distribution function
CMP	contamination monitor package
ELL	elipsometry
EOIM	Effects of oxygen interactions with materials
ESCA	electron spectroscopy for chemical analysis
ESD	electrostatic discharge
FGS	fine guidance system
GAS	Get Away Special
GSFC	Goddard Space Flight Center
INSAT	Indian National Satellite
ITO	indium tin oxide
LEO	low Earth orbit
MSFC	Marshall Space Flight Center
MSIS	mass spectrometer and incoherent scatter
PBI	polybenzimidazole
PFTA	payload flight test article
PIXE	proton induced x-ray emission
PMMA	polymethyl methacrylate
QCM	quartz crystal microbalances
RBS	Rutherford backscattering
RE	reaction efficiency
RMS	remote manipulator system
RTG	radioisotope thermoelectric generators
SEM	scanning electron microscope
SIMS	secondary ion mass spectroscopy
ST	space telescope
STS	Space Transportation System
TDS	total diffuse scatter
TQCM	temperature controlled quarts crystal microbalances
TS	tethered satellite
UV	ultraviolet
WDX	wavelength dispersive x-ray

1.0 INTRODUCTION

This technical memorandum represents a compilation of 15 technical papers and is organized by subject matter into three separate volumes. Volume 1 of this document summarizes the effects of atomic oxygen exposure upon typical spacecraft materials, such as polyimide films, thermal control paints, epoxies, silicones, and fluorocarbons. Volume 2 summarizes the effects of these interactions upon optical coatings, thin metallized films, and advanced spacecraft materials, such as high-temperature coatings and new coatings for infrared optical systems. In addition to these results, Volume 2 includes a description of a generic model proposed by the NASA Jet Propulsion Laboratory, which may explain the atomic oxygen interaction mechanisms that lead to surface recession and weight loss. Volume 3 presents a futuristic look into the atomic oxygen program and outlines requirements for follow-on studies to produce an accurate reaction rate data base for Space Station design. It also identifies Shuttle flight experiments and on-going activities underway at research laboratories in the United States to evaluate materials in a neutral, 5 eV O-atom environment and to develop a more thorough understanding of the chemical mechanisms leading to surface recession and space glow. This volume, entitled *Atomic Oxygen Effects Experiments: Current Status and Future Directions* includes a detailed discussion of atomic oxygen simulation techniques now under development in the United States. In light of these discussions, it is limited in its distribution to U. S. Government agencies and contractors only.

2.0 EFFECTS ON OPTICAL SYSTEMS FROM INTERACTIONS WITH OXYGEN ATOMS IN LOW EARTH ORBITS*

J. C. Gregory

University of Alabama
Huntsville, Alabama 35899

P. N. Peters and J. T. Swann

NASA Marshall Space Flight Center
Space Science Laboratory, Alabama 35812

Abstract

Modifications of material surface properties due to interactions with ambient atomic oxygen have been observed on surfaces facing the orbital direction in low Earth orbits. Some effects are very damaging to surface optical properties, whereas some are more subtle and even beneficial. Most combustible materials are heavily etched, and some coatings, such as silver and osmium, are seriously degraded or removed as volatile oxides. The growth of oxide films on metals and semiconductors which are considered stable in dry air was measured. Material removal, surface roughness, reflectance, and optical densities are reported. Effects of temperature, contamination, and overcoatings are noted.

2.1 Introduction

Optical systems are operated in space with increasing frequency for making astronomical, atmospheric, and Earth observations. While there are distinct advantages to observations from space, special problems unrelated to ground-based experience can arise.(1) One such problem is encountered in low earth orbits (200-600 km) where oxygen atoms that dominate the atmospheric composition and high orbital velocity can degrade surfaces. The atoms result from dissociation of oxygen molecules by solar UV, and recombination is slow due to a scarcity of three-body collisions. The oxygen atom number density varies not only with altitude and latitude but with sunspot activity and other parameters. Fluxes of atoms to surfaces are either calculated using models based on previous direct measurements (e.g., mass spectrometer and incoherent scatter (MSIS) data),[2] on drag measurements,[3] or on direct measurement made on the individual flight. A typical density at 300-km altitude and at 30° latitude and with mean annual and mean solar-cycle conditions is $N = 10^9$ atoms cm^{-3}. The flux to surfaces facing the orbital direction is given by $j = Nv$, where $v = 8 \times 10^5$ cm s^{-1} producing a flux of $\sim 8 \times 10^{14}$ atoms $cm^{-2} s^{-1}$.

Since little activation energy is required[4] for the oxygen atoms to react with most combustible surfaces, such surfaces are etched, even at room temperature, and unusual topographies, as shown in Figs. 1 and 2, are typically produced. Although few combustible materials are likely to be used for optical surfaces, supporting structures of a combustible nature may be inadvertently chosen, and recognition of potential problems from poor choices of materials is pertinent.

The removal of combustible material by active oxygen is not a completely negative effect. Numerous related processes have been used to clean surfaces (discharges in air prior to coating optics, an active oxygen cleaning technique studied for NASA,[5] plasma ashers used in the semiconductor industry for removing photoresist, etc.), and it has been proposed that the oxygen atom source in orbit can be used to clean combustible contaminants from surfaces,[6] which it appears to do. Oxygen atoms do not effectively remove silicones. This can be unfortunate in the case of contamination or fortunate if this protection is desired.

Reprinted from *Applied Optics*, Vol. 25, No. 8
15 April 1986

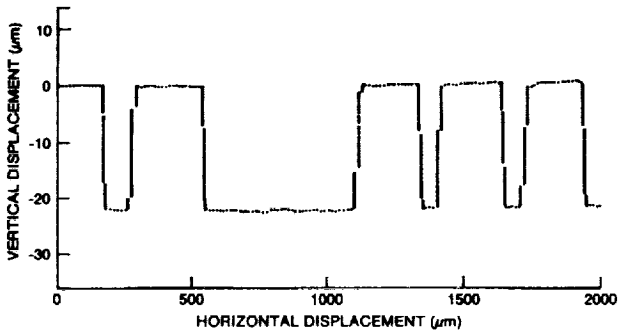

Fig. 1. Stylus profilometry tracing on CR-39 plastic showing heavy etching (21.5 μm) by atomic oxygen during exposure in the orbital direction. (Tops of the plateaus were protected by 200-nm thick Nb films.)

Fig. 2. Fine structure in the etched region of the CR-39 plastic shown in Fig. 1 (top portion protected by Nb film; bottom portion etched from exposure).

Metallic coatings have wide applications to mirror and grating surfaces and in a variety of thermal control systems. Alterations of reflection, scattering, and transmission properties are of great importance in the design of instruments and spacecraft for long-term performance in low earth orbit. Effects on metal surfaces which were examined included loss of metal by physical or chemical action and buildup of the protective oxide layer already present on most metals exposed to air.

Many of the effects observed for atomic oxygen interacting with spacecraft surfaces were predicted by Gregory and Peters in a 1975 proposal to NASA, Langley Research Center, for an experiment to be flown on the Long Duration Exposure Facility (LDEF). That experiment is being flown as LDEF Experiment A-0114.[7] Portions of that experiment and other oxygen atom interaction experiments[8-16] have been flown on recent Shuttle flights.

2.2 Experimental Approach and Exposure Parameters

Surfaces of various samples were exposed in the orbital direction as part of The University of Alabama in Huntsville module of the oxygen interaction with materials experiment (EOIM-2) which flew on Shuttle flight STS-8 in Sept. 1983.[4]

Approximately 95% of the total atom fluence of $\sim 3.5 \times 10^{20}$ oxygen atoms cm^{-2} was produced while surfaces were oriented within 1° of the orbital direction. Exposure parameters are shown in Table I.

The surfaces studied were of two types: high-purity thin films sputtered or evaporated onto 2.54-cm diam $\lambda/20$ fused silica optical flats, and highly polished bulk samples. Films were prepared with optical densities of ~2.5 or less, as listed in Table II. Measurement of optical densities using a Perkin-Elmer PDS scanning microdensitometer allowed sensitive determination of any changes to these thin films produced by the exposure. By masking one-half of each sample during flight as a control it was possible to measure changes in optical density of ~0.01, corresponding to a few percent change in thickness of ~10-nm thick films. (No increase in scattering was assumed, since most films became smoother; changes in reflection due to very small oxide thickness increases were also neglected.) In several cases the sensitivity of the method was ± 1 monolayer of surface atoms. Total film thicknesses were accurately measured by step height changes in stylus traces of the film/substrate surfaces using a Tencor Alpha-Step 200 stylus profilometer with a nominal 2-μm radius diamond stylus. Decreases in both the optical density and total film thickness were attributed to metal film removal. A decrease in optical density but an increase in total film thickness was attributed to film expansion due to formation of a nonvolatile oxide of lower density than the original film. To obtain optimum resolution of step heights

from stylus measurements, fine lines were scraped to the bare substrates, except for the niobium and nickel films, which could not be removed without damaging the substrate. The arithmetical average of the step plateaus (average absolute distance from a center line level for up to 2000 data points) gave indicated surface roughnesses of the order of 0.5 nm for the smoothest surfaces. Although some smoothing probably occurred from the stylus riding over microscopic defects and compressing the surface somewhat, changes of ± 1 nm in relative film heights between exposed and unexposed surfaces were measurable when averaging was used on both levels of sharp steps. Topographic measurements were also made on a number of surfaces with an optical heterodyne instrument using recent techniques.[17] These measurements provided an optical determination of surface roughnesses for comparison to stylus results as well as several correlation functions from the same measurement.

Estimates of metallic film thicknesses in exposed and unexposed areas were calculated from the optical density measurements using equations for transmission and reflection.[18] Published optical constants for metals[18,19] were used for calculations except for noted cases, such as for niobium, where a value of 28-nm thickness per unit optical density change had been accurately determined for our sputtered niobium films. Air, metal, and fused silica substrate media were assumed. This neglected the effect of very thin transparent oxides on absorption and reflection for normal incidence on these samples. Neglecting such effects on metals forming thick oxides, such as for silver, would introduce unacceptable errors, however.

Osmium and iridium films were purchased, the platinum overcoatings on the osmium were electron-beam evaporated, and most of the other films were sputtered.

Sensitive step height measurements on the bulk samples shown in Table III were obtained with the diamond stylus. Most of the bulk sample surfaces had 10-nm arithmetic roughness and were not very flat. In most cases this lack of precision for bulk sample measurements was unimportant since large effects were produced. Step height determination was enhanced on most bulk samples by sputtering a protective niobium film ~220 nm thick in a resolution pattern of small rectangles spaced over the whole sample surface before mounting for flight. Although both knife-edges and film masks were used, much sharper steps were obtained with films than with mask knife-edges, because intimate contact between substrate and film mask was assured, and effects due to shadowing of areas of the substrate next to taller mask structures did not occur. Accurate niobium mask thicknesses were obtained in the unexposed areas and subtracted from the step heights in the exposed areas. Typically, large negative steps were produced on combustible materials by oxygen exposure; however, in the case of silver, a large expansion occurred.

Table I. STS-8 Atomic Oxygen Exposure Data[a]

Flight dates	08/30/83 to 09/05/83
Period payload bay facing forward	$t = 41.2$ h
Altitude	225 km (120 nmi)
Speed	7.8 km s^{-1}
Mean oxygen atom density (calculated)	2.65×10^9 cm^{-3}
Surface impact frequency	2.07×10^{15} cm^{-2} s^{-1}
Integral fluence	3.5×10^{20} atoms cm^{-2}

[a] From Ref. 4.

Table II. Some Effects Observed on Thin Films Exposed to 3.5×10^{20} Oxygen Atoms cm^{-2} in Low Earth Orbits[a]

	Optical Transmission Results				Step measurements of films with 2-μm diamond stylus (nm)				Optical heterodyne measurements			
	Optical density		Metal thickness (nm) from optical absorption		Film thickness		Arithmetic average surface roughness		rms surface roughness (nm)		Estimated thickness changes (nm)	
Sample[b]	Unexposed	Exposed	Unexposed	Exposed	Unexposed	Exposed	Unexposed	Exposed	Unexposed	Exposed	Metal	Metal + oxide
Iridium film	1.78	1.65	32.3	29.4	32.2	29.7	0.5	0.5	1.88	1.84	−2.9	−2.5
Au/Nb film	1.29	1.29	–	–	35.5/39.5	35.5/39.5	1	1	–	–	None	None
Al film	0.28	0.21	3.4	2.6	15.0	16.5	0.5	0.5	2.08	1.77	−0.8	+1.5
Ni film	1.79	1.76	54.2	53.3	Unable to remove Ni except at pinholes which gave ~84 nm in both regions.		1	1	1.79	1.76	−0.9	–
W film	0.35	0.31	4.8	4.1	~17.0	~17.0	0.5–1	1–1.5	2.17	2.62	−0.7	–
Au/Ag film	2.51	2.55	–	–	100 Total	100 Total	0.5	0.5	2.13	1.98	Unable to separate any film thickness; apparently slight darkening.	
Nb film	0.60	0.54	16.8	15.1	Unable to remove Nb films except at one pinhole (55 nm) in exposed area of thicker film.		1	1	3.75	3.68	−1.3	–
Nb film	1.69	1.66	47.3	46.5			1	1	3.85	3.34	−0.8	–
10-nm Pt/Os	2.55	2.52	~73.2	~72.3	10/63	~73 Pt + Os	0.5	0.5	–	–	−0.9	Undetected
6-nm Pt/Os	[c]	[c]	[c]	[c]	6/30	~24 Pt + Os	0.5	2.5	–	–	[c]	−12

[a] Results were influenced by both contamination and temperature, as described in the text; results shown are for ambient temperature believed to be between 273 and 300 K.

[b] Films were deposited on fused silica flats described in text unless noted otherwise.

[c] See text for details; 6-nm Pt/Os was poorly protected; we were unable to make measurements of the 6-nm Pt/Os because the back of the substrate was rough ground.

The polycarbonate (CR-39) and polymethyl methacrylate (Lucite) bulk plastics were cut into disks and cleaned with ethanol. The other bulk materials in Table III, except for the diamond sample, were ground and polished reasonably flat with progressively finer abrasives (aluminum oxide or diamond) to ~10-nm arithmetic roughness and cleaned with strong solvents followed with alcohol.

2.3 Results

Effects on silver, osmium, and carbon thin film coatings have been previously reported.[20] Unprotected thin silver films which were strongly bonded to optical substrates were converted to clear silver oxide (Ag_2O) interference filters of low optical density that reverted to higher optical density after exposure. The Ag_2O is slightly unstable, especially under the beam of a scanning electron microscope. Outer surfaces initially developed a thin metallic appearance but became dark brownish with time. We have not investigated the effects of substrates, protective gas, and cold storage conditions, which should reduce changes in the Ag_2O, but under typical laboratory conditions the exposed silver samples should be investigated within a month of exposure to limit changes in optical density to appreciably $<10\%$. Even with the instability problems we have found silver films useful for atomic oxygen sensors because of their high reaction efficiency. Other stable oxide films do not experience this problem. Thick silver platings and bulk silver samples formed interference films for low exposure, but continued reaction produced such large expansions of the silver lattice (i.e., ~55% increase of the Ag–Ag spacing) that major topographic changes occurred. This expansion was very pronounced for a bulk sample heated to ~373 K, resulting in elevation of the exposed silver oxide surface to 2200 nm above the unexposed silver surface. Such expansions in thick samples caused considerable stresses in the exposed areas, and debonding and sometimes flaking from the parent silver have occurred.[9] Debonding from the silver apparently limited further reaction at the interface. Various silver samples behaved differently, partly as a result of their responses to such stresses, making it more difficult to specify what reaction kinetics to expect for arbitrary silver surfaces. Coating silver films with gold of >10-nm thickness provided considerable protection, but a slight discoloration and an optical density decrease still occurred in the exposed area. Similar exposure of a 35.5-nm thick gold film over a niobium interface film did not produce permanent discoloration or other effects.

Osmium films have been shown to disappear rapidly during orbital exposure presumably due to formation of volatile OsO_4; however, the superior properties of osmium for vacuum UV optics justify continued attempts to use it. An attempt was made to protect osmium films from erosion with an overcoating of platinum thin enough to permit the optimum XUV reflecting properties of the thicker osmium film to dominate the thin overcoating. The results in Table II indicated that osmium was not protected by a 6-nm Pt film and escaped as volatile oxide though gaps in the Pt film, reducing the film thickness by 12 nm and increasing the roughness by a factor of 5. Deposition of very thin films sometimes results in incomplete coverage (island formation etc.). Poor UV reflectance measurements on both the unexposed as well as exposed areas suggested poor quality coatings for the 6-nm platinum over osmium. Attempts to improve thinner overcoatings should be made before concluding thinner films are definitely nonprotective. A film of 10 nm of Pt provided almost complete protection. The very small optical density decrease in the exposed area indicated a thickness change, but no step was measurable with the stylus to ~1 nm. Vacuum UV measurements and calculated properties are listed for this sample in Table IV with other details in Table II. Thinner needed to take advantage of the osmium properties at much shorter wavelengths.

As shown in Fig. 3, differential etching was observed on crystallites of a bulk osmium sample producing results commonly observed after acid etching used in metallographic studies, and similar effects on other materials have been observed with sputtering.[21] As shown in Table III, over 1 μm of osmium was removed from the ambient temperature sample, and increased etch rates were observed at higher temperatures.[4] If the desorbed species were OsO_4, the overall efficiency for the reaction was ~8% in terms of osmium atoms lost for each four incident oxygen atoms.

Platinum was not flown as a separate film, but it does not appear to be affected by the atomic oxygen exposure. The iridium sample apparently lost some atoms since formation of known solid oxides[22] should have produced an increase in thickness based on reported mass densities.[23] Sputtering is not considered a likely mechanism based on our measurements of gold (see Sec. 2.4). Formation of IrO_4 has been reported but not substantiated,[22] and it is postulated that it formed and evaporated in orbit. This process, which has not been observed before for

Table III. Some Effects Observed on Bulk Samples Exposed to 3.5×10^{20} Oxygen Atoms cm^{-2} in Low Earth Orbits[a]

Sample	Effects
Polished tungsten carbide	No detectable change; surface roughnesses on exposed and unexposed areas ~10 nm.
Diamond	Least affected carbon. Etched 75 nm deep; etched surface not smooth but covered with a weak layer which was easily scraped off.
Edge oriented graphite	Etched ~2300 nm deep; very rough, separated, striated structure produced.
Basal oriented graphite	Etched ~2200 nm deep; smoother, orange-peel effect on surface.
Vitreous carbon	Etched ~4500 nm deep; rough surface resembling grass, misshapen cones or pyramid, etch depth slightly dependent on manufacturer and/or preparation and mounting.
CR-39 plastic	Heavily etched samples: 22,000 nm. Etched surface very rough (cones resembling grass, see Fig. 2).
Polymethyl methacrylate	Heavily etched: ~17,000 nm. Very rough surface also.
Silver	Thin films of optical quality are typically covered to transparent oxide with the film thickness expanding greatly (~55%). Results on bulk silver seem to vary. Beautiful interference colors are observed for the thin oxides. Thick oxide formations appear to create stress levels which produce buckling or scaling which limit, or modify, further oxidation. The oxide is not too stable. The oxide apparently has a high index of refraction, but attempts to measure its optical properties by ellipsometry have given very poor inconsistent results, possibly due to inhomogeneities or instability effects.
Osmium	Etched ~1100 nm; polycrystalline structure made visible by slight preferential etching.
Silicon	No measurable effect.
Germanium	Visual discoloration, ellipsometer indicated 159-nm film with index of 1.53; stylus gave no distinguishable step; one form of GeO_2 (tetra) has a density of 6.239 g/cm^3, which exceeds the density of Ge.
Copper	Polished OFHC copper disk exhibited a very slight surface discoloration estimated to be ~3.5 nm thick from step measurements.

Table IV. Ultraviolet Reflectance Measurements Made on a 10-nm Pt/Os Film on Fused Silica with a Portion Exposed to 3.5×10^{20} Atoms cm^{-2} of Atomic Oxygen

Wavelength (nm)	Reflectance (unexposed)	Reflectance (exposed)	Reflectance[a] (calculated)
125	0.18	0.18	0.206
130	0.17	0.17	0.195
135	0.17	0.17	0.188
140	0.16	0.16	0.185
145	0.16	0.16	0.180
150	0.16	0.16	0.179
155	0.18	0.18	0.185
160	0.18	0.18	0.204
165	0.20	0.20	0.203
170	0.22	0.22	0.211
175	0.24	0.24	0.227
180	0.26	0.24	0.245
185	0.26	0.25	0.266
190	0.28	0.26	0.289
195	0.28	0.28	0.313
200	0.29	0.28	0.344

[a] Calculated using Refs. 18 and 19 and media: vac/Pt/Os.

iridium, is much less efficient than that for osmium. Gold showed no permanent effects except for more particulates in the exposed area. Al, Ni, and W showed minor decreases in optical density and increased film thickness ascribed to growth of the oxide layer. Calculated thicknesses from optical properties given in Table II suggested protective oxide layers initially existed on the unexposed films and were only slightly increased by the exposure. Increases in oxide thickness were observed on two Nb films except the thinner film indicated a larger change, perhaps as a result of being at a higher temperature due to greater absorption of solar radiation. Optical heterodyne measurements of the rms surface roughnesses listed in Table II showed slight smoothing of all surfaces except those of tungsten and 6-nm Pt/Os. This is opposite to the rough textures produced on heavily etched materials. Optical heterodyne measurements of unexposed and exposed iridium are shown in Figs. 4 and 5, respectively.

Most carbonaceous surfaces exposed to appreciable oxygen atom flux in orbit have been heavily etched (as shown in Fig. 1) and roughened, often with a spike-shaped structure (as shown in Fig. 2). The material shown in Figs. 1 and 2 is poly(bis-allyldiglycolcarbonate) (CR-39), a plastic of high optical quality used for windows and lenses. Direct exposure of such materials to the orbital direction can be expected to destroy optical surface properties.

Pure carbons were heavily etched, with diamond being the least affected. The diamond surface exposed was an octahedral face of a natural stone. An etch depth of 75 nm was observed (~5% of that with graphite), but the exposed surface was left coated with a greyish-white solid much softer than diamond. This was not considered to be contamination from an external source, since adjacent surfaces were not similarly coated. While the surface has not been characterized, there are similarities with those obtained by the action of oxygen on diamond at elevated temperatures. While true reversion of diamond to graphite occurs above 1800 K in inert atmospheres, a black coating can form at ~900 K when oxygen is present.[24] The nature and composition of this coating was unclear. In the present case, however, we observe that the coating cannot be normal graphite, which is much

Fig. 3. Etching of a bulk osmium sample while in low Earth orbits.

more reactive to atomic oxygen than diamond. Characterization of diamond surfaces exposed to activated oxygen in the laboratory[25] has shown at least a two-monolayer uptake of oxygen,probably in the form of carbonyl ($=C=O$) and ether linkages ($C-O-C$). It appears that these residues cover the diamond surface and partially inhibit further oxidation. A unique form of white carbon has also been reported[26] which indicates that forms other than clear diamond and black structures may be possible with pure carbon. Scattering from a rough topography is another possible source for the coloration. The diamond flown was too small to permit optical measurements, but microscopic examinations indicated significant damage which would be expected to increase absorptance and scattering. Vitreous carbon and edge and basal crystalline planes of graphite were heavily etched with different topographies. The surfaces of vitreous carbon exhibited grasslike spikes. The graphite surfaces with exposed basal planes were roughened to a lesser degree, producing an orange-peellike texture, while the edge orientations developed accentuated striated structures.

Silicon did not appear to be affected. It should be noted that the stable layer of SiO_2 on silicon in air is one of the thinnest oxide coatings and probably one of the most protective against oxygen attack.[27] Germanium was slightly discolored, and ellipsometric measurements indicated a film of 159-nm thickness with index $n=1.53$ existing on the exposed portion. No distinguishable step was measured on the Ge sample with the stylus, however. One form of GeO_2 (tetra) has a mass density of 6.239 g cm^{-3}, which is greater than the density of Ge (5.35 g cm^{-3}). Stoichiometric production of this oxide should have resulted in the production of a step of 11-nm height. Excessive spacing between the sample and knife-edge mask may have produced such an ill-defined step so that detection was not possible on this bulk sample.

The oxide discoloration on an OFHC copper disk was very slight, and a step height of ~3.5 nm was measured. No effect was measured on a polished tungsten carbide sample.

We have also observed that etching in orbit is very sensitive to certain contaminants overlying the reactive materials (silicones over carbon, for example). Figures 6 and 7 show the effect on a carbon sample of an invisibly thin film deposited by outgassing from a nearby elastomer sealant used in an electrical feedthrough. Line-of-sight deposition from this point source of contamination created a shadow of the sample holder on the carbon sample. The contaminated area was not etched and remains reflective, while the area shadowed from contamination was heavily etched. Other features were created by a screen placed above this sample and by a resolution mask pattern of ~200-nm thick protective niobium film. A stylus profilometer trace across the surface is shown in Fig. 7. The screen produced a grid pattern by shadowing the contaminant. Attempts to measure the contaminant deposited as a screen pattern on the niobium surfaces were unsuccessful down to noise levels of 20 – 30 nm for the profilometer traces on these particular surfaces, suggesting that the contaminant was thinner than this. Also, no interference colors from the contaminant were visible.

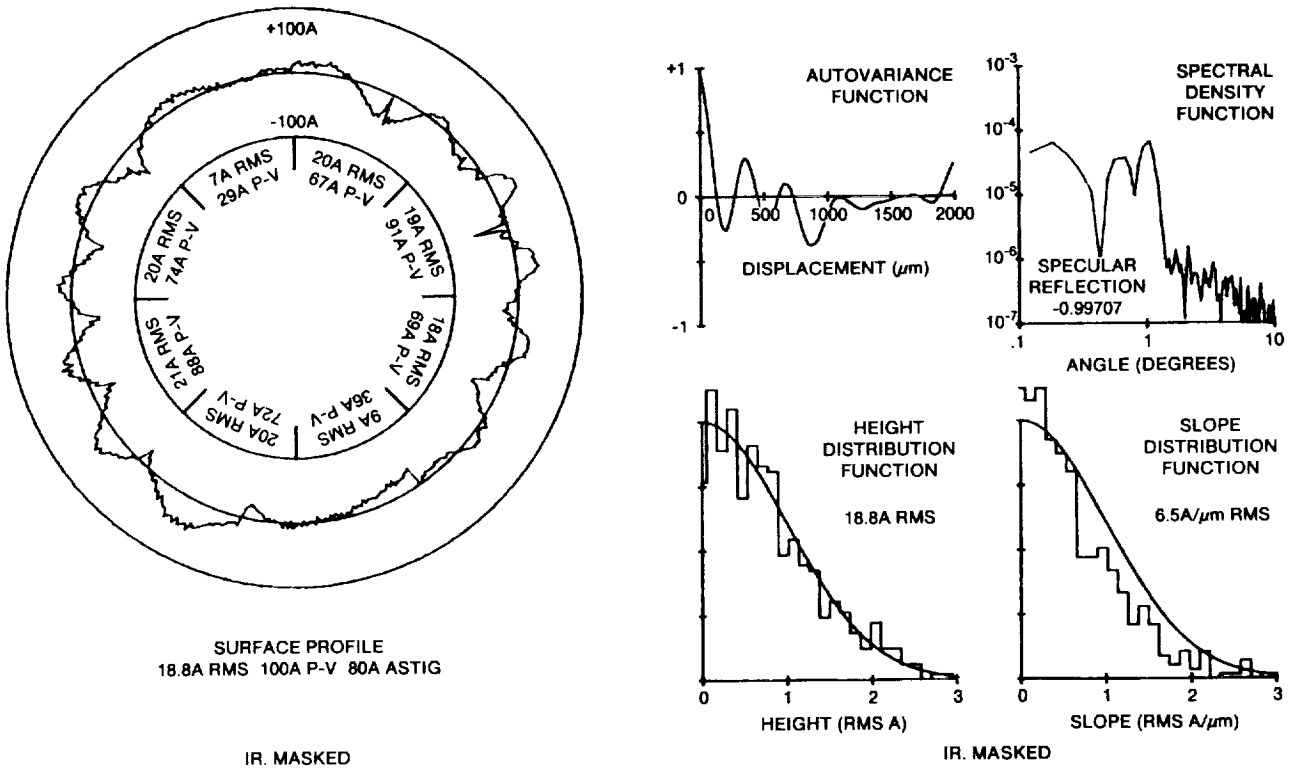

Fig. 4. Optical Heterodyne measurements of unexposed Ir sample.

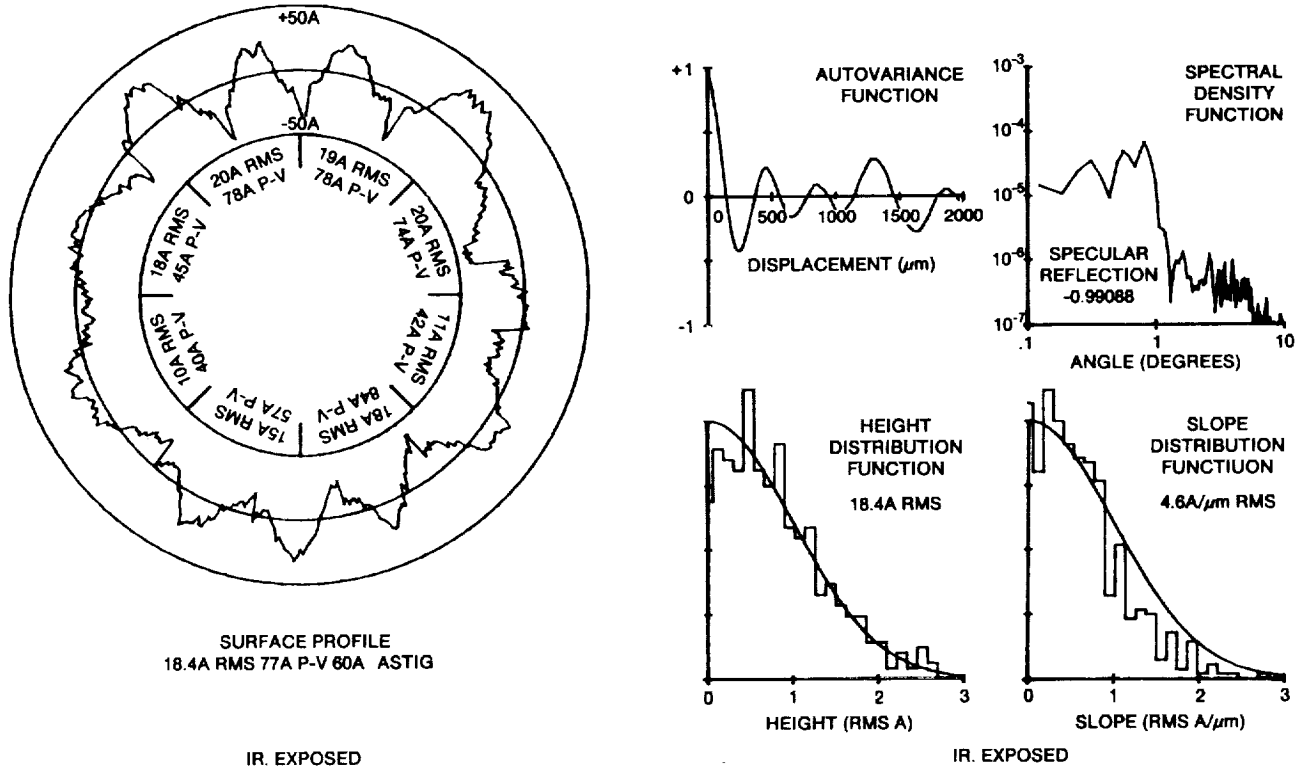

Fig. 5. Optical heterodyne measurements of exposed Ir sample.
Note: profile scale is twice that of Fig. 4.

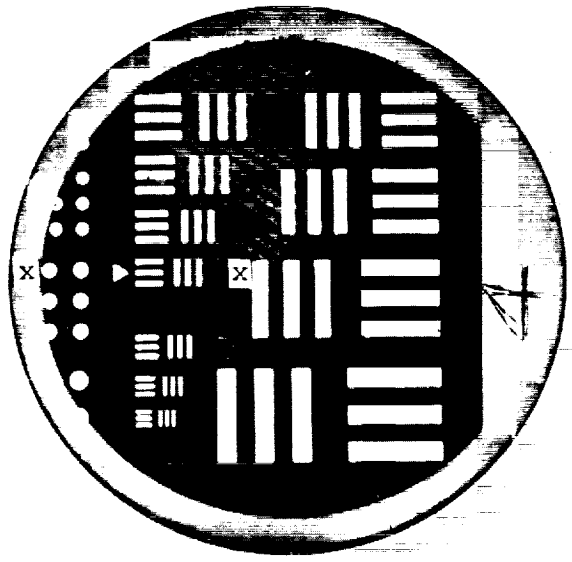

Fig. 6. Vitreous carbon surface showing polished finish where protected by holder, mask pattern, or contamination and dark finish where exposed to etching by atomic oxygen.

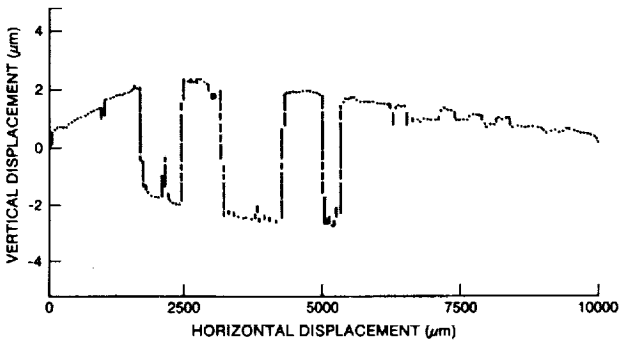

Fig. 7. Stylus profilometry tracing between the X's (X – X) on vitreous carbon surface shown in Fig. 6. Protected regions are elevated.

2.4 Discussion

We have also reported[4] temperature-dependent reaction rates observed for the etching in orbit which correspond to low activation energies (1-2 kcal/mole). The effects reported here are for ambient temperatures which were expected to be between 273 and 300 K; however, variations in film thickness, substrates, heat sinking, and solar radiation conditions could modify actual temperatures, as suggested by different oxide thicknesses observed on two different thicknesses of niobium.

Thin films of osmium should not be used in low Earth orbit if they will be exposed directly to the oxygen atom beam. Surfaces in more protected locations have been shown to survive,[28] but the effects of reflected oxygen atoms are as yet poorly understood. Even if osmium surfaces are not totally removed, mirror performance may be degraded by changes in surface topography on the microscopic scale.

Physical removal of films by momentum imparted from collisions with the incident atoms (sputtering) rather than by chemical reactions was studied by examining gold. Gold sputters with relatively high yields and is not reactive with oxygen. Thin film gold samples showed no permanent change in optical density between exposed and shielded portions. In this case, the sensitivity of the transmission measurement was ~2.5 nm or ten monolayers of gold. Assuming 1.5×10^{15}-atoms cm^{-2}/gold monolayer, an upper limit of 5×10^{-5} is obtained for the sputtering yield for 5-eV oxygen atoms incident on gold. This very small upper limit on physical sputtering yield resulting from 5-eV oxygen atoms bombarding gold is in agreement with our previous findings and the results of Colligon and Bramham for N^+, Ne^+, N_2^+, and Ar^+ bombarding gold at low energies.[29] Contamination cleaning and sputtering in orbit were reported by McKeown and Corbin.[30]

While graphite-epoxy and other carbonaceous composites may still be used for optical benches and other structural elements, mass loss and surface roughening are to be expected where the surface is exposed to atomic oxygen.

Growth in oxide film thickness on the exposed portions was observed for metals of Al, Ni, W, and Nb which are stable in dry air. The effect may not be important at visible wavelengths, and in any event such optics are usually coated with MgF_2, which appears resistant to atomic oxygen. There are, however, important exceptions to this. For example, x-ray optics may not be coated with light-element protective films. The growth of an oxide film on a surface under these conditions should be examined for any particular application in terms of total oxygen fluence expected at the optic.

Iridium is comparable to osmium in density and has potential applications for grazing incidence x-ray optics. Although we have not made x-ray measurements on our exposed surfaces, the similar

rms roughnesses before and after exposure suggest that such use is not denied by topographic changes. The small film loss observed from the iridium sample is being investigated further.

The smoothing effect observed on lightly oxidized metal films may indicate a mechanism for reducing scatter at optical surfaces in applications where scatter is critical.

2.5 Conclusions

Reactive effects in orbit have been described which could degrade the performance of optical systems. These effects are of relatively simple origin and associated with orbiting objects interacting with ambient atomic oxygen. Chemical changes and surface roughening effects can contribute to optical surface degradation. Deposited particles and contaminants can modify the observed results. Most of these problems can be controlled by selection of materials and operational procedures and by use of protective overcoatings where necessary and acceptable. Potentially beneficial effects have been noted.

We wish to thank Alice Dorries for obtaining scanning electron micrographs, Thomas E. Stephens and Robert DeHaye for assistance with film coatings, and Roger Linton, Walter Fountain, and James Carter for assistance with UV reflectance, optical transmission, and optical heterodyne measurements, respectively. We are grateful to the UAH Research Institute and the UAH Center for Applied Optics for grants for hardware fabrication and data analysis.

J. T. Swann is now a graduate student research fellow at the University of Alabama, Department of Physics & Astronomy.

References

1. J. P. Simpson and F. C. Witteborn, "Effect of the Shuttle Contaminant Environment on a Sensitive Infrared Telescope," Appl. Opt. 16, 2051 (1977).

2. L. G. Jacchia, "Thermospheric Temperature, Density, and Composition: New Models," SAO Report 375 (1977).

3. A. E. Hedin *et al.*, "A Global Thermospheric Model Based on Mass Spectrometer and Incoherent Scatter Data, MSIS 2, Composition," J. Geophys. Res. 82, 2148 (1977).

4. J. C. Gregory and P. N. Peters, "The Production of Glow Precursors by Oxidative Erosion of Spacecraft Surfaces," NASA CP-2391, Second Workshop on Spacecraft Glow (1985), pp. 174-179.

5. R. L. Shannon and R. B. Gillette, "Laboratory Demonstration Model Active Cleaning Technique Device, Final Report," Boeing Aerospace Report D180-18031-1 (1974).

6. P. N. Peters and E. R. Miller, "Utilization of Atomic Oxygen at Orbital Altitudes for In Situ Cleaning of Optical and Other Sensitive Surfaces," Marshall Space Flight Center Suggestion 79-49 (1979).

7. J. C. Gregory and P. N. Peters, "Interaction of Atomic Oxygen with Solid Surfaces at Orbital Altitudes," in *Proceedings, First LDEF Mission Working Group Meeting* (NASA, Langley Research Center, 1981), p. 48.

8. L. Leger, J. T. Visentine, and J. E. Kuminecz, "Low Earth Orbit Atomic Oxygen Effects on Surfaces," AIAA Paper 84-9548 (1984).

9. A. F. Whitaker *et al.*, "Atomic Oxygen Effects on Thermal Control and Optical Materials, STS8 Results," AIAA Paper 85-0415 (1985).

10. J. C. Gregory and P. N. Peters, "Measurement of Reaction Rates and Activation Energies of 5 eV Oxygen Atoms with Graphite and Other Solid Surfaces," AIAA Paper 85-0417 (1985).

11. T. R. Gull *et al.*, "Effects on Optical Surfaces at Shuttle Altitudes," AIAA Paper 85-0418 (1985).

12. W. K. Stuckey *et al.*, "Effects on Advanced Materials: Results of the STS-8 EOIM Experiment," AIAA Paper 85-0419 (1985).

13. B. A. Banks *et al.*, "Ion Beam Sputter Deposited Thin Film Coatings for Protection of Spacecraft Polymers in Low Earth Orbit," AIAA Paper 85-0420 (1985).

14. W. L. Slemp, B. Santos, and G. F. Sykes, "Effects of STS-8 Atomic Oxygen Exposure on Composite Polymeric Films and Coatings," AIAA Paper 85-0421 (1985).

15. G. S. Arnold and D. R. Peplinski, "Kinetics of Oxygen Interactions with Materials," AIAA Paper 85-0472 (1985).

16. J. J. Triolo *et al.*, "Degradation Studies of Materials Retrieved by the Solar Max Repair Mission, STS 41-C," AIAA Paper 85-0474 (1985).

17. G. E. Sommargren, "Optical Heterodyne Profilometry," Appl. Opt. 20, 610 (1981).

18. G. Hass and L. Hadley, "Optical Properties of Metals," in *AIP Handbook*, D. E. Gray, Ed. (McGraw-Hill, New York, 1963), Sec. 69.

19. D. W. Lynch and W. R. Hunter, "Comments on the Optical Constants of Metals and an Introduction to the Data for Several Metals," in *Handbook of Optical Constants of Solids*, E. D. Palik, Ed. (Academic, Orlando, 1985).

20. P. N. Peters, R. C. Linton, and E. R. Miller, "Results of Apparent Atomic Oxygen Reactions on Ag, C, and Os Exposed During the Shuttle STS-4 Orbits," Geophys. Res. Lett. 10, 569 (1983).

21. O. Anceilo and R. Kelly, Eds., *Ion Bombardment Modification of Surfaces, Fundamentals and Applications* (Elsevier, New York, 1970).

22. W. P. Griffith, *The Chemistry of the Rarer Platinum Metals (Os, Ru, Ir and Rh)* (Interscience, London, 1967).

23. É. Savotslu, *Physical Metallurgy of Pt Metals*, Translation, I. Savin (Mir, Moscow, 1978).

24. J. E. Field, Ed., *The Properties of Diamond* (Academic, New York, 1979).

25. S. Evans, "Depth Profiles of Ion-Induced Structural Changes in Diamond from X-ray Photoelectron Spectroscopy," Proc. R. Soc, London Ser. A 360, 427 (1978).

26. C. R. Hammond, "The Elements (Carbon)," in *Handbook of Chemistry and Physics*, R. C. Weast, Ed., (CRC Press, Cleveland, 1979), p. B-9.

27. H. J. Mathieu, M. Datta, and D. Landolt, "Thickness of Natural Oxide Films Determined by AES and XPS with/without Sputtering," J. Vac. Sci. Technol. A3, 331 (1985).

28. M. R. Torr, "Osmium Coated Diffraction Grating in the Space Shuttle Environment: Performance," Appl. Opts. 24, 2959 (1985).

29. J. S. Colligon and R. W. Bramham, "Low Energy Sputtering of Gold," in *Atomic Collison Phenomena in Solids*, D. W. Palmer et al., Eds. (Elsevier, New York, 1970), p. 258.

30. D. McKeown and W. E. Corbin, Jr., "Space Measurements of the Contamination of Surfaces by OGO-6 Outgassing and their Cleaning by Sputtering and Desorption," paper presented at Space Simulation Conference, NBS, Gaithersburg, MD, Sept. 1970.

3.0 A Measurement of the Angular Distribution of 5 eV Atomic Oxygen Scattered off a Solid Surface in Earth Orbit*

J. C.Gregory
Chemistry Department
The University of Alabama in Huntsville
Huntsville, Alabama 35899

P. N. Peters
Space Science Laboratory, ES64
NASA Marshall Space Flight Center, Alabama 35812

Summary

The angular distribution of 5 eV atomic oxygen scattered off a polished vitreous carbon surface was measured on a recent Space Shuttle flight. The experimental apparatus was of novel design, completely passive, and used thin silver films as the recording device for oxygen atoms.

We observed that most of incident oxygen was contained in the reflected beam, remained in an active form, and was probably still atoms. We allowed for 12 percent loss of incident atoms which are converted to CO at the carbon surface.

The scattered distribution, which was wide lobular peaking 15° in the forward direction, showed almost but not quite full accommodation. The method of Nocilla[1] was used to fit the shape of the lobe. The implications of this measurement for satellite lift and drag calculations are discussed in a companion paper by Karr, Peters and Gregory[2].

3.1 Introduction

In the scattering of beams of gas particles from solid surfaces, the angular dependence of the scattered particles has been found to be dependent on the incident angle of the beam, the temperatures of the gas and the surface, the masses of the gas and surface atoms, and the form of the surface (including roughness and contamination). For a full description of the scattering process, the velocity distribution of the scattered particles must also be known. Clearly, the present single measurement does not permit such a comprehensive description.

If incident particles are captured on a surface long enough to reach equilibrium (a period of at least several atom-lattice vibrations) the particles are accommodated energetically and their desorption typically exhibits a cosine angular distribution. Such behavior is often seen with low, or thermal, energy particles. If the particles were not accommodated, their reflection would be close to specular, if the surface is considered to be an ideal flat plane. This is sometimes observed with particles at higher speeds, but the increase in particle energy also causes a deeper penetration of the surface potential and a transition to a different scattering model, called "structure scattering," is indicated.

Transition from thermal to structure scattering has been postulated by Oman[3] to occur at some value of incident energy E_i at which the scattered lobe properties show a systematic change. This has generally been shown to be so in the cases of rare gases scattering from single crystal surfaces under UHV conditions (see for example Liu, Rodgers and Knuth[4]. At the energy of the present measurement, 5 eV, we might assume according to this theory that the cube model no longer holds and that the 'structure regime' is penetrated (Goodman and Wachman[5]).

In low Earth orbits, most of the atmosphere is atomic oxygen and the orbital motion of the spacecraft results in an interaction energy with the forward facing surfaces of approximately 5 eV per atom. Most reported laboratory studies of oxygen atom/surface interactions have been carried out at energies either considerably below, or in excess of this energy; lower or higher energies have been usually obtained by thermal or electrical techniques, respectively. Satisfactory, high density, 5 eV oxygen atom beams have been lacking for ground based studies due to technical difficulties. There is good

Reprinted from *Rarefied Gas Dynamics*, Vol. 15, 1987

reason to believe that this situation is now changing (Cross[6], Bareiss and Sjolander[7]).

3.2 Experimental Description

All gas-beam scattering experiments include three components: the gas beam, the target surface, and the detector. In this experiment the beam was provided by the relative velocity of the atmosphere past an orbiting spacecraft, and the detector was a passive silver-film device (described below) which is sensitive only to oxygen atoms. Our target surface was polished vitreous carbon and in some ways was the least well defined component because of our lack of knowledge of its surface condition during the experiment. A diagram of the reflectometer hardware is shown in Figure 1. This was originally designed for the Long Duration Experiment Facility (LDEF).

3.2.1 Beam Characteristics

While low Earth orbit does not provide the perfect beam for many experimental purposes (for example, the composition and energy can only be varied over a small range and then not independently) it does provide intense beams of atomic oxygen and molecular nitrogen at energies which have proven difficult to generate in the laboratory. The characteristic energy of around 5 eV, depending on the orbital altitude, is roughly equal to chemical bond energies so that reactive scattering processes may be studied. Enhanced reactivities have, in fact, been observed with 5 eV oxygen on carbon and other surfaces (Gregory and Peters[9, 10]).

The density, composition, and temperature of the atmosphere are highly variable, but have been extensively studied and modelled.

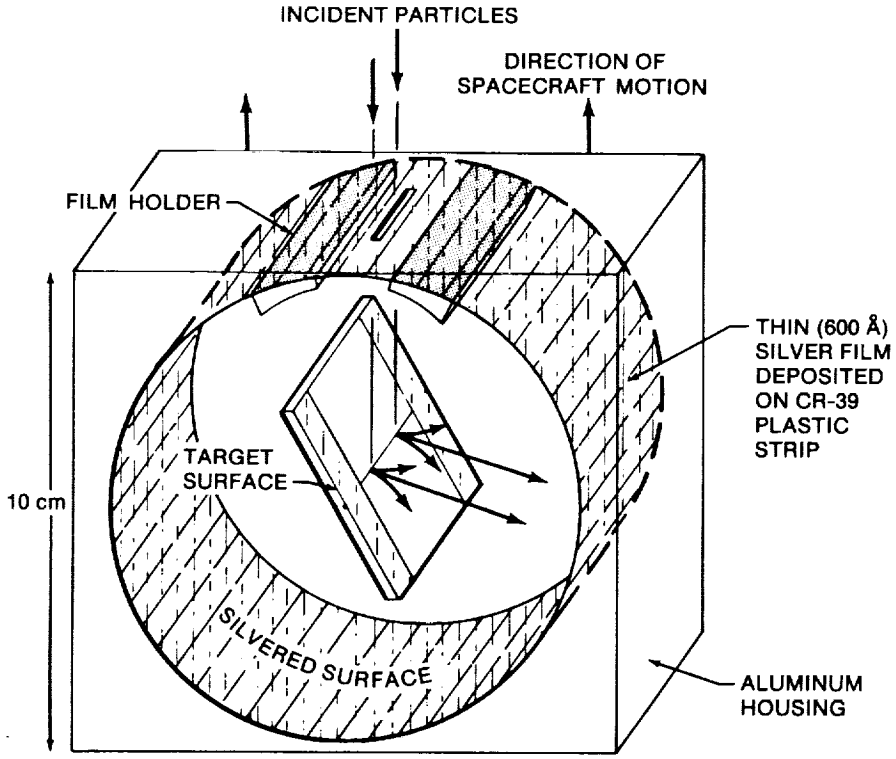

Figure 1.- The oxygen atom reflectometer flown on shuttle STS-8 and the long duration exposure facility.

The beam was formed by aligning the entrance slit and solid target with the velocity vector of the spacecraft. This was obtained in this case by controlling the attitude of the entire Shuttle Orbiter. The flight, designated STS-8, took place in September 1983, and was particularly well suited to the experiment discussed here since during the entire mission 95 percent of the 3.5×10^{20} atoms cm^{-2} fluence was accumulated with the experiments oriented within 1° of the orbital direction. Beam divergence (14° FWHM) was accurately known both from knowledge of the spacecraft velocity and ambient gas temperature, and from a direct measurement of the etch-profile of a shadowed carbon surface, which we have described elsewhere (Peters, Sisk, and Gregory[11]).

3.2.2 Atomic Oxygen Detector

The sensor was a thin silver film deposited on a strip of optically clear CR-39 plastic which fitted within the cylindrical reflectometer cavity in the same manner as x-ray film in a Debye-Scherrer camera. The Ag film formed a circle with the carbon target at its center. The use of Ag films as sensors was reported by Henderson and Schiff [12] and by Thomas and Baker[13]. Unlike these workers, we used the change in optical density of silver as it was converted to Ag_2O.

The film thickness chosen was designed to approach, but not exceed, saturation in the most heavily exposed area, thus providing maximum sensitivity for the measurement. The interior of the aluminum reflectometer housing was also silvered to act as a sink for any stray oxygen atoms. Most of the flight was flown with the reflectometer accurately aligned in the forward direction; a preflight decision was made not to further collimate the beam with tandem slits, for fear that orientational inaccuracies would limit knowledge of the actual flux reaching the surface or, worse, completely block the beam. Thus, a distribution of tangential components of velocity associated with thermal energies of the oxygen atoms are present. Since we know the gas temperature, as discussed above, this does not introduce serious error.

The optical density of the silver-coated sensor strip was measured at 1.0 mm intervals with a Perkin-Elmer Micro-10 scanning microdensitometer. Calibrations of silver thickness versus optical density were obtained by measuring 16 coatings of silver thicknesses on 1/20th-wave fused silica flats with a stylus profilometer. This data, which was corrected for different substrate absorptions, was used to determine the initial silver film thickness as a function of position on the sensor strip. This varied from approximately 630 Å to 770 Å over the region that received the reflected beam, with approximately 700 Å thickness where the maximum exposure occurred later. Postflight measurements of optical densities were used to determine changes due to exposure. The average optical properties of an Ag_2O film produced on an earlier flight were used to correct for overlying silver oxide on the postflight sensor strip. Since the silver film used in the reflectometer was approximately one-third as thick as the film totally converted on an earlier flight, and since we obtained a good mass-balance as discussed in section 3, the assumption of linearity between optical density changes and oxygen atom exposure seemed reasonable.

While the atmosphere at the flight altitude contained some 10% N_2 molecules, our detector did not respond to them; and we assumed their presence did not affect any measured process. Our detector gave angular intensities of scattering oxygen atoms with good sensitivity and linearity but, so far as is known, responded equally efficiently to oxygen atoms of all velocities. Consequently, the velocity distribution of the scattered beams was unknown.

3.2.3 The Scattering Surface

The structure and condition of the target surface, a vitreous, or glassy, carbon disc, cannot be described with any great certainty (as is frequently the case in some of the older beam-surface work). Vitreous carbon is formed by heating thermo-setting polymers to high temperatures (1000° to 2000° C). A refractory, non-porous, isotropic form of carbon is obtained which is much less reactive to thermal oxidation than graphite. The target was in the form of a one-inch diameter disc, the surface of which was polished, finishing with 1 μm diamond. Scanning electron micrography at 100,000X showed a smooth, featureless surface. The surface was slightly smoother after exposure than before. We discuss contamination of the surface in section 3.4.

3.3 Results

The variation in optical density of the exposed silver film is shown on a polar diagram in Figure 2. The bulk of the reflected atoms lie in a wide lobe whose maximum intensity lies at $\theta_r = 15°$. A small supraspecular peak (~2% of total) may be seen at $\theta_r =$

60°. It is not clear whether this is real or an absorption artifact. The figure also shows a cosine distribution for comparison, calculated for an equal number of oxygen atoms as the data contain.

No changes in optical density were observed on portions of the silver film which were shadowed from line of sight with the slit, providing good evidence that there were no stray oxygen atoms inside the reflectometer. The film holder cut-off may be seen at $\theta_i \sim 20°$. This prevented proper measurement of the backward region, and has been corrected in the latest design for future flights.

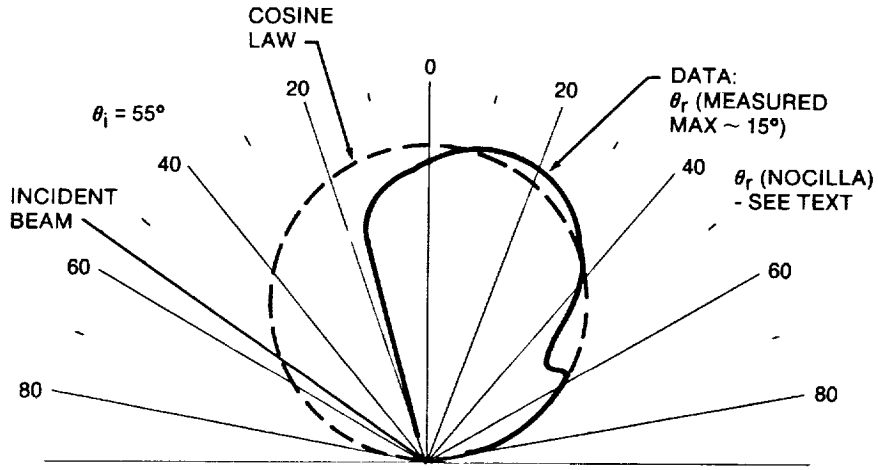

Figure 2.- Polar diagram of angular distribution of 5 eV oxygen atoms scattered from polished vitreous carbon (orbital flight data). A pure cosine law re-emission is shown for comparison. The cut-off in the backward hemisphere was caused by the detector film holder.

Optical densities were corrected for absorption by CR-39 and Ag_2O; and it was estimated that at lobe maximum, only 200 Å of Ag remained out of an initial thickness of 700 Å. Since we were given the atom fluence from the MSIS-83 model[14] and we know the slit size and the measured lobe shape, we can calculate the amount of Ag converted to Ag_2O. The best estimate for the total number of oxygen atoms striking unit area for the flight was $3.5 \times 10^{20}\,cm^{-2}$. Since the slit area was 0.024 cm^2, 8.4×10^{18} atoms should have struck the reflectometer carbon surface. Based on the 11.5 percent reaction efficiencies observed on etched external samples, 88.5 percent of the incident oxygen should have left the carbon surface as unreacted atoms or molecules. The result obtained was that approximately 600 Å of silver should have reacted at the maximum exposure location for the measured distribution.

This agreement within 20% between the measured and calculated values shows that the sensor is linear over the range used and that the recombination of O to O_2 on silver has a low probability. We note also that the errors in particle densities used in the MSIS model may not be better than 15 percent.

The method of Nocilla[1] was used to fit the observed scattered lobe. Nocilla's model treats particles emitted from (or impinging upon) a surface as the combination of normal random molecular motions associated with a particular temperature and a drift or ensemble velocity. The concept is called "drifting Maxwellian." We studied two cases, one in which there is assumed to be only one lobe, wide enough to include the small peaks at high θ_r, and the case with a slightly narrower main lobe with a small (2 percent) supraspecular lobe. The results of the fits are shown in Figures 3 and 4.

We have used Nocilla's notation. Note that the speed ratio (s) is the ratio of the ensemble velocity to the most probable velocity at the characteristic temperature, $C = (2kT/m)^{1/2}$.

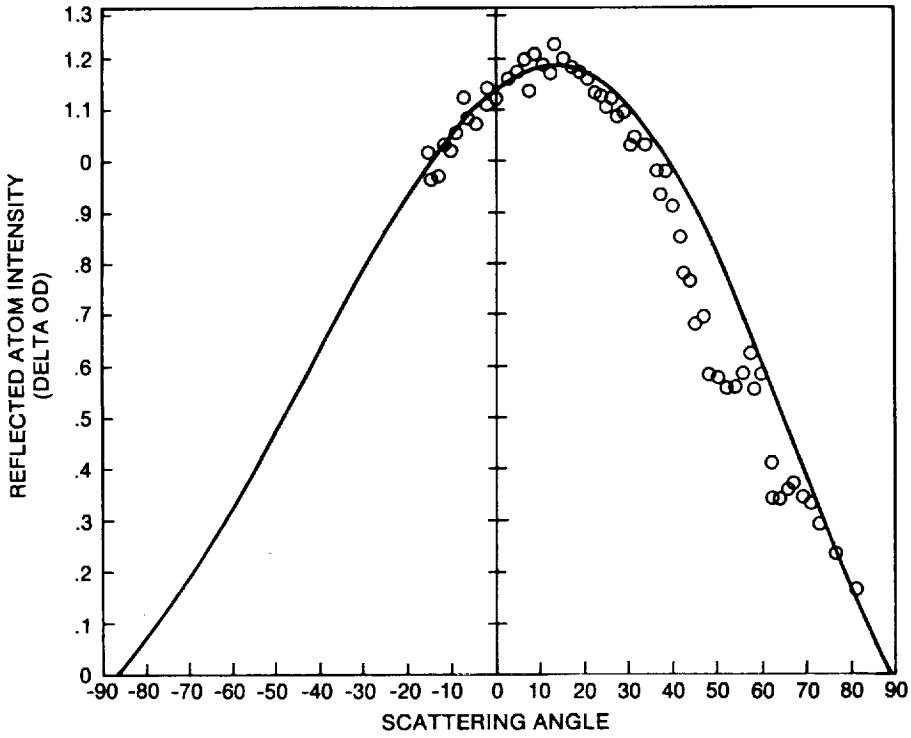

Figure 3.- Fit using Nocilla model to the outside envelope of the flight data. Discrepancies assumed due to absorption artifacts in the silver film θ_r. (Nocilla) = 40°: $S_r = 0.2$

	θ_i	S_i	T_i K	U_i km/s	θ_i deg	S_r	T_r K	U_r km/s
Case 1 (Single lobe)	55°	8.8	750	7.8	40°	0.2		
							(see text)	
Case 2 (excluding specular lobe)	55°	8.8	750	7.8	19°	0.6		

We may not solve further for T_r and U_r unless we either measure the scattered velocities or make some simplifying assumption. For example, if we assume the collision process is adiabatic, i.e., all the primary kinetic energy of the incident beam is converted into heating the scattered gas, we obtain a very high value of T_r ~30,000 K, close to the stagnation temperature of the primary beam. Since we know nothing about energy transfer at the surface, this merely represents a limit.

3.4 Discussion

The Nocilla fits gave speed ratios of 0.2 and 0.6 compared with the incident value of 8.8, and wide lobes of at least 80° FWHM. Generally, results of others with rare gases at similar energies but on clean single crystal surfaces show narrow peaks close to the specular angle. We are apparently seeing a high degree of accommodation, characterized by distributions approaching the cosine. It should be noted that our lobe width is affected by the beam divergence (14° FWHM) and by roughness and contamination effects. While the residual pressure in the reflectometer may have been of the order of 10^{-5} torr, this gas would have been chiefly O_2, CO, and N_2, none of which are considered to be strongly bound at carbon surfaces. Contamination by heavier organic molecules, while likely at first, was not expected to last long under the oxidative bombardment of energetic O atoms.

Calculations by Chiang and Knuth[15] have shown that physisorbed molecules are sputtered off by hyperthermal gas particles directed at the surface. This does not, however, preclude absorption from the beam itself and, though the oxidation mechanism of carbon is not understood in this regime, it is likely that the surface is covered with chemisorbed oxygen. However, since the masses of O and C are quite similar and the force constants of the C-O bond may be comparable to C-C bonds, it is not clear why a layer of chemisorbed oxygen should force the change from a specular to a cosine scattering pattern, as observed by others in well defined beam-surface experiments at lower energies.

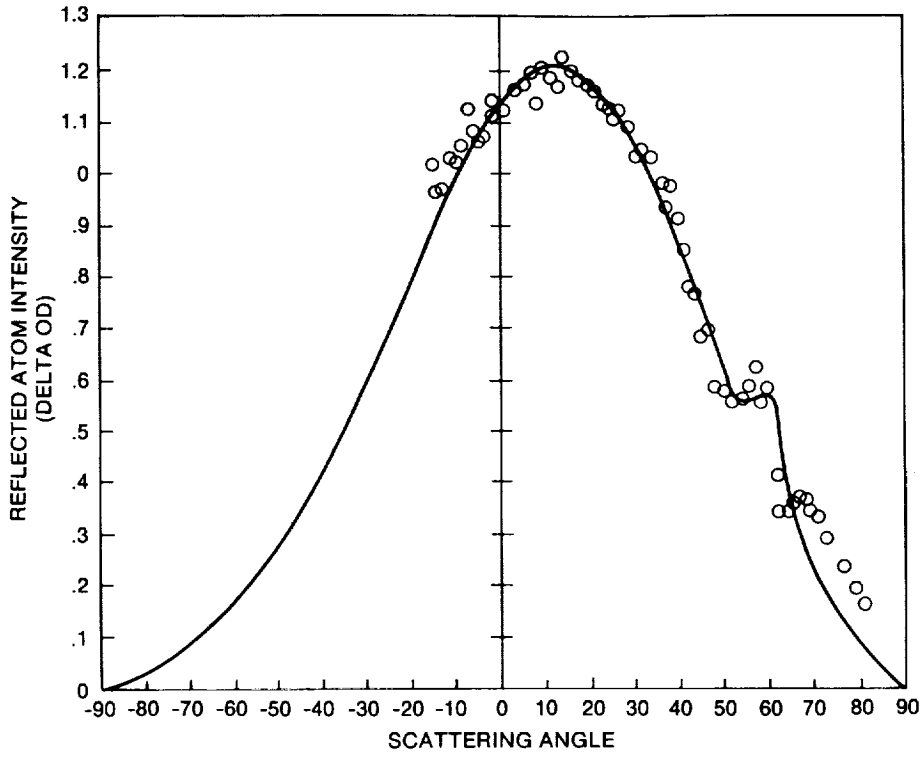

Figure 4.- Fit using Nocilla model to the flight data assuming a bi-modal distribution. Parameters where θ_r (Nocilla): Main lobe 19°, supraspecular lobe 62°: S_r (main lobe) = 0.6. Supraspecular lobe, 8.8. Only about 2% of the reflected atoms were in the supraspecular lobe.

Further experiments with hyperthermal atomic oxygen beams will be made with well characterized surfaces and scattered velocity measurements in the near future.

References

1. S. Nocilla, The Surface Re-emission Law in Free Molecular Flow, *Rarefied Gas Dynamics* 3 (1), 327, (1963).

2. G. R. Karr, J.C. Gregory and P. N. Peters, these proceedings.

3. R. A. Oman, *J. Chem. Phys.* 48, 3939, (1968); and in *Rarefied Gas Dynamics* 2, 1331, (1969), Academic Press, NY.

4. S. M. Liu, W. E. Rodgers and E. L. Knuth, Rarefied Gas Dynamics, p. E8-1, DFVLR-Press, Porz-Wahn, Germany, (1974).

5. F. O. Goodman and H. Y. Wachman in *Dynamics of Surface Scattering*, Chap. 7.

6. J. Cross, (1986), these proceedings.

7. L. Bareiss and G. Sjolander, (1985), Martin Marietta Corp., Denver, USA; private communication.

8. J.C. Gregory and P. N. Peters, The Interaction of Atomic Oxygen with Solid Surfaces at Orbital Altitude, (1974), proposal to NASA, LaRc; also in *The Long Duration Exposure Facility*, p. 14, NASA SP-473, NASA Headquarters (1984).

9. J. C. Gregory and P. N. Peters, the Production of Glow Precursors by Oxidative Erosion of Spacecraft Surfaces, Proc. 2nd Workshop on Spacecraft Glow, NASA, CP-2391, 174, (1985).

10. P. N. Peters, J. C. Gregory and J. Swann, Effects of 5 eV Oxygen Atoms on Optical Surfaces, *Applied Optics* 25, (8), 1290, (1986).

(continued on page 2-7)

11. P. N. Peters, C. Sisk and J. C. Gregory, A Measurement of the Thermospheric Gas Temperature by the Erosion of a Carbon Surface in Earth Orbit, submitted May 1986 to *Geophys. Res. Lett.*

12. W. R. Henderson and M. I. Schiff, A Simple Sensor for Atomic Oxygen in the Upper Atmosphere, *Planet. Space Sci., 18*, 1527, (1970).

13. R. J. Thomas and D. J. Baker, Silver Film Atomic Oxygen Sensors, *Can. J. Phys.* 50, 1676, (1972).

14. A. E. Hedin, A Revised Thermospheric Model Based on Mass Spectrometer and Incoherent Scatter Data: MSIS-83, *J. Geophys. Res.*, 88, 10,170, (1983).

15. K. C. Chiang and E. L. Knuth, *J. Chem. Phys.* 53, (6), 2133, (1970).

Acknowledgements

The authors gratefully acknowledge the assistance of Charles Sisk with the Nocilla calculations. This work was supported in part at the UAH by NASA grants NGW-812 and NAS8-36189.

4.0 THE REACTION OF 5 eV OXYGEN ATOMS WITH POLYMERIC AND CARBON SURFACES IN EARTH ORBIT

J. C. Gregory
Consortium for Materials Development in Space and
Department of Chemistry
The University of Alabama in Huntsville,
Huntsville, Alabama 35899

and P. N. Peters
Space Science Laboratory, ES64
NASA Marshall Space Flight Center, Alabama 35812

Abstract

An experiment to study the interaction processes of oxygen atoms striking materials surfaces at 8 km s^{-1} in low Earth orbit was performed in 1983. Reaction rates for two polymers, single crystal graphite, glassy (or vitreous) carbon and diamond were measured. For some of these, the temperature dependence of reaction rate could be measured and the activation energy determined. Some of the many uncertainties involved in comparing the results to the available literature on $O(^3P)$ reactions with organic materials are discussed. A model for the reaction sequence involves both kinetically activated adsorption and thermally activated reaction steps.

4.1 Introduction

A few hundred kilometers above the surface of the Earth, the most abundant constituent of the atmosphere is atomic oxygen. Formed by dissociation of molecular oxygen by ultraviolet radiation, the atoms are a major repository of solar energy in this region of the atmosphere through which low-orbit satellites pass. While the chemical reactivity of this environment has been realized for some time[1,2], only recently have observations been made of chemical and physical processes taking place involving interaction of the stream of oxygen atoms and a variety of material surfaces exposed on satellites[3,4,5]. Since satellite velocity at typical low orbital altitudes is about 8 km/s^{-1}, much discussion has focused on the effect of this translational kinetic energy (an oxygen atom strikes a satellite surface with a relative kinetic energy of 5 eV) on the rates of chemical reaction. This kinetic energy is approximately equal to typical chemical bond energies, and the possibility of enhanced reaction cross-sections seems real.

Because of the technical difficulties of producing ample beams of oxygen atoms at several eV, few studies have been made at these energies in the laboratory, and no materials chemistry experiments have been performed in space since 1983 using the source available there. While there is a wealth of data available on thermal energy ground state, $O(^3P)$, atom reactions with organic molecules, and some using atoms in the first-excited state, $O(^1D)$, very little has been reported on surface reactions[6], and much of that is such that it is difficult to make quantitative comparisons with the present work.

4.2 The Flight Experiment

In 1983, a materials experiment was flown to investigate the effects of 5 eV oxygen atoms on surfaces in orbit.[4] The University of Alabama in Huntsville provided a version of its Long Duration Exposure Facility instrument[1] (currently still in orbit) which had been designed for the same purpose.

The experimental approach used was necessarily very simple as no electromechanical devices such as lids, shutters, etc. were available, and no intermediate measurements could be made; thus only a single integral effect could be measured for each sample. Samples were nominally 1-inch discs, with the hot-plate discs only being one-fourth inch diameter. For the case of the erodible materials discussed here, a bar-pattern of small rectangles of niobium was deposited on the surface, using a photo-resist technique.[3] The niobium was sputtered on as a uniform film ~200 nm thick. Although it oxidized heavily, it still served to protect the underlying carbonaceous materials. The scanning electron microscope picture in Figure 1 shows both the eroded

portion of a CR-39 surface and the part covered and protected by the niobium film. The height of the step on this sample was about 22,000 nm. The bar-pattern allowed multiple measurements of the step-height to be made using a stylus profilometer. Amplitudes were checked using SEM micrographs. Half of each sample was covered at all times before and during the flight, and served as a control.

Erodible surfaces studied included single crystal graphite (basal and prismatic planes), vitreous (or glassy) carbon from various manufacturers, polymethyl-methacrylate, bisallyl diglycol carbonate (CR-39, a high quality optical plastic), and diamond.

Figure 1. Micrograph of CR-39 surface exposed on the STS-8 flight (see text). Magnification 1800 X

The exposure obtained during the STS-8 mission was ideal from the point of view of the materials experiment, in that about 95percent of the atom fluence was accumulated while the vehicle attitude was held so that the ambient atom beam was within 1° of the normal to the material surfaces. The rest of the mission was spent at much higher altitudes or with the payload bay doors closed. Pertinent exposure data are shown in Table 1.

TABLE 1.- STS-8 ATOMIC OXYGEN EXPOSURE DATA

Payload bay forward facing:	t = 41.2 hrs.
Altitude:	120 nmi (225 km)
Velocity:	7.8 km s^{-1}
Mean oxygen atom density (calculated):	2.65×10^{9} cm^{-3}
Surface impact frequency:	3.07×10^{15} $cm^{-2}s^{-1}$
Integral fluence:	3.5×10^{20} atoms cm^{-2}

Erosion observed by this experiment ranged from 100 nm for diamond (which appears to be particularly resistant to oxidation under these conditions) to about 20, 000 nm for the polycarbonate resin, CR-39, which was the most heavily eroded material reported on any space flight exposure.

The temperature dependence of the oxidative effects was measured by conducting the erosion measurements at three temperatures spanning about 100°C. The Arrhenius activation energy, E, was estimated, assuming: $r = A \exp[E/RT]$, where r is the rate of the reaction and A is a constant assumed independent of temperature T. These studies were performed for six materials, vitreous carbon, two graphites, CR-39, silver, and osmium. All activation energies were small and positive.

4.3 Results

The conclusions from the measurements on various forms of carbon exposed in the STS-8 mission appear applicable to organic solids in general. They may be summarized as follows:

1. Measured erosion was linear with total fluence

2. No induction time was observed before onset of erosion.

3. Erosion rate linear with oxygen flux (i.e., reaction probability independent of flux) measured over a small range, 1.5 to 2.5×10^{15} atoms $cm^{-2}s^{-1}$.

Our experiments used very pure materials, but standard or engineering materials may be contaminated either on the surface or by inclusions in the bulk. Such contamination, if less oxidizable than the matrix itself, may then serve to protect the rest of the matrix material from erosion. As erosion proceeds, the density of these screening particles or films on the surface grows, and the erosion rate may drop from its prior value. Such protection may result in erosion measurements and derived rates considerably less than those for pure or unprotected material. We have shown that thin films of silicone deposited in space were converted to a layer of SiO_2 2 to 3 nm thick by the ambient oxygen atoms. This film, which overlaid a carbon surface, provided protection from attack by oxygen atoms.

The temperature-dependent rate data for CR-39 were as follows:

Temperature °C	0-20	65	115
Erosion (nm)	22,600	25,000	29,000

Similar data were obtained for the other substrates. Arrhenius activation energies for some of these were calculated to be:

Material	E (cal mol^{-1})
CR-39	650
vitreous carbon	1200
graphite (basal plane)	1400

These values are quite consistent with literature values of activation energies of $O(^3P)$ with some organic compounds in the gas phase.

While reaction probabilities for carbon surfaces may be simply expressed in terms of C atoms lost per incident O atom (we have measured such probabilities with 5 eV oxygen in the range 0.1 to 0.15 atoms per atom), for more complex substrates, reaction probabilities have been expressed in $cm^3 \times 10^{-24}$ of material lost per incident O atom. Probabilities for some polymer films were summarized by Leger et al.[4]

Typical values were, at about 300 K (in the units cm^3) $\times$ (10^{-24} $atom^{-1}$) as follows:

CR-39 $(C_{12}H_{18}O_7)_n$ (this work)	6.0
Kapton (an aromatic imide) (ref. 4)	3.0
PMMA (this work)	4.8

4.4 Discussion

Comprehensive reviews of atomic oxygen reactions with organic compounds are available.[7,8] It is now well established that the first step of the reaction of $O(^3P)$ with alkanes is abstraction of hydrogen:

$$RH + O \rightarrow R + OH,$$

though other possibilities may still occur. In the case of second and further interactions of the same residue with oxygen atoms, however, the picture is very complex and obscure. For the case of surfaces of solid polymers under consideration here, subsequent addition reactions almost certainly occur; but after each addition or abstraction, the possibility exists for rearrangement and loss of a volatile fragment.

Reactions with halo alkanes proceed via abstraction of available hydrogen since abstraction of halogen is too endothermic, at least in the case of thermal energy $O(^3P)$. This may not be the case for 5eV oxygen atoms, though polyfluorinated hydrocarbons are clearly less reactive in the space environment. Reaction with completely halogenated hydrocarbons may also proceed by addition mechanisms[9], which may be facilitated by a kinetic energy of 5 eV. The massive erosion of fluorinated polyethylene observed on materials returned from the solar maximum repair mission was a surprise. The result has been interpreted in terms of the hydrogenated fraction of the material. The reaction rate of fully fluorinated polymers with 5 eV oxygen atoms remains unquantified.

For alkanes and alkynes, $O(^3P)$ adds to the unsaturated bond either forming stable products or rearranging and fragmenting. The relative frequency of these processes depends on the ability of the molecule to accommodate the excess energy according to Cvetanovic[10]. This ability is high in the case of surface reactions, but the behavior with 5 eV atoms is quite uninvestigated.

Reactions of $O(^3P)$ with aromatic compounds is the least well understood. Oxygen atoms may add to a carbon atom in benzene forming a radical which may rearrange to give phenol:

If a free radical remains in the surface after the first atom reaction, then reaction may occur with another atom. Since the atom-arrival rate of oxygen atoms in low Earth orbit is about 1 per surface atom per second, the radical lifetime must be at least this long. Laboratory data on atom-radical reactions is sparse, with a considerable amount of data available only for methyl radical reactions. There is ,however, much published information on decomposition pathways of radicals, including those containing oxygen, and these allow deductions to be made on probable reaction paths.

$$O + R \rightarrow [RO]^* \rightarrow \text{products.}$$

As Huie and Herron point out, however, even in the case of thermal $O(^3P)$ the produced radicals are most probably excited, and other pathways become energetically possible.

The situation is further complicated in the present case if 5 eV kinetic energy is available (though this may not be the case; see conclusion). Also there is a greatly increased possibility of de-excitation of various species at the solid surface. Thus, although a good deal of data exists on reaction pathways of free-radicals with oxygen atoms, the number of possibilities for reaction with polymeric surfaces is so large that elucidation of actual reaction pathways needs experimental measurement *in situ* of chemical species present on the surface and mass spectrometric measurement of product composition and energy. A number of general conclusions can be drawn from the extensive literature on rates of reaction with $O(^3P)$. Some of these are:

- The attack of $O(^3P)$ on carbon compounds is electrophillic in nature.

- For alkanes, secondary hydrogen atoms are 10 to 20 times more likely to be abstracted than primary hydrogen atoms.

- Results for $O(^3P)$ reactions with substituted benzenes show this electrophilic nature, with rate constants varying 2 orders of magnitude from $C_6H_3(CH_3)_3$ to C_6H_5F and $C_6H_5CF_3$.

These conclusions are modified in the case of $O(^1D)$ reactions and may also not be valid with 5 eV $O(^3P)$.

4.5 Conclusions

Activation energies have been measured for 5 eV $O(^3P)$ reactions with solid polymer and carbon surfaces in orbit in the range 4-7 kJ mole^{-1} These are similar in magnitude to those observed in a variety of reactions of thermal $O(^3P)$ with organic compounds. This fact would be consistent with a model in which the rate-controlling step in the reactions of 5 eV oxygen atoms with solid organic surfaces actually involved thermalized O atoms bound at the surface, perhaps in a mobile precursor state. This is also consistent with a measurement of the angular distribution of 5 eV oxygen atoms scattered from a carbon surface,[11] which showed almost (but not quite) complete energy accommodation. The present authors have also shown, however, that the absolute rate of the reaction of 5 eV atoms with carbon surfaces is several times that of thermal atoms. This dependency of rate on kinetic energy only applied, according to this model, to the adsorption step of oxygen into the precursor state. The actual reaction with the organic moiety in the surface to form products may not need to consider the inclusion of 5 eV of excitation energy that has already been dissipated. The following reaction sequence is postulated:

activated adsorption	$O\ (fast) + S \rightarrow O_s^*$
dexcitation	$O_s^* + S \rightarrow O_s + S$
re-emission	$O_s \rightarrow O_g$
reaction	$O_s + RH \rightarrow [RHO]^*$
	$[RHO]^* \rightarrow$ products

This conclusion means that the extensive data on thermal $O(^3P)$ reactions may be useful (in so far as gas-phase reactions may be correlated with surface reactions) in interpreting surface reactions of $O(^3P)$ at 5 eV.

It should be noted that this does not apply to gas-phase reactions of oxygen atoms with molecules surrounding the Shuttle Orbiter which have been postulated to give rise to the extended Shuttle glow[12]. In this case, intermediates and products will be produced in high energy electronic and vibrational states.

4.7 References

1. Gregory, J. C., and P. N. Peters, "The Interaction of Atomic Oxygen with Solid Surfaces at Orbital Altitudes," experiment proposal to NASA, Langley Research Center, June 1975; see also, "The Long Duration Exposure Facility (LDEF) Mission One Experiments," NASA SP-473, p. 14, NASA Headquarters (1984).

2. Lundquist, C. A., "Skylab's Astronomy and Space Sciences," NASA SP-404, p. 107 (1979).

3. Peters, P. N., Gregory, J. C., and Swann, J., *Applied Optics* 25, 1290, (1986).

4. Leger, L. J., Visentine, J. T., and Kuminecz, J. F., AIAA Paper No. 84-9548, January (1984).

5. Whitaker, A. F., et al, AIAA paper 85-0415, (1985).

6. Hansen, R. H., Pascale,J. V., Benedictis, T., and Renzepis, P. M., *J. Polymer Sci:PtA, 3,* 2205, (1965). 183, (1984).

7. Cvetanovic and Singleton, *Rev. of Chem. Intermed. 5,* 183, (1984).

8. Huie, R. E., and Herron, J. H., *Prog. React. Kin. 8,* (l), p. 1-80, (1975).

9. Ung, A. Y-M., and Schiff, H. I., *Can J. Chem, 40,* 486, (1962).

10. Cvetanovic, R. J., *Advan. Photochem.I,* 115, (1963).

11. Gregory, J. C., and Peters, P. N., *Rarefied Gas Dynamics 15,* 644, (1986).

12. Gregory, J. C., and Peters, P. N., *Second Workshop on Spacecraft Glow,* NASA CP-2391, p. 174, (1985).

4.6 Acknowledgements

The authors are indebted to Ms. Alice Dorries, NASA, MSFC for the electron micrograph. At UAH, the work was supported by Martin Marietta Corp., NASA and the Alabama-NSF EPSCoR program.

5.0 EFFECTS ON ADVANCED MATERIALS: RESULTS OF THE STS-8 EOIM EXPERIMENT*

M. J. Meshishnek, W. K. Stuckey
J. S. Evangelides, L. A. Feldman, and R. V. Peterson
Materials Sciences Laboratory

and

G. S. Arnold and D. R. Peplinski
Chemistry and Physics Laboratory
The Aerospace Corporation
El Segundo, CA 90245

Abstract

A variety of metals was exposed to the low Earth orbit space environment on Shuttle flight STS-8 as a part of NASA's "Effects of Oxygen Atoms Interaction with Materials" experiment. These materials included carbon filters and graphites, infrared optical materials, organic and metal films, Kevlar and fiberglass fabric, and high-temperature coatings. The effects noted on these materials included oxidative erosion of the carbon and graphite, loss of tensile strength for the Kevlar fabric, erosion and oxidation of organic films, partial oxidation of infrared optical materials, and loss of reflectance for the high-temperature coatings.

5.1 Introduction

The Aerospace Corporation participated in the National Aeronautics and Space Administration (NASA) Effects of Oxygen Interaction with Materials (EOIM) experiments on Shuttle missions STS-5 and STS-8. These experiments were designed to study the reactions of a wide variety of typical spacecraft materials with oxygen in low Earth orbit.[1] The results obtained from the STS-8 experiment will be described, along with some comparisons to previously unpublished STS-5 results.

The samples on STS-8 were contained in one of the trays provided by NASA's Langley Research Center as well as in an Aerospace-designed tray. The samples in the Langley tray are listed in Table 1. Table 2 shows the locations of the samples in the Aerospace tray. Samples A, B, and C were 1 inch in diameter; the others were 0.5 inch in diameter. Sample locations for both trays were indicated in Figs. 1a and 1b. In addition, Aerospace designed and built two additional fixtures for specific experiments. These two fixtures contained the organic and metal film experiment and the Kevlar and fiberglass experiment. (These fixtures are described in Sections III and IV, respectively.) Thus, four separate trays were the responsibility of The Aerospace Corporation in the EOIM experiment on flight STS-8.

The following technical discussion applies to those samples analyzed at Aerospace. Some of the samples in the trays were contributed by others -- Jet Propulsion Laboratory, Aerojet, Martin-Marietta -- and will be reported independently. The samples are divided into the following categories: optical materials and coatings, organic and metal films, Kevlar and fiberglass, carbon fibers and graphites, and high-temperature coatings.

5.2 Optical Materials and Coatings

5.2.1 Infrared Optical Materials

1. Sample Description

An increase in the background noise level of the Earth sensor assembly (ESA) of the DMSP spacecraft and their sister craft from the NOAA/TIROS program has been observed on orbit. This increase is consistent with a decrease of approximately 20 percent in the transmission of the objective lens of the ESA. The timing and geometry of the anomaly suggest that atomic oxygen in the atmosphere may play a role in that degradation.[2]

*Aerospace Corporation Report SD-TR-87-34, 20 July 1987

Table 1.-STS-8 Aerospace Disk Specimens (Langley Research Center Holder Assembly, Tray 2)

Specimen	Quantity	Location
graphite/Mg	1	1-1
bare graphite coating	1	1-2
pyrolytic graphite ("a" face)	1	1-3
Ir on Mo	1	1-4
Mo (polished)	1	1-5
Be	1	1-6
graphite/Mg/Ti	1	2-1
siloxane-treated graphite coating	1	2-2
black epoxy paint on A1	1	2-3
black Rh on Mo	1	2-4
sputtered black Rh	1	2-5
Ti ("tiodized")	1	2-6
Flamemaster S1023 on A1	1	3-1
IR optics	1	3-2
Ti 6-4 ("tiodized")	1	3-3
Ir foil	1	3-4
M-diethynyl-benzene + ethynyl-benzene (1:1)	1	3-5
Kevlar (up)/Ag (down)	1	4-1
IR optics	1	4-2
Z306 on Kapton	1	4-3
Rh foil	1	4-4
Mg foil AZ61A	1	4-5
Total	22	

Table 2.-STS-8 Aerospace EOIM Disk Specimens

Specimen	Quantity	Location
ITO/Kapton composite	1	A
SAS on A1	1	B
black Kapton	1	C
ZnO	1	D
AG	1	E
pyrolytic graphite ("c" face)	1	F
fibers (HM 3000/Kevlar/ low-temperature PAN/KGF 200/mesophase pitch/T300)	1	G
AXF-5Q-POCO graphite	1	H
silicone	1	I
Total	9	

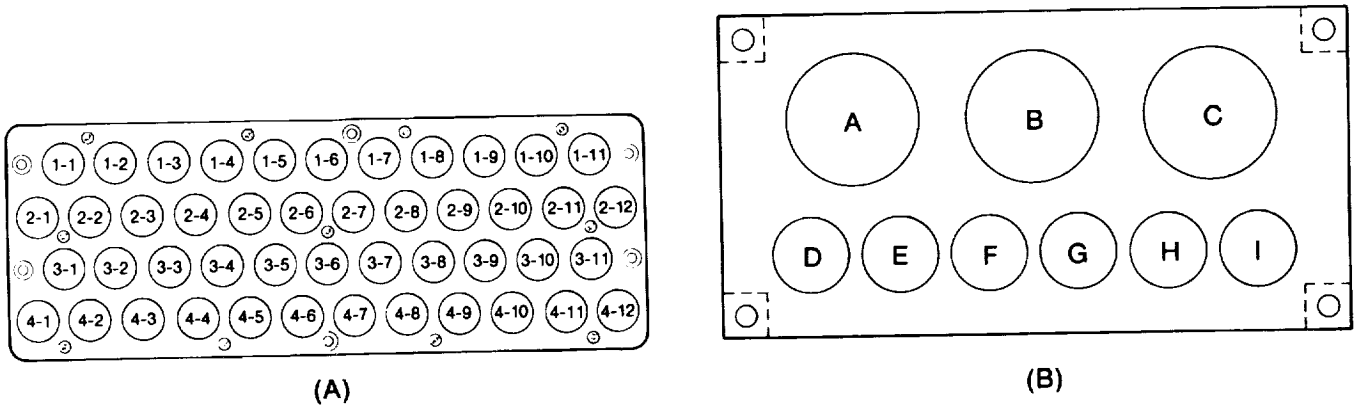

Figure 1.- STS-8 Specimen Identification Format. (a) Langley Research Center disk holders. (b) Aerospace tray.

To investigate the role of atomic oxygen (O) in the DMSP ESA offset anomaly, samples of coated infrared optical materials were flown on both the STS-5 and STS-8 EOIM experiments. These samples are described in Table 3.

Samples on the STS-5 experiment were flown in duplicate, one in the "up" (exposed) position and one in the "down" (unexposed) position. Only one exposed sample each was flown on STS-8.

2. Experimental Procedure

a. Chemical Composition. Postflight measurements of the surface chemical composition of the disks were made by x-ray photoelectron spectroscopy (XPS) using a McPherson ESCA-36 spectrometer. The chemical depth profiles of two of the STS-5 samples were measured with a Physical Electronics model 590 scanning Auger microprobe equipped with a 5-kV argon-ion sputtering beam.

b. Infrared (IR) Transmission. IR transmission spectra of the disks from 2 to 20 μm were measured with a Nicolet MX-1 Fourier transform infrared (FTIR) spectrophotometer having a beam diameter of 7 mm. Pre- and postflight measurements of the STS-8 samples were performed, and transmission spectra of the STS-5 samples were compared to those of replicate samples maintained in the laboratory.

3. Results

a. Chemical Composition. XPS measurements revealed that all of the flight samples with ZnS coatings were partially oxidized, although the "up" sample from STS-5 was more heavily oxidized than the "down" sample. In each of these samples less sulfur (S) was present than in the laboratory control sample. Comparison of the intensity ratios of O and S to zinc (Zn) as zinc oxide (ZnO) and zinc sulfide (ZnS) showed that the stoichiometry of the samples changes as a function of O-atom exposure. The ZnS found in the exposed and unexposed samples was sulfur deficient compared to that in the laboratory sample; the ZnO was more oxygen rich. Chemical depth-profile measurements of the "up" ZnS sample showed a ZnS layer of approximately 2 μm, with an initial intermixed oxide layer of approximately 20 nm. Surface contaminants of carbon (C) and chlorine (Cl) were also observed.

The XPS results for the STS-8 ZnS samples differed from those for the STS-5 samples. ZnS was less completely oxidized, appearing as a $ZnSO_4$ layer -4 A thick, or as a 0.4:1 mixture of $ZnSO_4$ and ZnS in the 30-A sampling depth of the instrument. This result is surprising, inasmuch as the fluence in the STS-8 exposure was approximately three times as great as that on the earlier flight.

Table 3.-Infrared Optical Material Samples

Sample No.	Flight	Substrate	Coating
A51A	STS-5	germanium	MLAR,* with ZnS as its outermost coating
A51B	STS-5	germanium	MLAR,* with ThF_4 as its outermost coating
A51C	STS-5	silicon	MLAR,* with SiO_x as its outermost coating
3-2	STS-8	germanium	same as 51B
4-2	STS-8	germanium	ZnS, 1/4-wave optical thickness at 15 μm

*Multilayer antireflection coating

XPS measurements of thorium fluoride (ThF_4)-coated samples from both flights showed that exposed samples were oxidized. A layer of thorium dioxide (ThO_2) 10 A thick, or a 1:1 mixture of ThO_2 and ThF_4 throughout the sampled depth of 30 A, was formed. In the STS-5 samples, the relative amount of F with respect to Th present as ThF_4 remained constant: ThO_2 replaced some of the ThF_4, but the fluoride remained stoichiometric. This was unlike the case for ZnS, where the ZnS in the flown samples was sulfur deficient compared to that in the laboratory samples. The STS-8 sample exhibited higher oxygen content than did the STS-5 sample, which is qualitatively consistent with the higher fluence on the later flight. No oxidation was observed on the unexposed STS-5 sample. The chemical depth profile of the STS-5 ThF_4 "up" sample revealed a multilayer structure, including ThF_4 layers. Carbon and oxygen were interspersed throughout the multilayer structure, suggesting that they may have been incorporated in the manufacturing process.

b. Infrared Transmission. No significant changes in the infrared transmission of any of the ThF_4-or ZnS-coated samples were observed. A slight decrease in transmission of the SiO_x-coated samples (compared to a laboratory control sample) was measured.

4. Discussion

Oxidation of the ZnS on the flight samples is not a surprising result, inasmuch as the high-temperature oxidation of ZnS in air is a well-known process.[3] However, since the infrared transmission spectra of ZnO and ZnS exhibit only subtle differences in the midwavelength IR, one would not expect the thin oxide layer formed to produce a significant change in the coating absorbance.

The result, that the STS-5 "up" and STS-8 ThF4 samples were oxidized while the STS-5 "down" sample was not, is intuitively satisfying. Assuming that oxidation proceeds via the reaction

$$ThF_{4(s)} + 2O_{(g)} + ThO_{2(s)} + 2F_{2(g)}$$

one might expect the process to be endothermic by as much as 2.9 eV. However, if one includes the additional translational energy of the incident atomic oxygen in the accounting, the process can be exothermic by more than 7 eV. Indeed, the lack of oxidation of the ThF_4 "down" sample (when other "down" samples of silver and ZnS were oxidized) lends some credence to the notion that the initial translational energy of the atomic oxygen is effective in promoting the oxidation of ThF_4. However, this is thin evidence on which to base a firm conclusion.

The surface analysis of the SiOx samples provided no explanation of the apparent decrease in transmission of these materials. They were, however, located nearest to the 250°F tray on the STS-5 experiment. It is possible that some contamination was produced by the hot tray, although the infrared spectra neither confirm nor deny this notion. Since transmission spectra of the STS-5 samples were compared to laboratory control samples rather than to preflight measurements, the possibility of systematic error must be admitted. Otherwise, the origin of this apparent transmission loss remains unclear.

5.4.2 Indium Oxide and Indium Tin Oxide

Conductive, transparent coatings of indium tin oxide (ITO) are normally applied to spacecraft surfaces to inhibit charging. Three types of samples with ITO or indium oxide (In_2O_3) coatings were included: (1) silica disks with 200, 400, and 600-A-thick coatings of ITO; (2) an In_2O_3-coated second surface mirror, or optical solar reflector (OSR), from Optical Coating Laboratories, Inc.; and (3) six strips of ITO-coated Kapton film (maintained at three different temperatures).

The van der Pauw technique[4] was used to measure the electrical properties of Hall resistivity, carrier density, and Hall mobility of the ITO-coated disks and the OSR before and after flight. No changes in these properties were observed for any of the samples.

Optical constants and coating thicknesses of the ITO-coated disks were measured by ellipsometry before and after flight. No changes were observed.

The specular reflectivity of the OSR after flight was measured in the range of 200 to 800 nm (using a Cary 17 spectrometer), and from 2 to 25 μm (using a Nicolet MX-1 Fourier transform infrared spectrophotometer). No differences in reflected intensity or in the spectral shape of the reflectivity were discernible among the two flight samples and a number of laboratory control samples.

To examine the ITO-coated Kapton films for changes in mass, 0.9-in.-diam disks punched from the samples were weighed. Comparison of the measured masses of the flight samples to those of disks punched from material kept in the laboratory showed no change in the masses of the films.

Taken together, these measurements lead to the conclusion that ITO films are not affected by the low Earth orbit atmosphere; furthermore, they indicate that ITO coating of Kapton will inhibit its erosion by atmospheric atomic oxygen. One caveat must accompany this conclusion: laboratory studies show that the heating of conductive ITO coatings above 200°C in air results in their complete loss of conductivity. One expects that the heating of ITO in the oxidizing atmosphere of low Earth orbit would produce a similar result.

5.4.3 Polished Nickel Mirror

Observations of the surface erosion of a variety of materials raised the concern that the reflective surfaces used to line sunshields on orbital sensors might be affected in such a way as to increase scatter, or nonspecular reflection. Four samples of polished, chemically deposited ("electroless") nickel, supplied by Westinghouse Electric Corporation (WEC), were flown on STS-5. Sample 1 was mounted in position A53-C-UP; sample 2 was mounted in position A53-C-DOWN. Samples 3 and 4 were kept as laboratory controls.

Measurements of the scatter of the mirrors, as quantified by the bidirectional reflectance distribution function (BRDF), were made by WEC on all four disks, both before and after the flight exposure of samples 1 and 2. The light source used in their measurements was a 5-mW helium-neon laser (6328 A). The angle of incidence of the laser beam on the samples was 10° from normal.[5]

Table 4 shows the results of postflight measurements of the BRDF value at a 20° angle of incidence. Changes in samples 3 and 4 are subjective, because the substrates were not flat enough for a reliable measurement.[6]

Visual observation under high-intensity illumination supports the results in Table 5. Low-magnification electron micrographs clearly show differences between the exposed the unexposed areas of the sample.

Table 4.-Postflight BRDF Summary

Sample No.	Location	Preflight BRDF, 20° [W/W-Sr]	Postflight Increase (Decrease) at 20°
1	up	1.3×10^{-4}	6.4/1
2	down	1.5×10^{-4}	17/1
3	control	4.8×10^{-4}	2/1
4	control	7.1×10^{-4}	(2/1)

Table 5.-Materials and Results of Organic Thin Films

Sample	Thickness, mil	Result
Kapton sheet	0.5	eroded/pitted through
Apiezon L grease	0.1 - 0.2	removed
McGhan-Nusil G-9042 silicone grease*	1 - 2	oxidized and darkened
Epon 1001 epoxy**	0.2 - 0.3	eroded through

* The ZnO pigment was removed by filtration prior to coating.
** Cured with BDMA (benzyl dimenthylamine).

The surfaces of the nickel mirrors were chemically analyzed by x-ray photoelectron spectroscopy (XPS). The nickel XPS spectra of flight samples 1 and 2 show the presence of only oxidized nickel, while the spectra of laboratory samples 3 and 4 contain signals for both oxidized and metallic nickel. The oxide layer on the flight samples is thus thicker than that on the laboratory samples, since the substrate metallic-nickel signal is not visible in the spectra. Given the escape depth of the electrons involved in the analysis and the geometry of the spectrometer, one can estimate that the oxide on the laboratory samples is on the order of 10 A thick; on

the other hand, the oxide on the flight samples is more than 30 A thick, which is the sampling depth of the spectrometer.

This experiment has shown that the exposure of polished electroless nickel reflectors to the low Earth orbit atmosphere results in a significant degradation in performance, as measured by the BRDF of the surfaces. Surface analysis by x-ray photoelectron spectroscopy indicates that this degradation is the result of oxidation of the surface by the ambient atmosphere. It is of particular significance that the sample that was nominally shielded from direct atmospheric impingement showed a larger effect as measured by both XPS and BRDF. This is consistent with the observation that silver foils, flown on tray A53, showed more extensive oxidation on the "down" sample than on the "up" sample. This result shows that significant oxidation of the nickel surface can occur from atomic oxygen that has struck one or more spacecraft surfaces before reaching the nickel.

5.3 Organic and Metal Films

The purpose of this experiment was to determine the effects on organic and metallic films of exposure to atomic oxygen in low Earth orbit. The potential of atomic oxygen impingement to remove contaminants by an accelerated oxidative process, and the possibility of contaminants being transferred to other surfaces via reactive chemical sputtering are two important mechanisms of contamination. This experiment was designed to measure simultaneously the degradation of various organic films as well as to detect sputtered material from these films by using Fourier transform infrared (FTIR) spectroscopy. Metal films were analyzed by nuclear backscatter and ion microprobe mass analysis (IMMA) to study effects of exposure to atomic oxygen as well as of possible metal atom sputtering.

5.3.1. Experimental Procedure

This experiment used a special fixture, a tray designed by Aerospace. Figure 2a is a photograph of the assembled tray with the cover removed, and Fig. 2b is a schematic of this fixture showing how the films were layed out. A schematic showing how the tray functions is presented in Figs. 3a and 3b, for organic and metal films, respectively.

A beam of atomic oxygen, collimated by slits in the tray cover, impinges on a germanium FTIR plate that contains a film. Close to the sample is another FTIR plate used to catch any sputtered material. Four of these sample-witness plate pairs (Figs. 2a and 2b, foreground) were used, and they occupied one half of the fixture. The other half of the fixture (Figs. 2a and 2b, background) contained the metal film experiment, wherein an oxygen beam, collimated by slits in the tray cover, strikes metal film targets and sputters metal atoms to the side collectors; here three such assemblies were used.

The organic films, prepared by the use of solvent airbrush techniques, were a hydrocarbon grease, a methyl silicone grease, and an epoxy. Kapton was a commercial film material. The identification and thickness ranges of these materials are presented in Table 5. The metal films used were gold, aluminum, and silver; these were vacuum deposited to a thickness of 1000 A. In addition to this experiment, thicker silver foils were

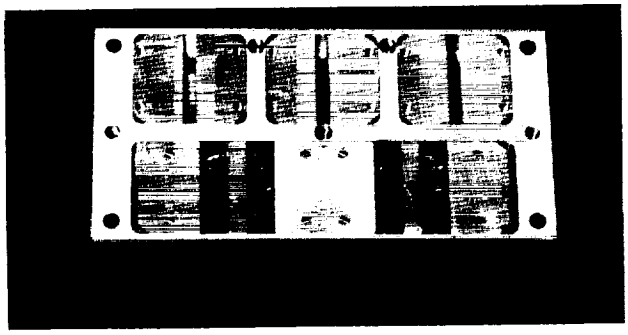

(A)

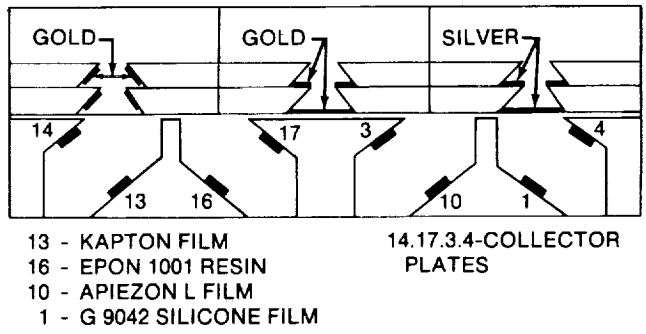

(B)

Figure 2.- The Aerospace Organic and Metallic Thin-Films Tray. (a) Photograph of the tray with the collimating cover removed. (b) Cross-sectional schematic of the sample layout.

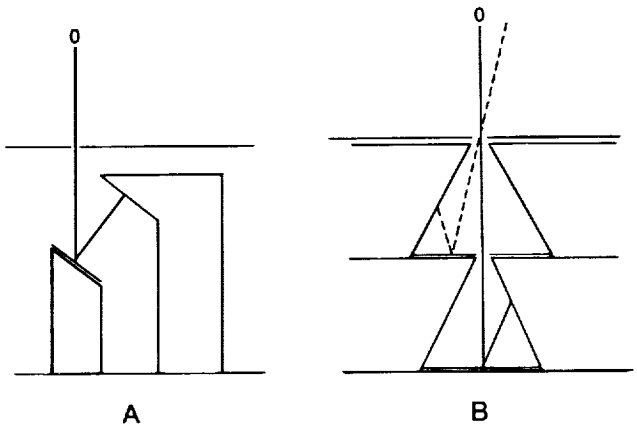

Figure 3.- Schematic of Tray Function.
(a) Organic Film configuration.
(b) Metal film configuration

also placed in the Aerospace sample tray at location E (see Fig. 1b) for comparison with the results of this metal-sputtering experiment as well as with the results obtained from STS-5 with respect to oxide formation on silver foils.

5.3.2 Results

The initial analysis of the metal film collectors using nuclear backscatter indicated that roughly a monolayer ($10^{15}/cm^2$) of both gold and silver had been transferred to the side collectors from their respective targets. However, closer examination indicated that this layer was present on all faces of the collectors and was therefore the result of poor or inefficient masking of the parts during the metal coating process. Aluminum could not be detected on the collector because of background noise. Control samples run through the metal coating process showed the same contamination on their unexposed faces.

Interestingly, the silver target showed intense color changes as a result of exposure to oxygen. A dark-brown pattern was present at the point of maximum impingement and changed to a dark green; outward from the center, several different shades were observed. No unique oxide could be identified by ion microprobe mass analysis (IMMA) or x-ray analysis. Silver-coated collectors showed dark-brown areas, indicating that a large amount of oxygen atom reflection had occurred.

For the organic films the results are fairly clear. The 0.5-mil Kapton sample showed severe degradation and pitting. The FTIR spectra of protected and exposed areas show changes in the intensity ratios of the various bands. The 0.2-mil Apiezon film was essentially destroyed; FTIR spectra indicate that very little of the film remained. The 0.2-mil epoxy film was similarly degraded, as seen both visibly and by FTIR. The 1-mil film of methyl silicone grease was visibly intact, but darkened. However, FTIR analysis of the surface indicated that almost all of the hydrocarbon backbone had been removed, and the remaining material was oxidized to a silicate. The FTIR spectra are shown in Figs. 4 through 15. Spectra were obtained by using both the attenuated total reflectance (ATR) and transmission modes for each sample. The most relevant spectra are presented for each sample.

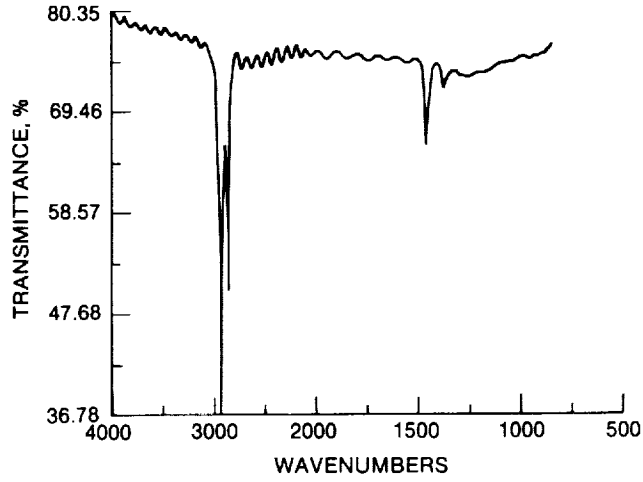

Figure 4.- FTIR Spectrum of Organic Thin Films: Preflight Apiezon (ATR Mode)

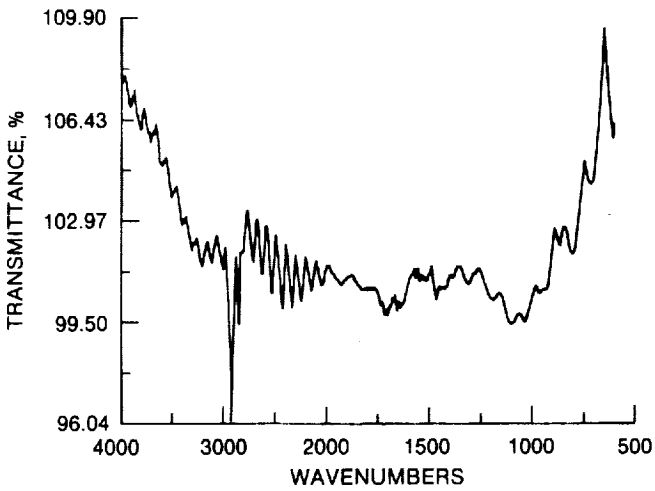

Figure 5.- FTIR Spectrum of Organic Thin Films: Postflight Apiezon (ATR Mode)

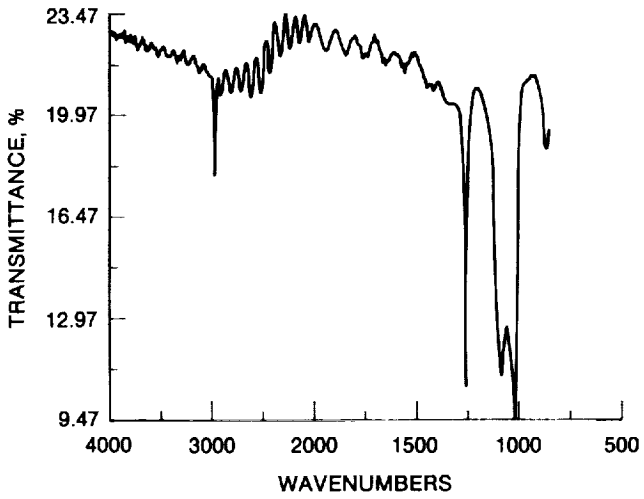

Figure 6.- FTIR Spectrum of Organic Thin Films: Postflight Silicone (ATR Mode)

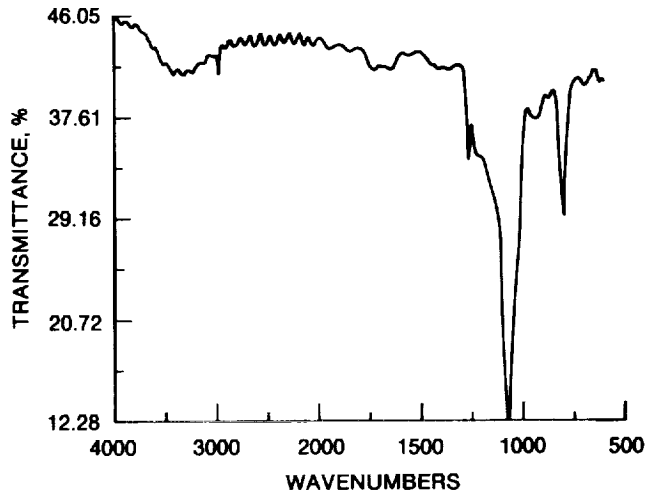

Figure 7.- FTIR Spectrum of Organic Thin Films: Postflight Silicone (ATR Mode)

The collector plates do not lend themselves to such obvious interpretation. Material has been collected on at least three, and possibly all, of the plates. The amounts of material are very small and the FTIR spectra obtained are quite noisy. The plates opposite the Apiezon and methyl silicone grease samples had identical spectra. Very little, if any, material seems to have been collected opposite the Kapton and epoxy.

These silver samples were 99.97% pure in the form of foils 0.0127 mm thick. Identical samples were flown facing up and facing down, about one-half inch above the mounting plate for the experiment; these were identical to the silver foils also flown in the very same tray on STS-5. Three other silver samples, attached to the temperature-controlled film trays on STS-5, were also analyzed.

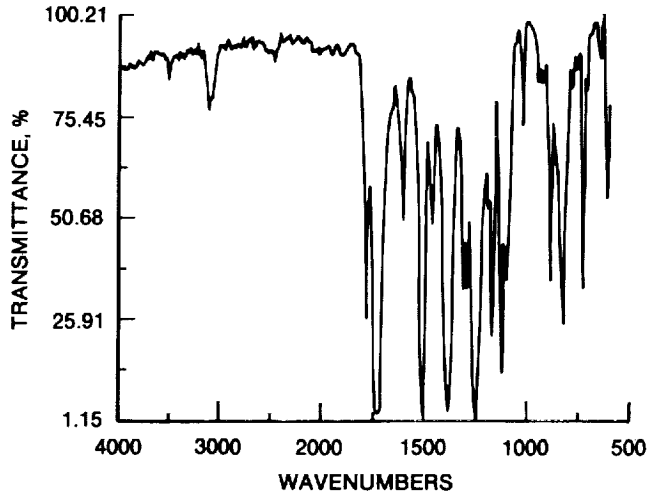

Figure 8.- FTIR Spectrum of Organic Thin Films: Kapton, Exposed Area (Transmission Mode)

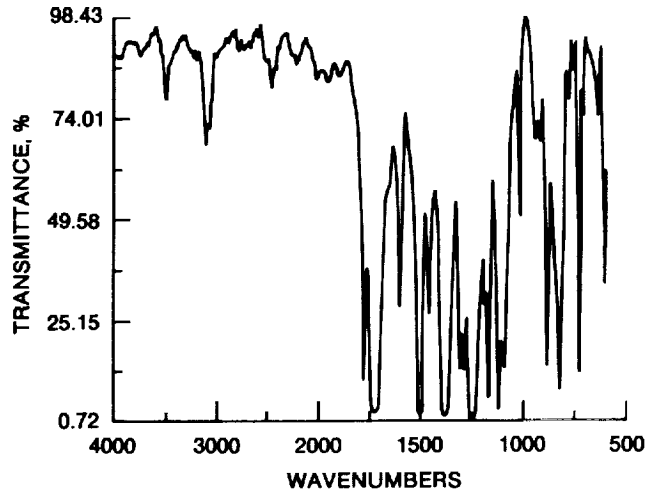

Figure 9.- FTIR Spectrum of Thin Films: Kapton, Masked Area (Transmission Mode)

Results from STS-8 are shown in Table 6, along with the results previously obtained on STS-5 for comparison. Each result is an average of three depth profiles taken with an ion microprobe mass analyzer (IMMA). A typical profile for an "up" sample is shown in Fig. 16. The "down" samples did not generally show as sharp a step between the oxide and the silver but instead a more gentle drop in concentration, one consistent with more diffusion into the sample. On some samples the oxygen

persisted to depths of over 3000 A. The thicknesses in all cases were taken at the 50% intensity point on the profile. The oxide thickness is greater on the STS-8 sample, but the thickness is obviously not linear with oxygen atom fluence in this range of fluences. The downfacing samples are thicker in both cases; this is apparently caused by their reaction with oxygen atoms -- not from direct impingement along the velocity vector, but from scattering, reflection, or other unknown processes. Depth profiles taken in those areas of the silver foil masked from exposure to atomic oxygen showed less than 140 A of native oxide thickness.

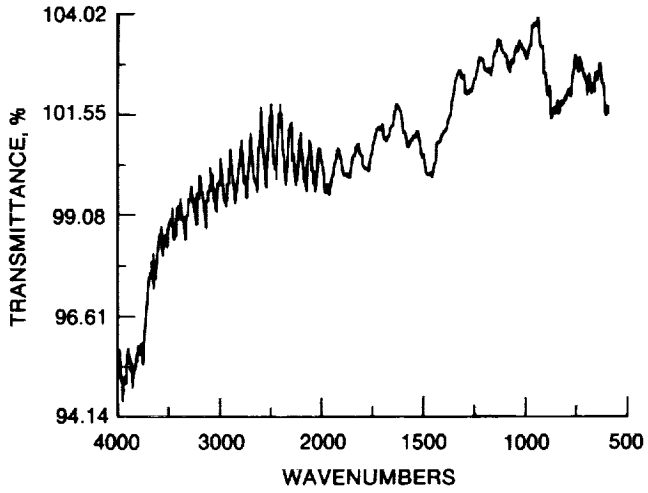

Figure 10.- FTIR Spectrum of Organic Thin Films: Epoxy, Exposed Area (Transmission Mode)

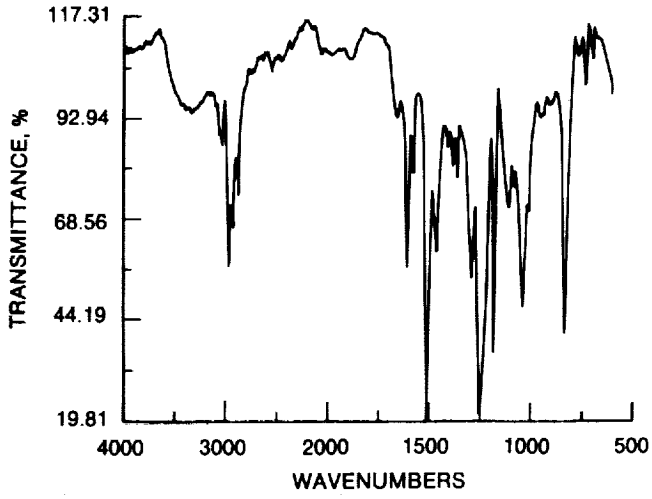

Figure 11.- FTIR Spectrum of Organic Thin Films: Epoxy, Masked Area (Transmission Mode)

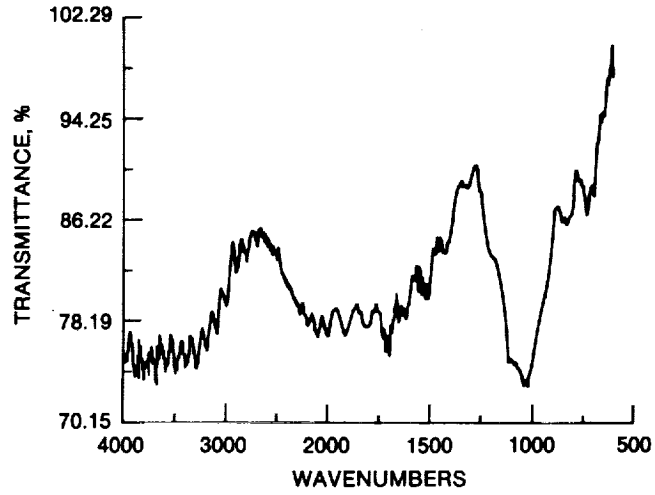

Figure 12.- FTIR Spectrum of Collector Plates: Silicone Collector Plate (ATR Mode)

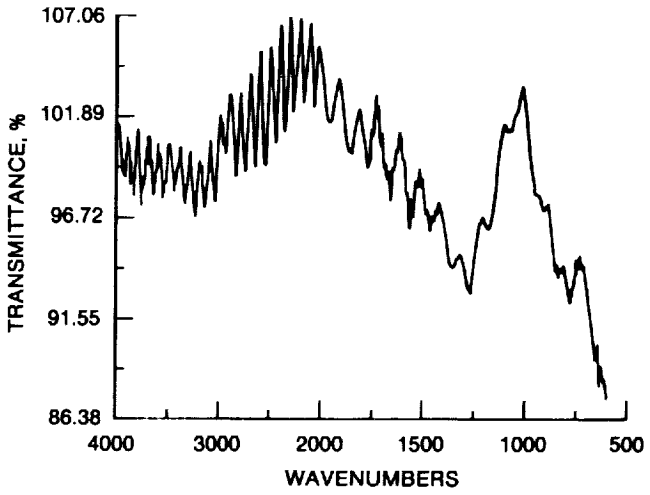

Figure 13.- FTIR Spectrum of Collector Plates: Kapton Collector Plate (ATR Mode)

5.3.3 Conclusions

Metal sputtering, if it occurs at all, must have a yield of less than 10^{-5}. With respect to metal film stability, only the silver showed a tendency to oxidize. From both experiments, oxidation of the silver-coated specimens indicates that oxygen atom reflection is a significant phenomenon.

From the organic and metal film experiment it appears that hydrocarbon contamination can be removed by atomic oxygen impingement, although silicone contamination will not be removed but will be altered and darkened by this exposure. Epoxies

and Kapton will be eroded by atomic oxygen exposure. Material sputtered or transferred to another surface by atomic oxygen impingement was not observed. The nature of the contamination on the collector witness plates is unknown, but it would seem to be silicone related. The possibility that contaminants can be removed by reflected atomic oxygen cannot be dismissed; such removal may in fact be a significant mechanism by which materials are oxidized.

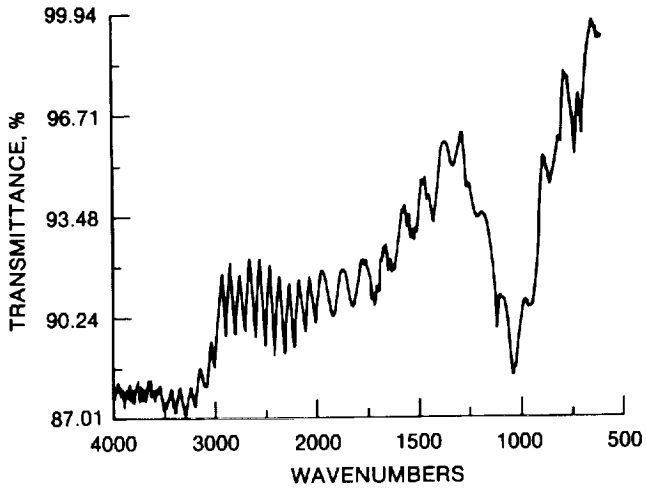

Figure 14.- FTIR Spectrum of Collector Plates: Apiezon Collector Plate (ATR Mode)

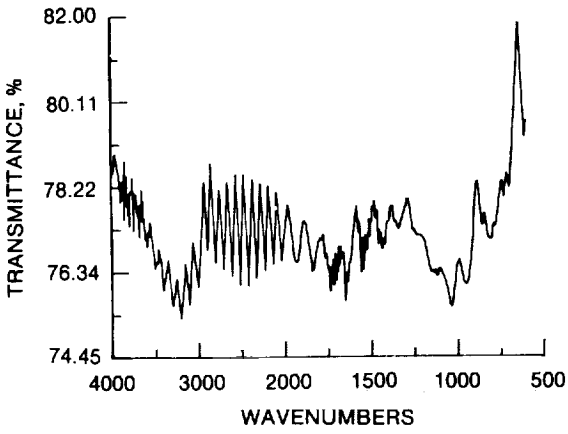

Figure 15.- FTIR Spectrum of Collector Plates: Epoxy Collector Plate (ATR Mode)

Table 6.-Thickness of Oxide Film on Silver

Sample	Thickness, A	
STS-5:	Up	Down
A53	850	1060
2-75-7A	2900	1500
1-250-7A	2200	2600
2-250-7A	1700	2600
STS-8:		
E	1100	2100

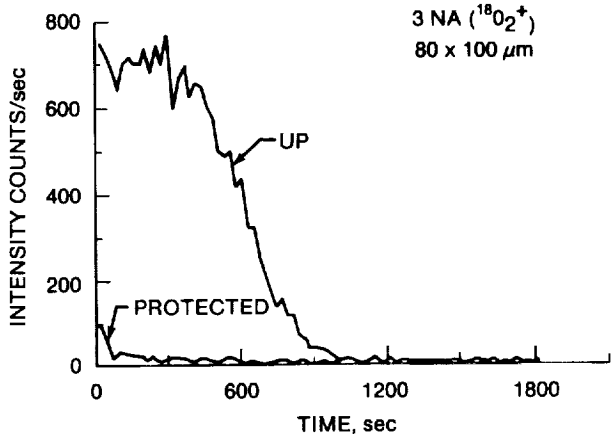

Figure 16.- Typical IMMA ^{16}O Depth Profile for an "Up" Sample of Silver

5.4 STS-8 Kevlar and Fiberglass Samples

5.4.1 Experimental Procedure

Samples of plain, square-weave Kevlar 29 were placed in two locations in the EOIM experiment. A 1-in.-diam piece was inserted into the Langley disc sample tray (Fig. 1a), while a fourth tray, an

Aerospace-fabricated aluminum holding fixture, housed a sample approximately 7 1/2 × 4 inches The Aerospace tray, 4 × 9 inches × 1 inch deep (see Fig. 17), also held a fiberglass sample (exposed) and O-atom-protected Kevlar and fiberglass samples on the back of the aluminum frame. The large Kevlar sample was held in the Aerospace tray at three different angles to the incident O-atom flux: at normal, 45°, and 60°. The fiberglass sample was positioned normal to the incident flux. Kapton tape was placed around the edges of the Kevlar and fiberglass samples to prevent the fabric from unraveling.

The purpose of mounting the Kevlar at different angles to the incident flux was to obtain different levels of O-atom exposure, thereby also obtaining physical-spectrophotometric properties as a function of dose for the Kevlar.

The two major concerns for the fabric were changes in mechanical strength and optical properties of the material as a result of O-atom exposure. Several analytical methods were chosen to measure any changes in mechanical strength or optical properties resulting from the O-atom environment.

5.4.4 Results

1. Macrophotography and Microscopy

The surface sheen of the 1-inch-diameter Kevlar sample was visibly dulled by O-atom exposure. The exposed areas of the Kevlar from the holding fixture were again obviously dull in appearance when compared with the unexposed areas (Fig. 18). The shiny areas were protected by the aluminum frame, as well as by Kapton tape placed around the Kevlar edges. There was no visible effect of O-atom exposure on the fiberglass sample.

Samples of the exposed and unexposed fabric were viewed with the optical stereo microscope. Again, although the dull surface of the exposed Kevlar fibers was apparent, to the eye there did not initially appear to be any breakage or erosion of fibers, and the fiberglass sample did not at first reveal any visible change as a result of exposure to the O-atom flux. However, when the exposed Kevlar fabric was viewed in the scanning electron microscope (SEM), it was obvious that the surface had been eroded. This erosion probably gives the appearance of dullness or loss of sheen to the eye. There was no apparent change to the exposed fiberglass when it was viewed in the SEM.

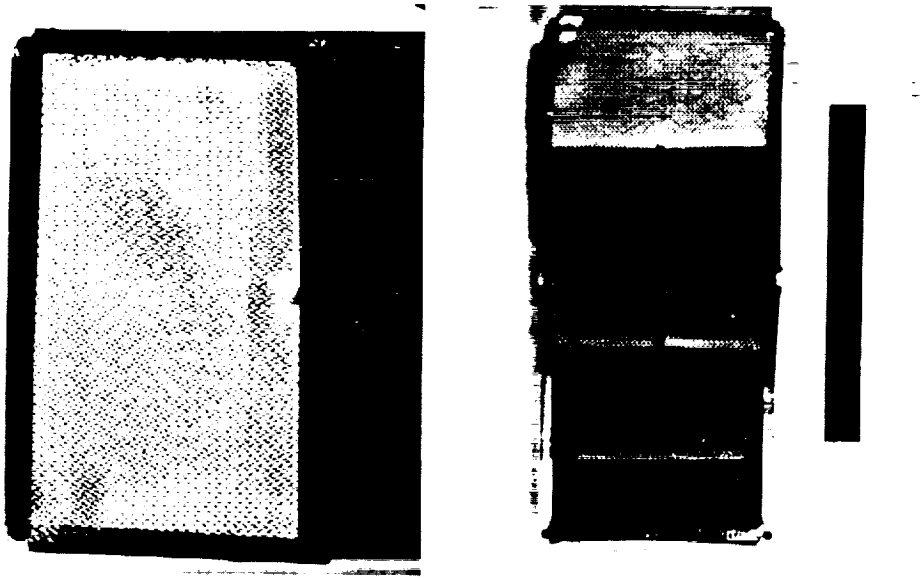

Figure 17.- Photographs of STS-8 Aerospace-Fabricated Holder for Kevlar and Fiberglass Samples (Preflight). (a) Front. (b) Back.

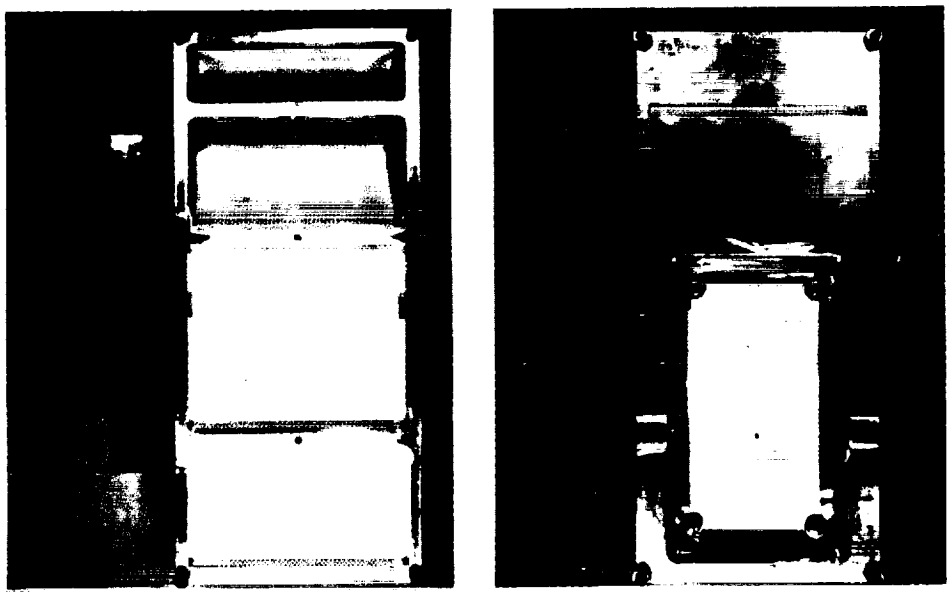

A B

Figure 18.- Photograph of Kevlar from Flight Tray 2, Showing Surface Sheen Dulled by O-Atom Exposure. (a) Exposed. (b) Unexposed.

A sample of the Kevlar fabric exposed under normal conditions was cross-sectioned and examined by means of optical and scanning electron microscopy in an attempt to see the extent of fiber damage. Most fibers on the exposed side appeared undamaged, with the possible exception of the outer surface of some of the fibers. In any case, the erosion or damage does not appear to penetrate the fiber to any significant depth.

2. Mechanical Testing

Mechanical testing of the Kevlar and fiberglass consisted of pulling samples to failure in an Instron model 1127 mechanical tester. Samples were tested from each of the three exposed areas of Kevlar and the one of fiberglass, as well as from unexposed laboratory and flight samples. Samples were mounted for testing in capstan-type holders to minimize clamping stresses. Fracture occurred at the center of the gage length in all samples.

The exposed Kevlar samples showed a 25-to-30-percent loss of strength compared with the unexposed Kevlar. The angle the Kevlar fabric made with the incident flux had little effect on the strength of the material. This was probably due to the nature of the fabric. The O-atoms strike normal to the fiber, damaging individual fibers regardless of their weave-exposure angle. Consistent with the fact that no damage could be detected via microscopy, the fiberglass sample exhibited no loss of strength as a result of the O-atom exposure.

3. Spectrometric Measurements

Specular reflectance and absorption spectra of the pre- and post-flight Kevlar and fiberglass samples were measured from 4000 to 400 cm^{-1} by means of the Nicolet MX-1 FTIR spectrophotometer. The absorption measurements were obtained on the fabric surfaces by pressing the fabric against a KRS-5 internal reflectance crystal and using the attenuated total reflectance (ATR) attachment to the FTIR. There were no significant changes in either the specular reflectance or absorption IR spectra between the exposed and unexposed samples of either the Kevlar or fiberglass.

Spectral hemispherical reflectance measurements were made with a Beckman 5240 spectrophotometer, while normal emittance values were obtained from measurements on a Gier Dunkle DB-100 spectrophotometer. The pre- and postflight solar absorptance α_s and emittance ε_N and ε_H (normal and hemispherical) values were obtained. Small changes due to O-atom exposure were noted in the absorptance and emittance values of the Kevlar. No significant changes were measured for the fiberglass sample.

5.4.4 Conclusions

The optical and mechanical properties of the Kevlar 29 fabric changed as a result of its exposure to the atomic-oxygen atmosphere at Shuttle Orbiter altitudes. The surface sheen of the Kevlar was noticeably dulled, and the solar absorptance emissivity values decreased. No spectrometric changes were observed in the exposed fiberglass.

Mechanical testing revealed a 25-to-30-percent loss of strength in the Kevlar as a result of the O-atom exposure. The mechanical test data are presented in Table 7. Scanning electron microscopy revealed that the exposed fibers were eroded, though only the outer surface of the fibers appeared to be affected. However, this erosion was presumably insufficient in itself to cause the observed loss of strength. The mechanism causing fiber weakening is not known. The FTIR did not reveal any observable molecular change in the exposed fibers.

It has been suggested that the vacuum environment in space contributed to the loss in strength of the Kevlar, although the flight control sample exposed to the same vacuum and temperature history, but not to the incident oxygen flux, exhibited only a 6 percent loss of strength. Geometry should have prevented the oxygen atoms from reaching the sample.

Since we have only the one data point from which to extrapolate, there are insufficient data to determine the rate of change of the optical or mechanical strength properties in Kevlar with O-atom dose levels.

Table 7.-STS-8 Kevlar Mechanical Testing Data

Sample*	Orientation	No. of Tests	Average Fracture Load, lb.	Breaking Strength, lb/in.	Normalized Strength, %
lab control sample	X (fill)	3	270	759	100
	Y (warp)	13	237	667	88
unexposed flight control sample	X	4	254	714	94
exposed sample (angled section at end)	X	3	202	568	75
exposed sample (angled section at center)	X	4	203	571	75
exposed sample (flat section)	X	6	187	526	69

* All samples have 8 strands.
Weave is approx. 22.5 strands/in. (warp and fill directions).
Breaking strength = $\frac{22.5}{8}$ (fracture load).

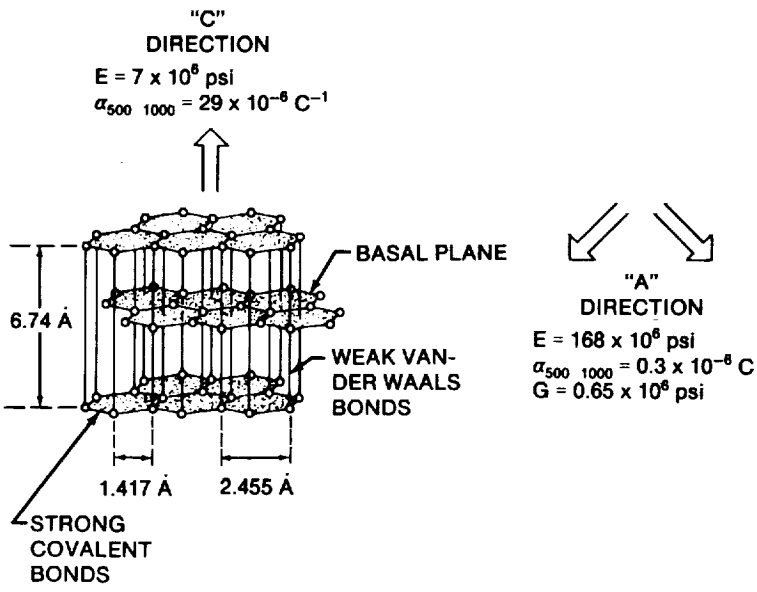

Figure 19.- Graphite Crystal Structure Showing Large Anisotropy. α is the coefficient of thermal expansion, E is the elastic modulus, and G is the shear modulus.

Table 8.-Filament Property Data

Filament	Manufacturer	Precursor	Diameter μm	Density g/cm3	Tensile Modulus, msi
KGF 200	Kureha	pitch	10	1.6	10
Thornel 300	Union Carbide	PAN	7	1.75	33
HM 3000	Hercules	PAN	8	1.83	50
VSB 32	Union Carbide	mesophase pitch	11	2.02	55
Kevlar	DuPont	polyamide	12	1.44	18
low-temp. PAN	Celanese	PAN	–	–	–

5.5 Carbon Fibers and Graphites

5.5.1 Sample Description

Carbonaceous materials were selected to ensure a meaningful representation of the range of structures and morphologies available. The large anisotropy of a single crystal of graphite is shown in Fig. 19. The materials consisted of five carbon fibers, one polymer fiber (Table 8), one bulk polycrystalline graphite, and a highly oriented pyrolitic graphite. The five carbon fibers ranged from a high-modulus, highly graphitic fiber (VSB 32) to a low-modulus, amorphous fiber (KGF 200). The one polymer-based fiber was a medium-modulus fiber having good fibril orientation. The bulk graphite was selected to represent the class of carbonaceous composites consisting of aggregates. The graphite had a bulk density of 1.86 g/cm and an open porosity of 16.7 percent, with essentially isotropic properties. Single crystals of graphite were represented by a highly oriented pyrolytic graphite.

5.5.2 Experimental Procedure

The materials were prepared for the experimental trays in a manner that would enhance the observation of microstructural and morphological changes caused by oxidation via atomic oxygen (O). All six fibers were mounted in an epoxy resin and metallographically prepared in the transverse direction.

The axial plane of the bulk graphite sample was metallographically prepared and xenon-ion etched for exposure to atomic oxygen. To bring out the orientation of the graphite basal planes of the matrix phase in these materials, the polished surface was xenon-ion etched; this was also done for the a- and c-planes of the pyrolytic graphite. If the structure of the material is not overly refined, etch lines or laminae that indicate the graphite basal plane orientation will develop (Fig. 20).

5.5.3 Results and Discussion

The changes after oxidation in the morphology and microstructure of the carbon and polymer filaments, bulk polycrystalline graphite, and pyrolytic graphite were qualitatively characterized by optical and scanning electron microscopy (SEM). However, the very slow rates of reaction for the carbonaceous materials prohibited quantification in

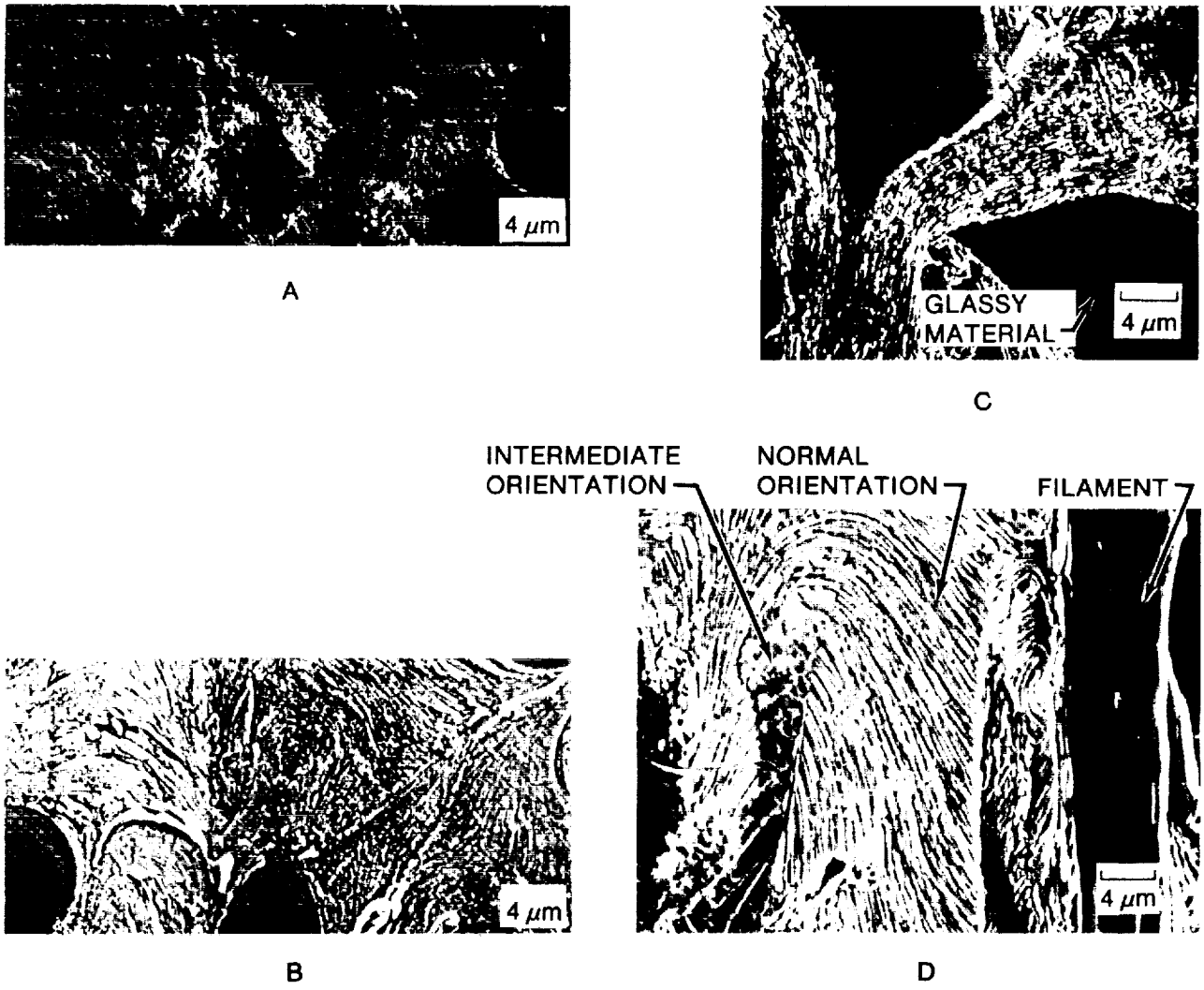

Figure 20.- Photomicrographs of Xenon-Ion Etching of Polished Surface to Enhance Viewing of Graphite Basal-Plane Orientation. (a) As polished. (b) Ion etched. (c) Phenolic resin matrix system. (d) Pitch matrix system.

this experiment. After exposure, the epoxy-based mounting compound used for the transverse sections of filament had oxidized at a faster rate than the filaments themselves, leaving the various filaments protruding above the oxidized plane of the mounting compound (Fig. 21). The changes in the filaments were a function of precursor-pitch, polyacrylonitrile (PAN), mesophase pitch, and polyamide, and the degree of graphitic order as reflected by the axial (longitudinal) tensile modulus. The carbon filament with an amorphous structure, KGF 200, appeared to have the least amount of in-depth oxidation (Fig. 22). The axial plane (transverse surface) was pitted with pores of varying shape and size which resulted from the oxidative attack of existing micropores; these micropores are present in amorphous carbons as a result of their low density, 1.6 g/cm^3, compared to the density of a single crystal of graphite, 2.25 g/cm^3.

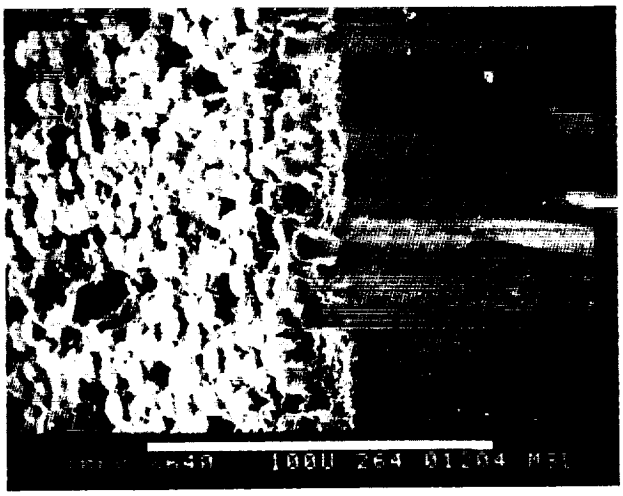

Figure 21.- Scanning Electron Micrograph of Mounted Carbon Filaments in Cross Section. Filaments protrude above oxidized plane of mounting compound.

The extent of surface and in-depth oxidation was found to decrease with increasing tensile modulus and density for the PAN-based filaments (Figs. 23 through 25). The low-temperature PAN with the lowest tensile modulus also had the greatest surface, transverse and longitudinal, and internal oxidation of the three PAN filaments. The appearance after oxidation suggests the fibril structure of PAN filaments which has been proposed by many researchers[7] (see Fig. 23). The degree and extent of oxidative attack was reduced for the filaments having an intermediate modulus (Thornel 300, Fig. 24), and even more so for the filament having a high modulus (HM 3000, Fig. 25) The Thornel 300 filament also had a fibril appearance after oxidation. However, as this structure became more refined, resolving the fibrils became more difficult because of the smaller interfibril spacing (as in the high-modulus HM 3000 filament).

Another observation of the oxidative structure of the HM 3000 filament was that resistance to oxidation of the center core of the filament was apparently higher than that of the outer annulus (Fig. 26). Under more severe conditions, with flowing air at atmospheric pressure and a temperature of $-3900°C$, the outer annulus was oxidized away, leaving the resistant center core (Fig. 27).

The post-oxidative characteristics of the transverse surface of the mesophase-pitch filament, VSB 32 (Fig. 28), were similar to those of the other high-modulus carbon filament, HM 3000. This fibril structure, which was common among the medium- and high-modulus carbon filaments, was also found in the medium-modulus filament made of Kevlar polyamide (Fig. 29). The development of this coarse fibril structure, a structure similar to that of the low-temperature PAN shown in Fig. 22, was not unexpected, considering the degree of alignment of the polymer planes required to achieve a tensile modulus of 18×10^6 psi.

Although the post-oxidative microstructural characteristics of the a- and c-planes of pyrolytic graphite were similar, the a-plane characteristics were an order of magnitude smaller. The fine conical structure after oxidation of the a-plane is shown in Fig. 30. The laminae shown in this micrograph of the a-plane clearly indicate the perpendicular orientation of the graphite basal planes to the plane of section. Micrographs of the c-plane before and after oxidation are shown in Fig. 31. Cross-sectional views of these conical features are shown in Fig. 32. The lack of a greater difference in the post-oxidative characteristics between the a- and c-planes was somewhat surprising, considering the large differences in the properties of the planes. The bulk polycrystalline graphite had microstructural features and coarse conical structures (Figs. 33 and 34) similar to those of the pyrolytic graphite. The microstructure suggested that oxidation resulted in the enlargement of micropores.

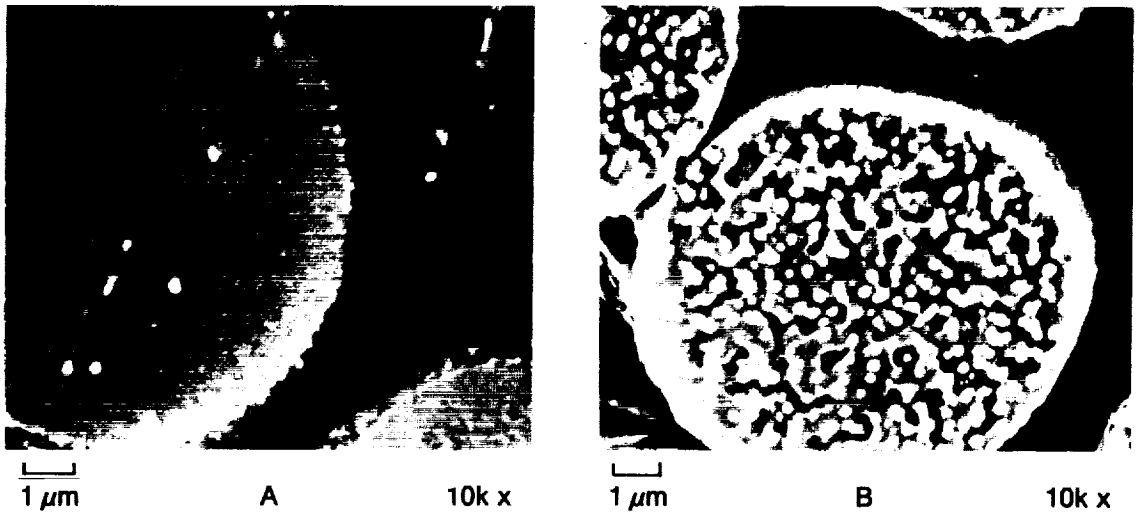

Figure 22.-Scanning Electron Micrographs of KGF 200. (a) Preflight. (b) Postflight.

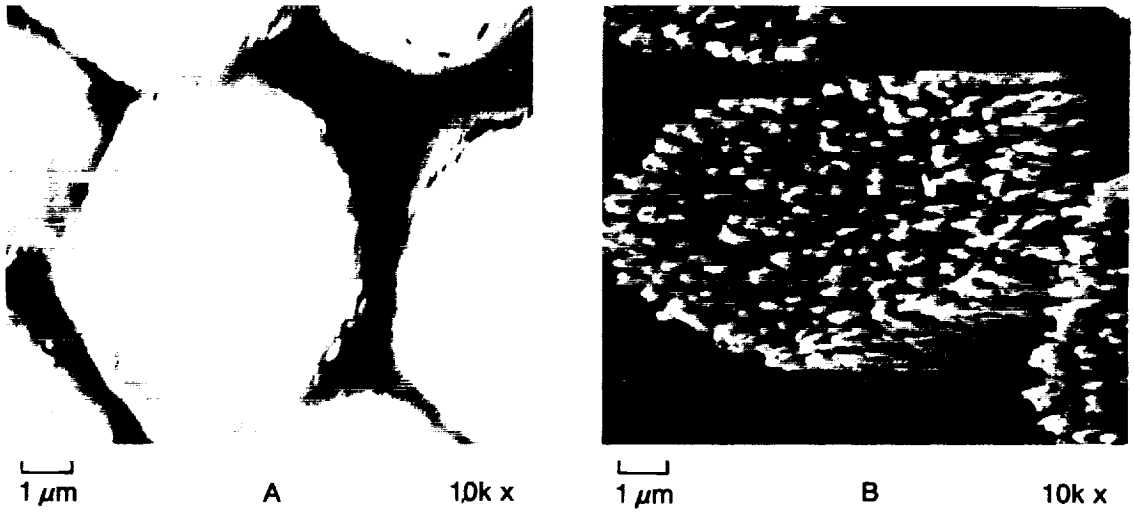

Figure 23.-Scanning Electron Micrographs of Low-Temperature PAN. (a) Preflight. (b) Postflight.

5.5.4 Summary and Conclusions

The results indicate that carbonaceous materials oxidize when exposed to atomic oxygen at the Shuttle altitude. Although reaction rates for the carbonaceous materials could not be obtained, the epoxy was found to oxidize faster than the carbon filaments. The extent of microstructural changes in the materials depended on the degree of graphitic order and on the type of precursor. Carbons with an amorphous and highly graphitic structure, the extremes in structure, were the more resistant to oxidation as determined by the qualitative observations of microstructural changes in these materials. The relative reactivities at Shuttle altitude are consistent with the relative reactivity observed from high-temperature oxidation.

5.6 High-Temperature Coatings

5.6.1 Introduction

Materials resistant to high temperatures are being developed for spacecraft applications. Coating materials and processes are necessary to provide thermo-optical properties that minimize heating caused by absorption of solar radiation, allow dissipation of heat, and also tolerate brief high-temperature excursions.

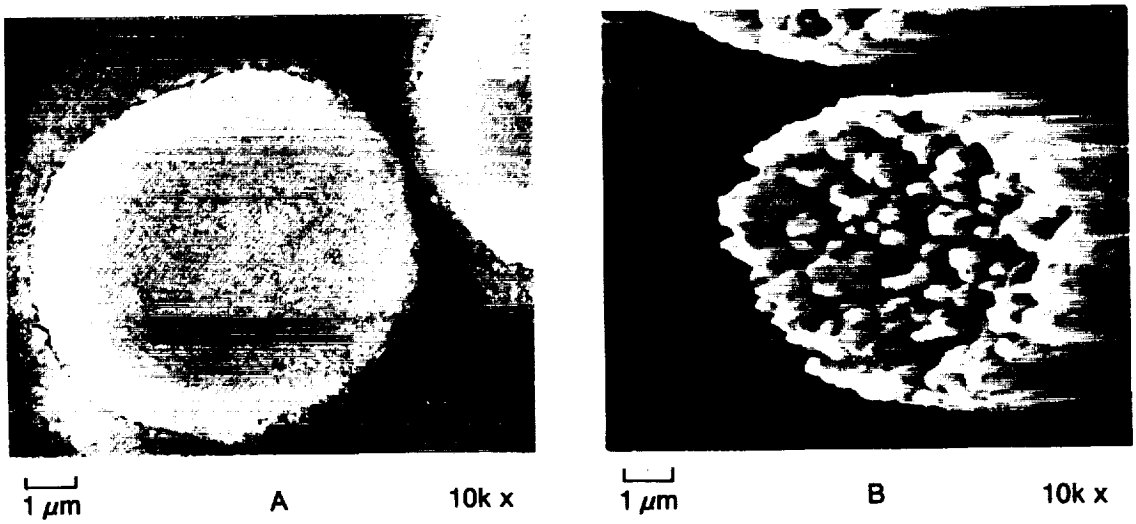

Figure 24.-Scanning Electron Micrographs of Thornel 300. (a) Preflight. (b) Postflight.

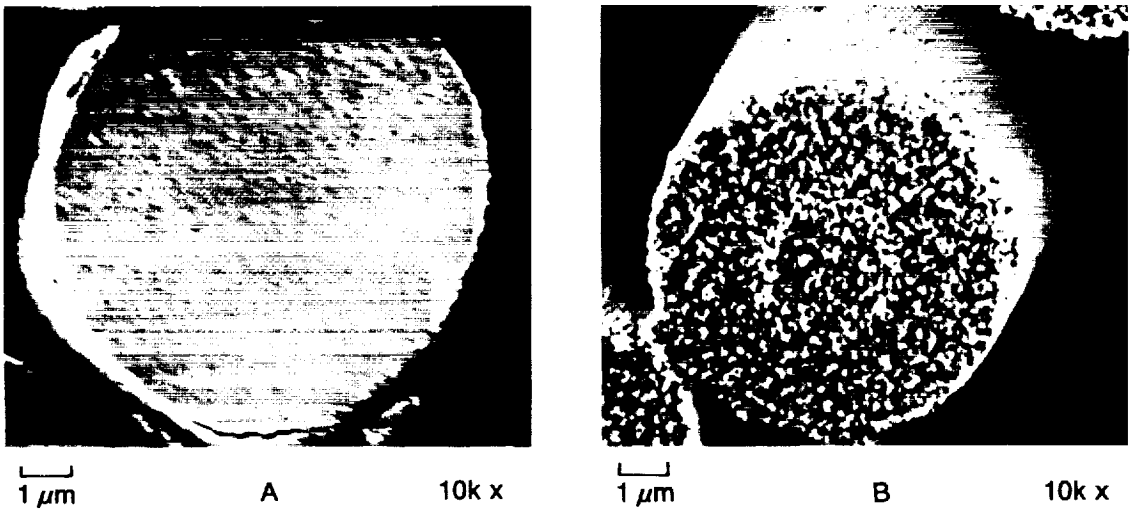

Figure 25.-Scanning Electron Micrographs of HM 3000. (a) Preflight. (b) Postflight.

Of concern is the behavior of these materials in the orbital environment, as specific changes in their thermo-optical properties can cause problems. A number of candidate high-temperature coating and substrate materials are being considered for satellite thermal control; however, the effects of exposure to the Shuttle environment are not well known. This is partly because, in previous space flights, samples of materials have not been given definite exposures and then retrieved for later examination. In addition, the exact conditions encountered on orbit are difficult to duplicate in the laboratory.[8] Results from STS-4 are severe erosion of osmium and carbon films and changes in the appearance of silver films. Gold films, which appeared unchanged, indicated that sputtering was not the mechanism of degradation.[9] There is thus reason for concern over the effects of this environment on other materials that may be used in the future.

The aim of this experiment was to expose samples of thermal-control coating materials to atomic oxygen bombardment in low Earth orbit and investigate any resulting changes in the infrared emissive and reflective properties and any correlated microstructural or textural effects.

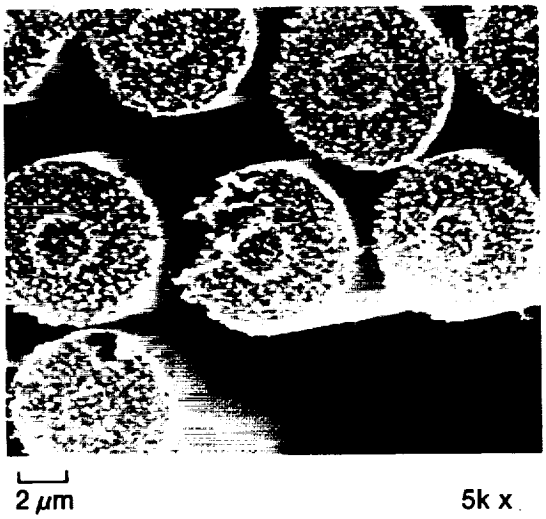

Figure 26.- Scanning Electron Micrograph of HM 3000, Showing Center Core Region

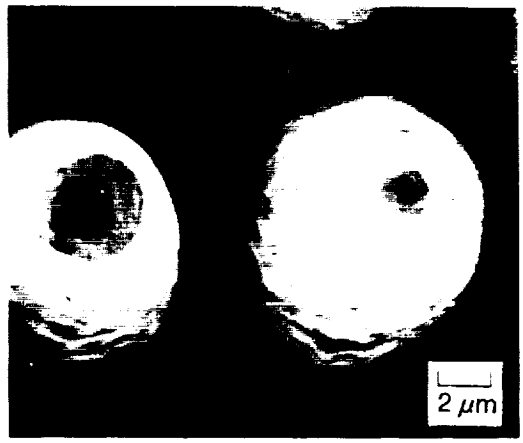

Figure 27.- Scanning Electron Micrograph of HM 3000 Filament after Oxidation in Air at Atmospheric Pressure and a Temperature of – 3900°C

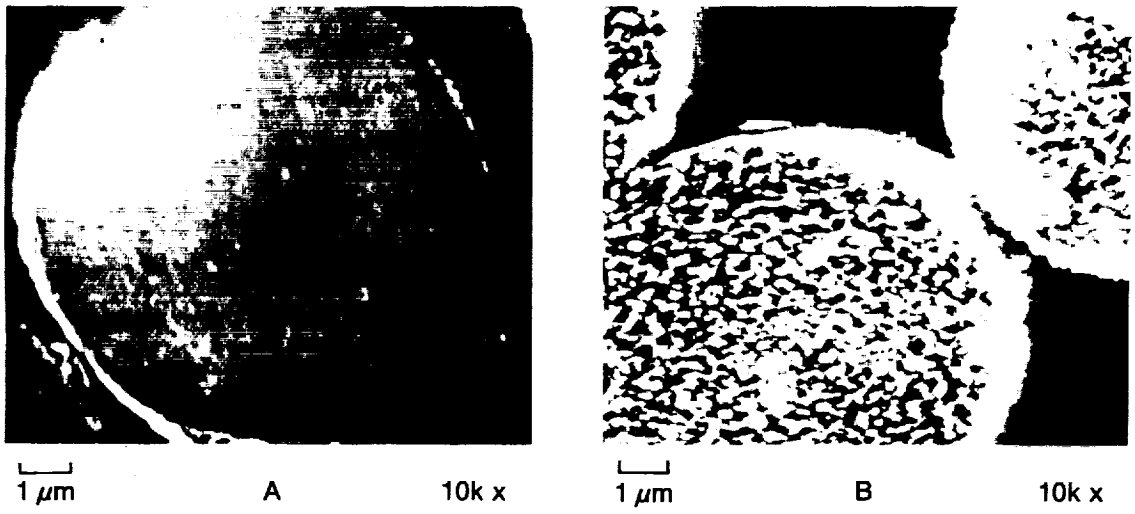

Figure 28.-Scanning Electron Micrographs of VSB 32. (a) Preflight. (b) Postflight.

5.6.2 Sample Description

The coatings were applied to sample disks 1 inch in diameter and 0.125 inch thick. The disks were located in the Langley tray (see Fig. 1a). Various coating materials were applied to substrates of polished molybdenum (Mo), aluminum (A1), and titanium (Ti). The ten coatings investigated are described below.

1. Black rhodium on molybdenum (specular) - A rhodium (Rh) coating that was sputter-deposited to approximately 1 μm thickness from a Rh target onto a polished Mo substrate, using a vacuum sputtering unit (Edwards model 150B, under nitrogen at 0.3 mb). The coating had a shiny black appearance.

2. Black rhodium on Mo (matte) - Sputtered coatings of Rh on polished Mo, using conditions similar to (1); dull black in appearance.

3. Black iridium on Mo - Sputtered coatings of iridium (Ir) on polished Mo; black in appearance.

4. Black Cr on Cr on Mo - Mo substrates plated with Cr metal and coated with a high-emittance layer of black Cr.

5. Rh foil on aluminum - Highly reflective Rh foil applied to an A1 disk by means of an adhesive.

6. Ir foil on A1 - Same as for (5), but with reflective Ir foil.

7. Polished Mo - Disks of polished Mo.

8. KAT glass - Molybdenum sealing-glass composition coating, formed by sol-gel processing and doped with cobalt (Co) as a dark coloring agent, on a Mo substrate.

9. Ti/"tiodized" CP - Titanium anodized coating on a pure Ti substrate (a proprietary process, analogous to anodizing for A1, that consists of the electrolytic formation of a thick Ti oxide layer on Ti).

10. Ti/"tiodized" alloy - "Tiodized" coating on a Ti alloy (Ti-6Al-4V) substrate.

5.6.3 Experimental Procedure

Two identical sets of samples were prepared; one set was flown and the other served as a control. Samples were photographed both before and after flight. To assess quantitatively the changes in the absorption and reflection properties of the samples, measurements of the infrared reflectivity in the 4000 to 500 cm^{-1} (2.5 to 20 μm) region were made before and after flight, using a Nicolet Fourier transform infrared (FTIR) spectrophotometer. Specular reflectance was measured, with the incident beam at 10° off normal.

Surface composition analysis and depth profiles were studied by means of a scanning Auger microscope (SAM), and surface morphology was examined with a scanning electron microscope (SEM). The bonding of the coatings to the substrate was also examined by means of a tape-peel adhesion test.

5.6.4 Results

1. Visual Observation, Pre- and Postflight

Some visual changes were observed on comparison of the postflight and control specimens, mainly on the Ir, Rh, and black Cr coatings. This is summarized in Table 9. The gross visual changes noted were mainly an apparent clouding or fogging of the surface, or the formation of small holes in the coating. Changes were also observed in the IR spectra of the coatings as a result of exposure to atomic oxygen.

2. FTIR Results

Table 10 summarizes the changes observed in the IR spectra of samples that had accompanying visual changes. Except for the black Cr coating, the "fogging" is seen to decrease the measured IR reflectance. This can be interpreted as either an increase in the absorption of the sample, an increase

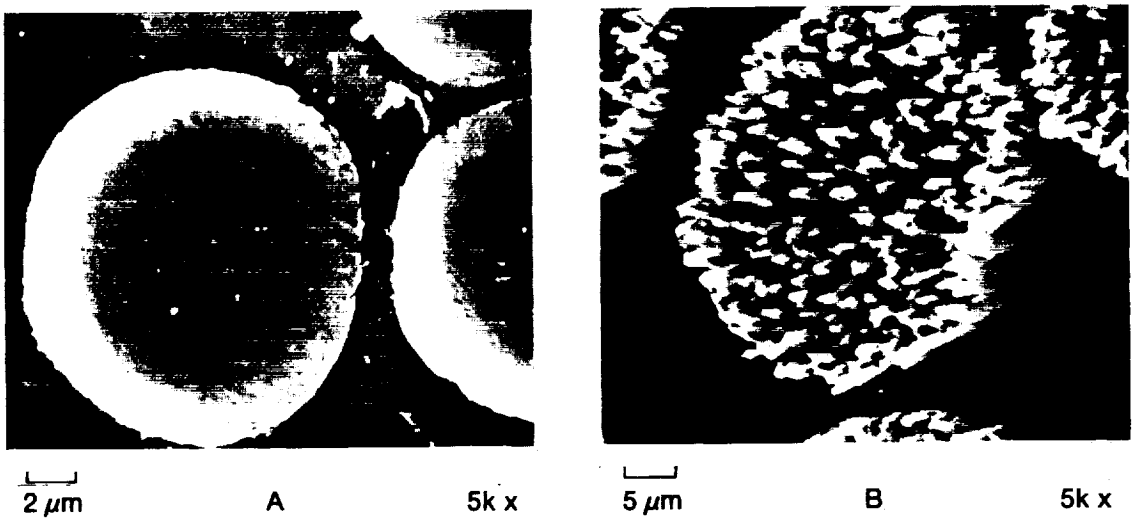

Figure 29.-Scanning Electron Micrographs of Kevlar Polyamid. (a) Preflight. (b) Postflight.

in the diffuse reflectance, or some combination of each. However, it is to be expected that an increase in texturing of the surface such as that caused under various conditions of sputtering can lead to increased absorptance.[10,11] Total reflectance over the maximum solid angle would be necessary to account for any changes in absorption compared to those caused by diffuse reflectance, although the changes induced in the coated samples (as indicated by the appearance of fogging) would likely be associated with an increase in absorption. In the case of the exception where reflectance increased, it seems likely that this increase is caused by the formation of actual holes in the coating, which causes the reflective metal substrate to be exposed and thus increases overall IR reflectivity. The changes in the IR spectra listed in Tables 10 and 11 are an indication of the change in average reflectance over the entire IR range measured. No major changes in spectral shapes or new peaks resulting from the exposure were observed.

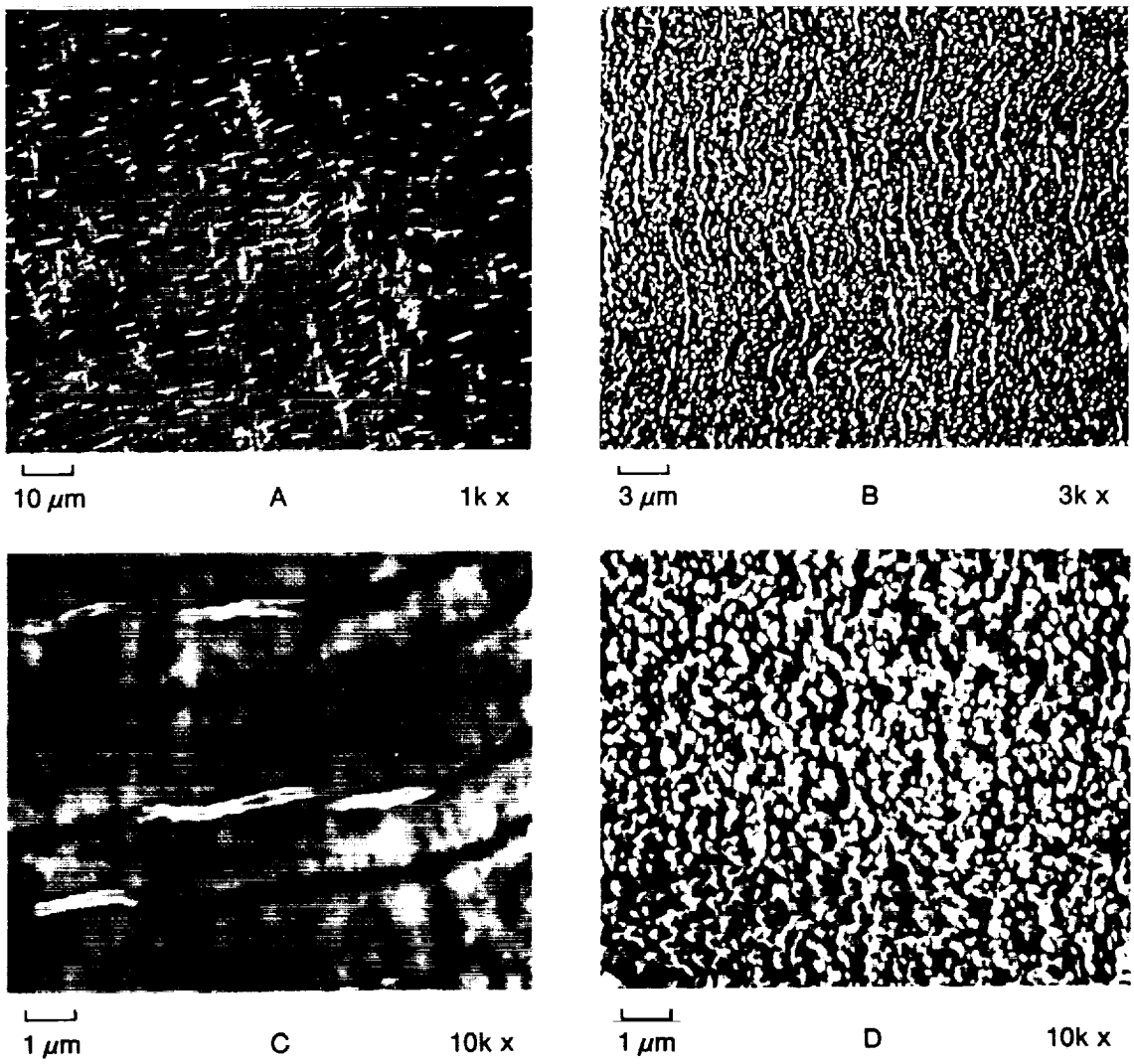

Figure 30.- Scanning Electron Micrographs of the A-Plane in Pyrolitic Graphite. (a) Preflight. (b) Postflight. (c) Preflight. (d) Postflight.

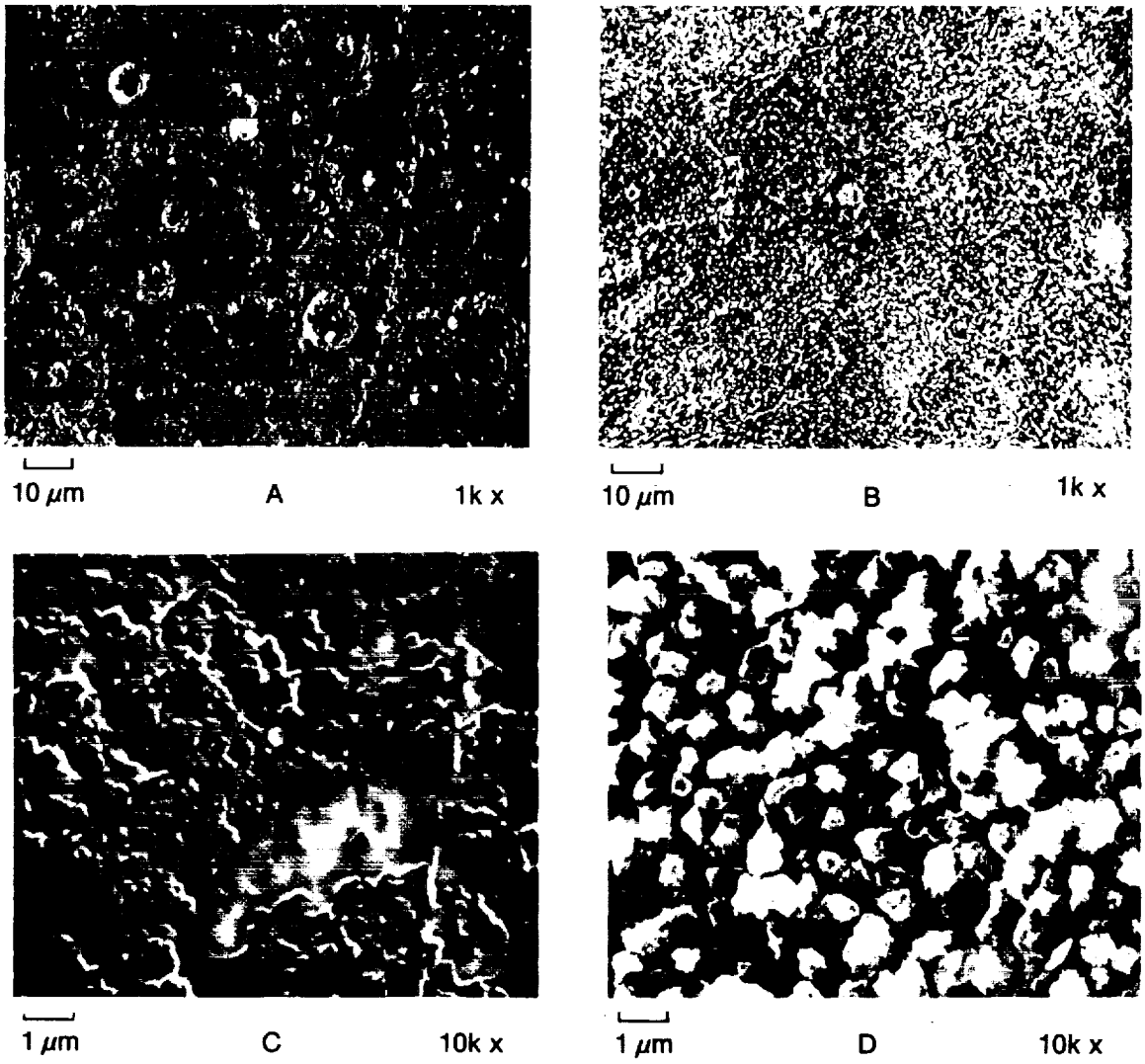

Figure 31.- Scanning Electron Micrographs of the C-Plane in Pyrolitic Graphite. (a) Preflight. (b) Postflight. (c) Preflight. (d) Postflight.

Table 11 summarizes the IR changes observed in the remainder of the specimens, which did not exhibit visual changes. Some decreases in reflectivity were noted in the last three samples in the table. The low value of the reflectivity of the KAT glass samples made it difficult to determine the change in reflectivity. The Ti/"tiodized" (titanium anodized) (CP) sample showed similar spectral changes in both the control sample (over a six-month period) and the postflight sample. The changes in the coating may have occurred gradually over a period of time, perhaps because of moisture absorption. Spectral changes occurred in both the postflight and control Ti/"tiodized" (alloy) samples, but the changes were somewhat different, as is indicated when the pairs of spectra are subtracted. This shows that, while the control sample may have changed during storage, there are also signs that the flight sample was affected by exposure to atomic oxygen.

3. Adherence Test.

The degree to which the coatings adhered to the substrates, both controls and postflight samples, was examined by a simple tape-peel test.[12] Adhesive cellophane tape was applied to the coatings, then was peeled off and examined to determine if the coating had debonded from the substrate. The results are summarized in Table 12.

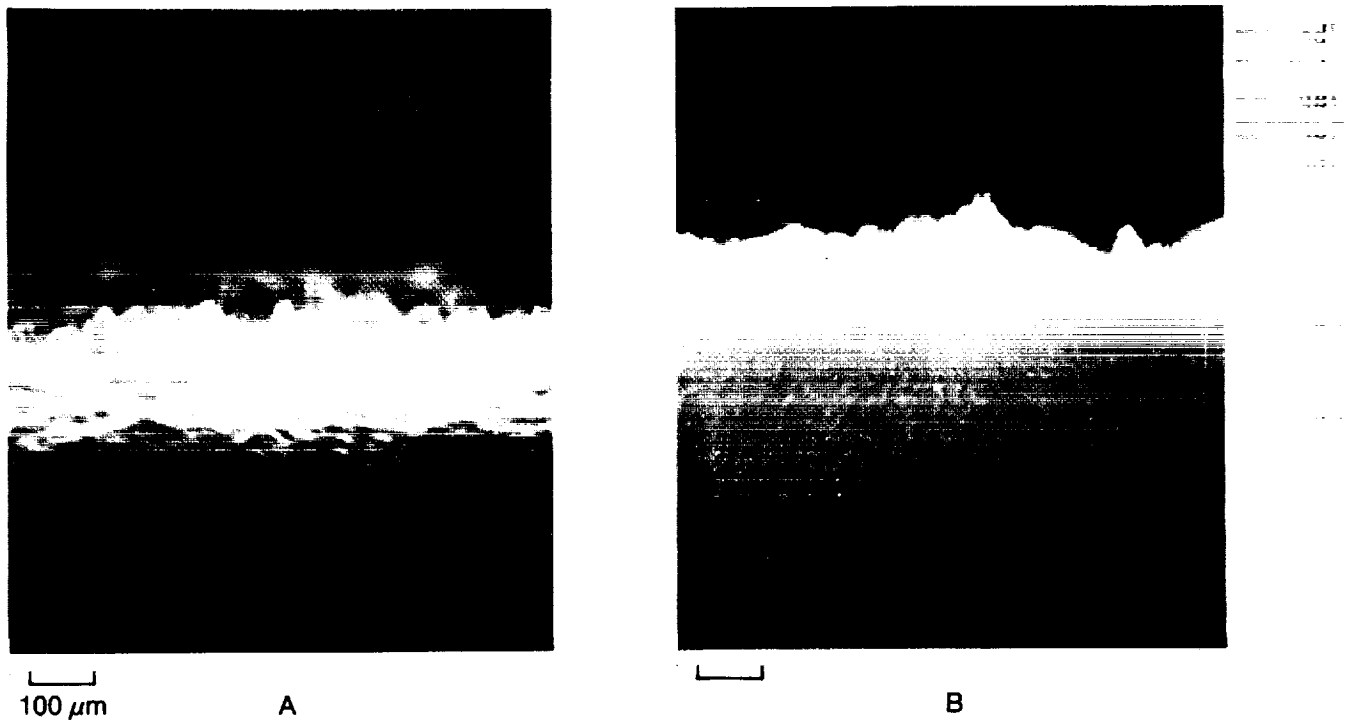

Figure 32.- Scanning Electron Micrographs (Cross-Sectional View) of Conical Features in Oxidized Pyrolitic Graphite. (a) A-plane. (b) C-plane.

It is also noted that no major changes in adherence were found as a result of exposure to the atomic oxygen environment, except for the case of the black Cr coating. The adherence of that coating, which contained numerous small holes, was much less after the exposure.

4. SAM and SEM Results.

Observation of the pre- and postflight samples by means of scanning Auger microscopy (SAM) showed some effects of exposure to atomic oxygen. Polished Mo showed a higher concentration of oxygen on the surface of postflight samples than on preflight ones. Surface profiling was performed in the instrument by sputtering away surface material with argon-ion bombardment and repeating Auger analysis. Oxygen was detected for a longer time (i.e., to a greater depth) in the postflight (Fig. 35a) than in the preflight samples (Fig. 35b), indicating that the energetic O-atoms create a significant oxidized surface layer.

Black Cr samples, both pre- and postflight, had similar composition profiles under Auger analysis. The Mo/Cr/black Cr structure was evident from the results. The coating appeared scaly and cracked into numerous, typically four-sided sections roughly several microns in diameter (see Fig. 36). The Auger analysis of the coating showed the material to be composed mainly of Cr and O, consistent with black Cr being a mixture of Cr and Cr_2O_3 (Fig. 37). Results were similar to SAM sputtering profiles obtained by Lampert[13] on commercial black-Cr solar absorber coatings on nickel-plated copper, where further analysis by transmission electron microscopy (TEM) showed the coating to be composed of Cr_2O_3 particles interspersed with Cr particles. Regions in the cracks between the black Cr scales were found to be predominantly Cr (i.e., the metallic Cr undercoating), with small oxygen content. The Auger oxygen peak of the undercoating disappeared after brief sputtering, indicating the existence of only a superficial oxide layer. Comparison of the pre- and post- flight black Cr oxygen content showed no significant differences attributable to atomic oxygen bombardment, although the microstructures of the black Cr scale had differed somewhat in appearance, probably because of differences in the surface finish of the substrates before coating.

An unusual debonding phenomenon illustrating the difference in adherence of the black Cr coatings in the pre- and postflight samples was observed in the SAM under electron beam bombardment. Under irradiation by the electron

beam at 10 kV, some of the surface scales of the post-test samples were seen to debond spontaneously and appeared to fly off the surface, leaving an exposed area of the Cr undercoating (see Fig. 38). This was not observed in the pretest samples. It is believed that this may indicate charging of the surface scale, along with low adherence, so that the scales fly off as a result of electrostatic repulsion from the substrate. This would require the electrical contact between scale and surface to be poor. However, the bright voltage contrast due to charging, which one would expect to see in SEM images of the area, was not observed.

An interesting effect is the presence of a light-colored border along the edges of the surface platelets of black Cr, which is visible in areas where the platelets have debonded. This may indicate exposure of the Mo substrate, where O impinging through the crack has removed the Cr layer; however, it was not possible to probe the electron beam close enough to the base of the ledge to determine if the Mo was exposed. Another possible cause of debonding under the beam may be local heating, leading to thermal stresses that might also cause detachment of the scale when there is a reduced adherence to the surface. In summary, adherence changes are seen in

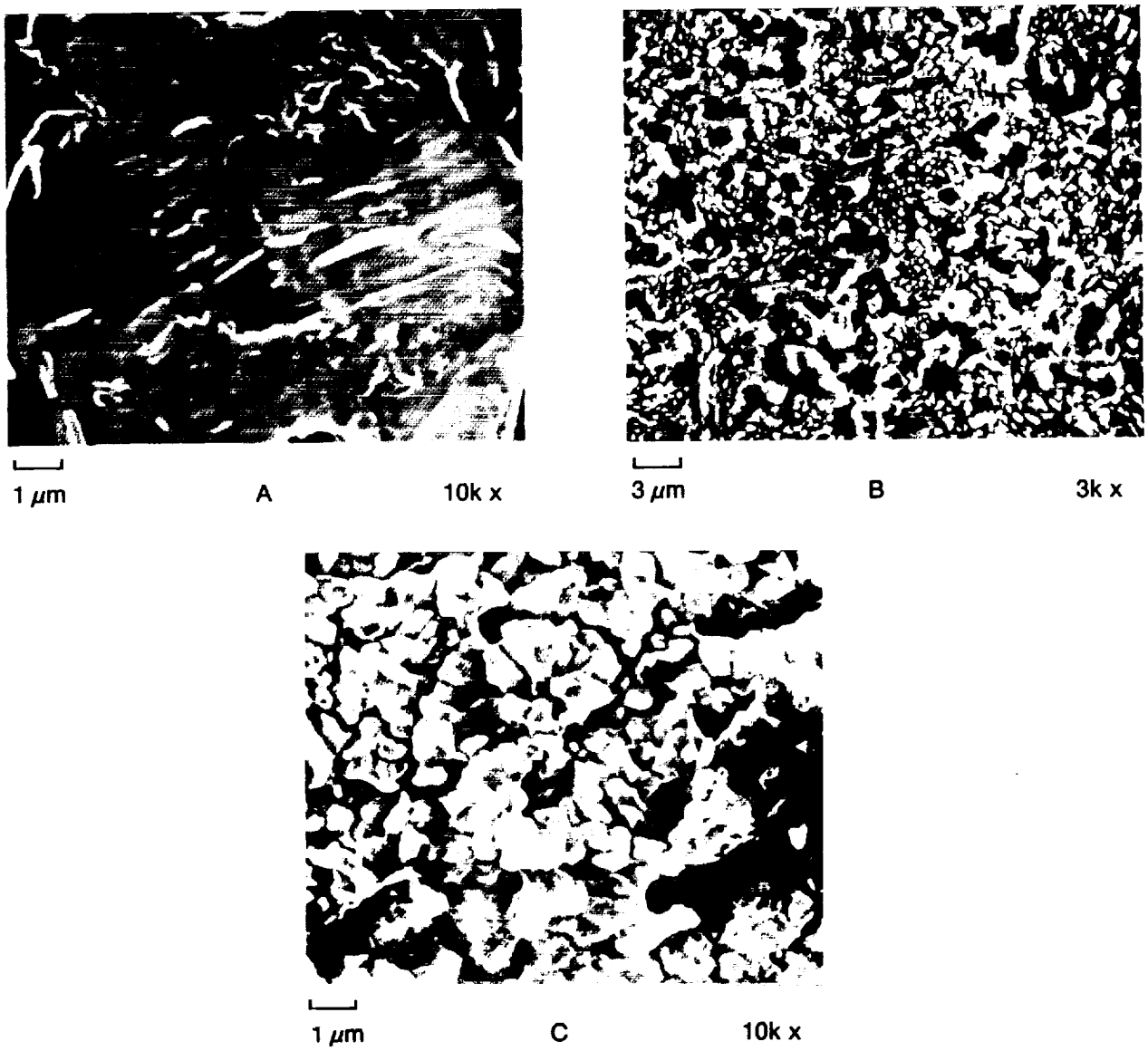

Figure 33.- Scanning Electron Micrographs of POCO 5Q Polycrystalline Graphite. (a) Preflight. (b and c) Postflight.

the oxygen ram-exposed samples, but no major induced microstructural or compositional effects are found. Thus, the cause of the reduced adherence is not fully apparent.

Depth profiling of oxygen on the black Ir coating flown on STS-8 (Fig. 39) showed a decrease in oxygen by a factor of about two, going from the immediate surface into the bulk. SEM observation showed a "furrowed" surface (Fig. 40a) after atomic oxygen exposure, compared to the control sample (Fig. 40b), indicating some attack of the surface has occurred. In addition, regions of exposed substrate were observed.

No major microstructural damage was seen in the black Rh coating, as compared to the black Ir coating. However, at low magnification the coating exhibited a pattern of ring-like mottling (Fig. 41) whose origin is uncertain, suggestive of an etching effect. It has been noted that varied surface morphologies can arise as a result of sputtering of surfaces under various conditions; these morphologies include cones, rods, hillocks, and other structures. [14]

The samples of KAT glass showed no major microstructural changes caused by the exposure. A comparison of the STS-8 and lab control samples is shown in Fig. 42.

E. Conclusions

High-temperature coatings underwent some changes as a result of exposure to the atomic oxygen environment in the STS-8 experiment. Large changes occurred in the black metal samples. This may be supported by the fact that previous and ongoing studies have shown that the black Ir and Rh samples prepared by sputter deposition are unstable at elevated temperatures, undergoing microstructural changes that are associated with changes in reflectivity. The increase in reflectivity of the black Cr coating is probably due to the exposure of the metallic substrate, because atomic oxygen erodes the coating.

Further work will involve examining the diffuse reflectance of the materials in the 0.3 to 25 μm range (30000 to 400 cm^{-1}) to determine the solar absorptance (α_s) and thermal emissivity (ε).

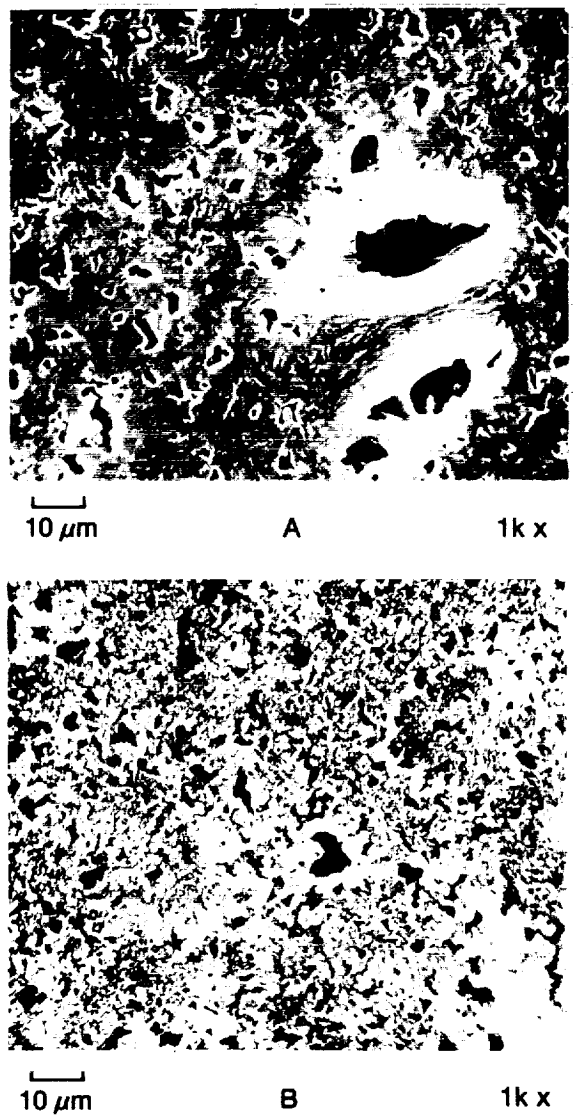

Figure 34.- Scanning Electron Micrographs of POCO 5Q Polycrystalline Graphite, Showing Changes in Micropore Diameters. (a) Preflight. (b) Postflight.

Table 9.-STS-8 High-Temperature Coating Experiment: Visual Observations

Sample No.	Description	Postflight	Control
1	black Rh on Mo (specular)	clouded	no change
2	black Rh on Mo (matte)	clouded	no change
3	black Ir on Mo	clouded	no change
4	black Cr on Cr on Mo	pinholes	no change
5	Rh foil on Al	no change	no change
6	Ir foil on Al	no change	no change
7	Mo (polished)	no change	no change
8	KAT glass	no change	no change
9	Ti/"tiodized" CP	no change	no change
10	Ti/"tiodized" alloy	no change	no change

Table 10.-STS-8 High-Temperature Coating Experiment: FTIR Difference Spectra (4000 to 500 cm^{-1}) for Samples Having Changes in Appearance

Sample No.	Description	Postflight Change in Average Reflectance, %
1	black Rh on Mo (specular)	−50
2	black Rh on Mo (matte)	−25
3	black Ir on Mo	−75
4	black Cr on Cr on Mo	+20*

*More reflective as a result of the exposed Mo substrate

Table 11.-STS-8 High-Temperature Coating Experiment: FTIR Difference Spectra (4000 to 500 cm^{-1}) for Samples Having No Change in Appearance

Sample No.	Description	Postflight Change in Average Reflectance, %
5	Rh foil on Al	no change
6	Ir foil on A1	no change
7	Mo (polished)	no change
8	KAT glass	−5 to 10*
9	Ti/"tiodized" CP	−40**
10	Ti/"tiodized" alloy	−25†

* Low absolute reflectance (-0.5 to 1%).

** Aging effect similar in STS-8 and control - no exposure effect.

† Contrast in difference spectra between STS-8 and controls - possible aging effect on controls.

Table 12.-STS-8 High-Temperature Coating Experiment: Adherence Test

Sample No.	Description	Postflight	Control
1	black Rh on Mo (specular)	good (some debris)	good
2	black Rh on Mo (matte)	poor	poor
3	black Ir on Mo	good (some debris)	good
4	black Cr on Cr on Mo	poor	fair
8	KAT glass	good	good
9	Ti/"tiodized" CP	good	good
10	Ti/"tiodized" alloy	good	good

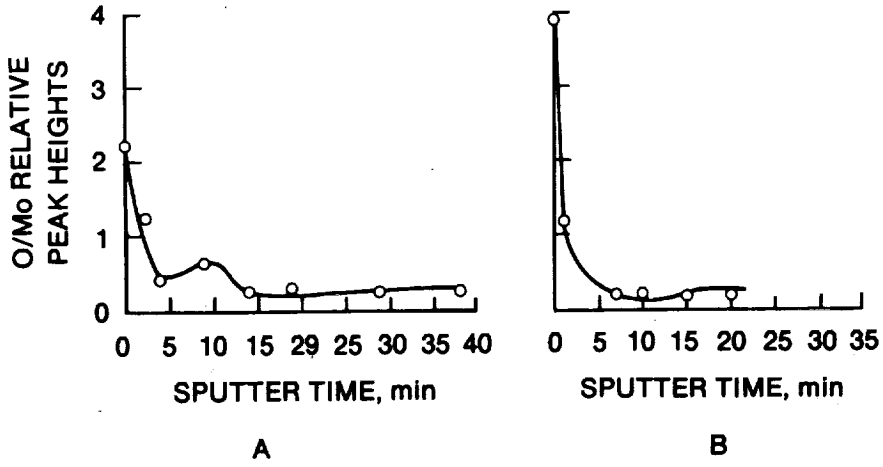

Figure 35.- Auger Surface Profiles of Polished Mo, Showing Oxygen Depth Profile. (a) STS-8 flight sample. (b) Laboratory control sample.

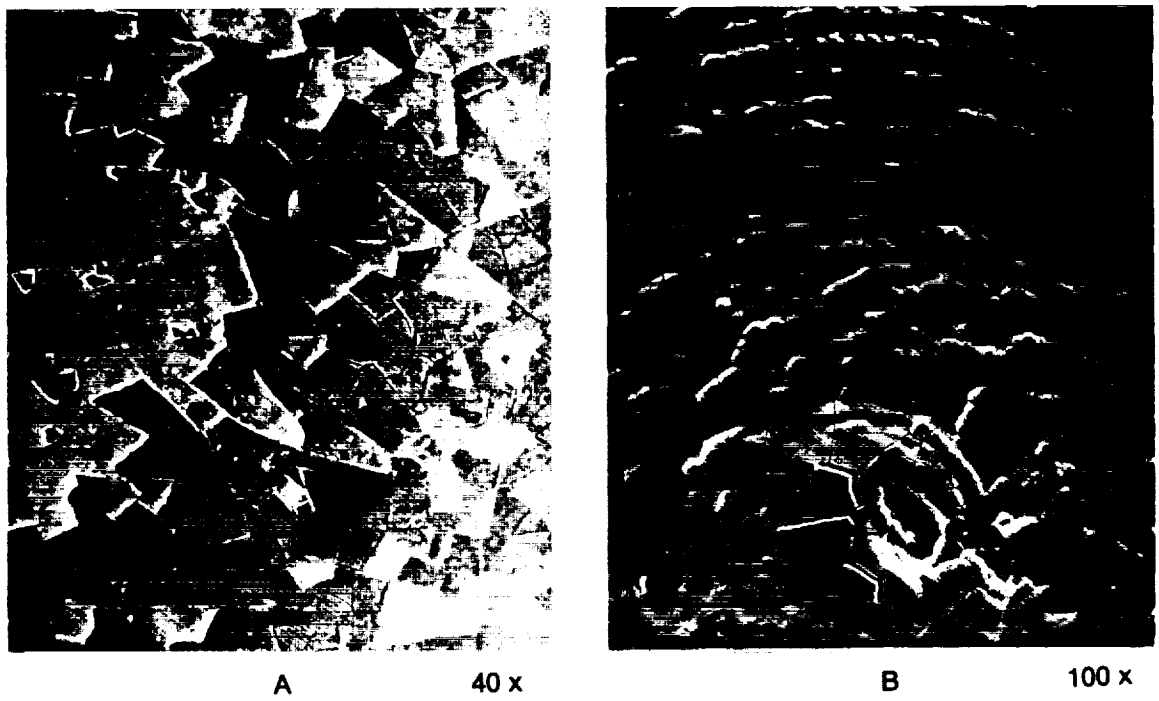

Figure 36.- Photomicrographs of Mo/Cr/Black Cr Sample, Showing Cracking and Scaling Caused by Exposure. (a) STS-8 flight sample. (b) Laboratory control sample.

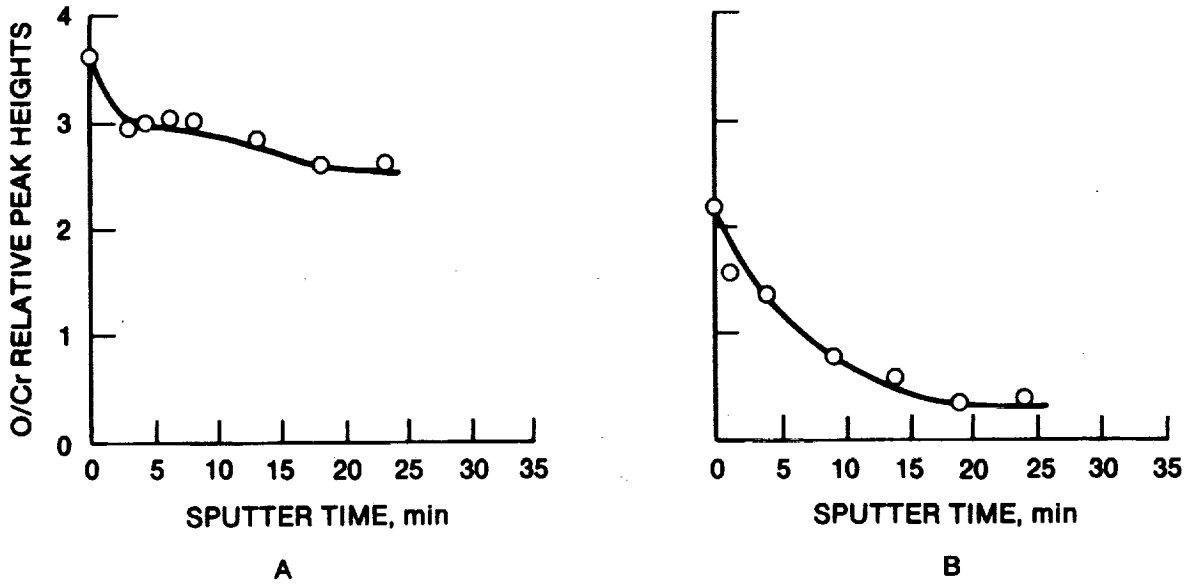

Figure 37.- Auger Surface Profiles of Black Cr on Cr on Mo, Showing Oxygen Depth Profile. (a) Laboratory control sample, showing oxygen content of oxide. (b) STS-8 flight sample, showing exposed Cr substrate.

Figure 38.- Photomicrograph of Mo/Cr/Black Cr Sample, Showing Debonding of Surface Layer and Exposed Cr Undercoating

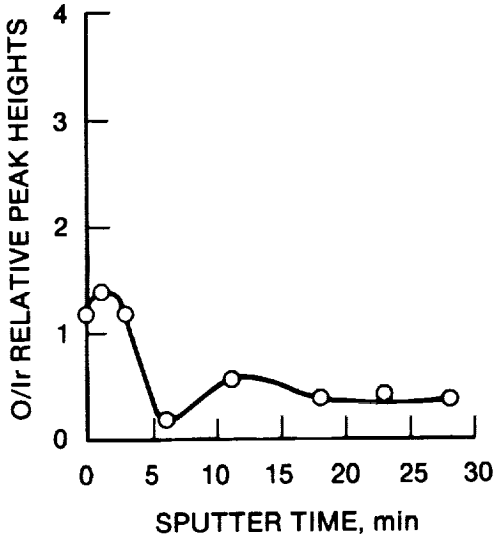

Figure 39.- Auger Depth Profile of Black Ir Coating, Showing Oxygen Depth Profile

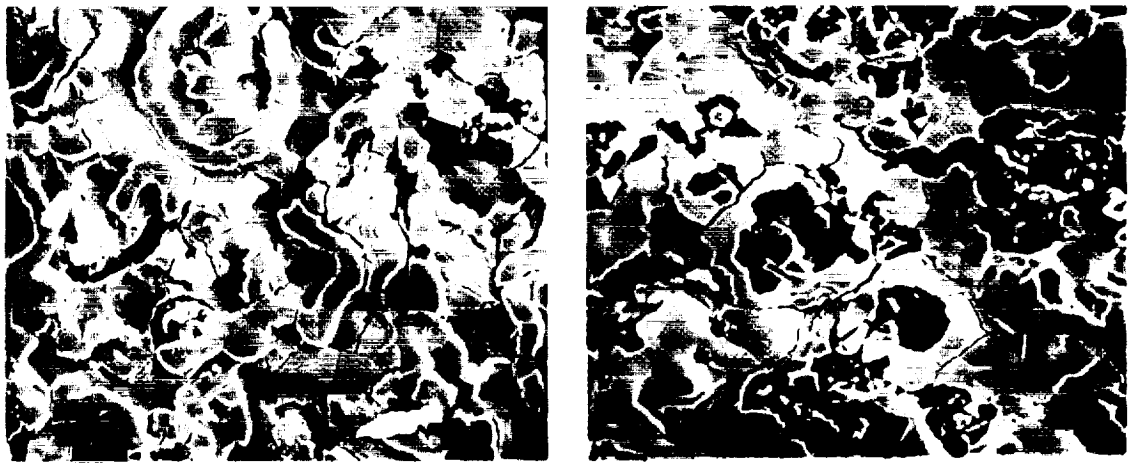

Figure 40.- Scanning Electron Micrographs of Black Ir on Mo Coating. (a) Laboratory control sample and (b) STS-8 flight sample, showing "furrowing" caused by exposure to atomic oxygen.

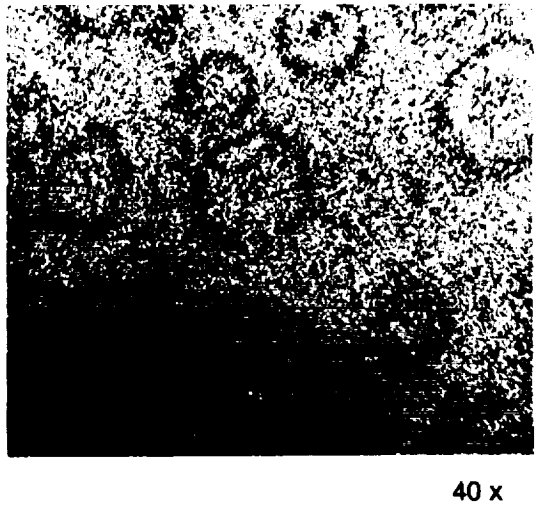

Figure 41.- Photomicrograph of Black Rh on Mo Coating of STS-8 Flight Sample, Showing Pattern of Ring-Like Mottling

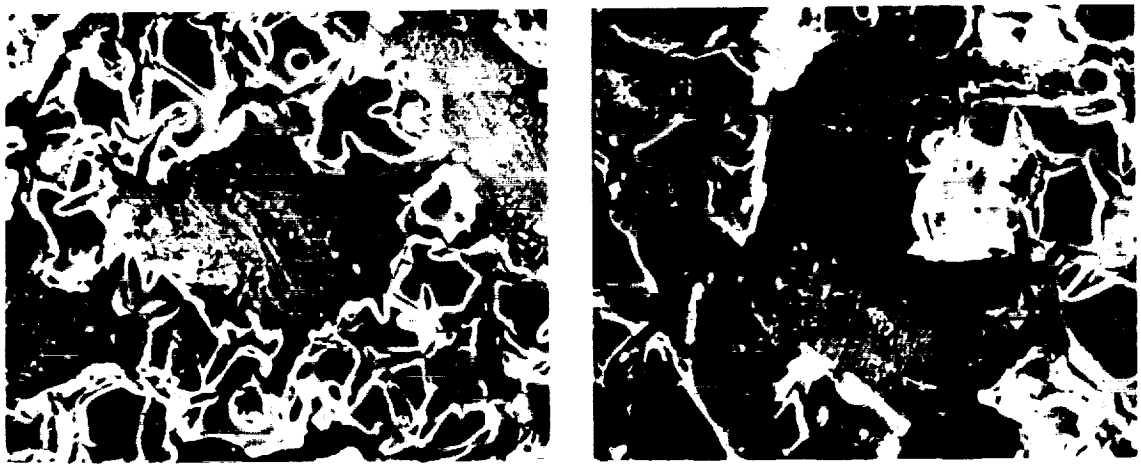

Figure 42.- Photomicrographs of KAT Glass on Mo Coating. (a) Laboratory control sample. (b) STS-8 flight sample.

References

1. J. T. Visentine, L. J. Leger, J. F. Kuminecz, and I. K. Spiker, "STS-8 Atomic Oxygen Effects Experiment," paper presented at AIAA 23rd Aerospace Sciences Meeting, Reno, Nev. (January 1985).

2. G. S. Arnold, R. R. Herm, and D. R. Peplinski, "Atmospheric Effects in Low Earth Orbit and the DMSP ESA Offset Anomaly," SD-TR-82-81, The Aerospace Corporation (30 September 1982)

3. J. C. Bailar, H. J. Emeleus, Sir Ronald Nyholm, and A. F. Trotman-Dickenson, Comprehensive Inorganic Chemistry, Vol. 3 (Pergamon Press, 1973), p. 229.

4. L. J. van der Pauw, "A Method of Measuring Specific Resistivity and Hall Effect of Discs of Arbitrary Shape," Philips Res. Rep. 13, No. 1 (1958).

5. Westinghouse Electric Corporation, Defense and Electric Systems Center, Specification #9RA3974 (30 October 1979).

6. M. R. Comer, Westinghouse Electric Corporation, private communication.

7. R. J. Diefendorf and E. Tokarsky, "High-Performance Carbon Fibers," Polymer Engineering and Science 15 [3] (1975).

8. G. S. Arnold and D. R. Peplinski, "A Facility for Investigating Interactions of Energetic Atomic Oxygen with Solids," ATR-84 (8540)-3, The Aerospace Corporation (16 September 1985).

9. P. N. Peters, R. C. Linton, and E. R. Miller, "Results of Apparent Atomic Oxygen Reactions on Ag, C, and Os Exposed during the Shuttle STS-4 Orbits," Geophys. Res. Lett. 10, 569-571 (1983).

10. G. D. Pettit, J. J. Cuomo, T. H. DiStefano, and J. M. Woodall, "Solar Absorbing Surfaces of Anodized Dendritic Tungsten," IBM J. Res. Dev. 22, 372-377 (1978).

11. G. Zajac and A. Ignatiev, "Percolation-Type Behavior in Black Chrome Selective Solar Films," Appl. Phys. Lett. 41, 435-437 (1982).

12. "Standard Methods for Measuring Adhesion by Tape Test," American National Standard ASTM D3359-78.

13. C. M. Lampert, "Metallurgical Analysis and High-Temperature Degradation of the

Black-Chrome Solar-Selective Absorber," Thin Solid Films 72, 73-81 (1980).

14. R. S. Berg and G. J. Kominiak, "Surface Texturing by Sputter Etching," J. Vac. Sci. Tech. 13, 403-405 (1976).

Acknowledgments

This work was supported by the U.S. Air Force Systems Command, Space Division, under Contract F04701-85-C-0086. The authors wish to thank the following individuals for their technical assistance in this work: Ann Bertrand, Eugene Borson, Richard Brose, Paul Chaffee, Sandra Gyetvay, David Hanna, Martin Leung, Nicholas Marquez, Thomas Park, Gloria To, Lucio Tolentino, and Clark Williams.

6.0 MECHANISTIC STUDIES OF POLYMERIC SAMPLES EXPOSED ABOARD STS-8

Ranty H. Liang
Amitava Gupta
Shirley Y. Chung
Keri L. Oda

6.1 Abstract

The early Shuttle flights and the attendant opportunity to deploy material samples to the near-earth space environment, along well defined trajectories and accompanied by detailed characterization of these samples prior to and following the flight exposure, have brought to light several novel phenomena associated with interaction of these materials with the space environment. The Jet Propulsion Laboratory (JPL), in coordination with other National Aeronautics and Space Administration (NASA) centers, has carried out a research program to study the material degradation and oxidation processes caused by interaction of these materials with atomic oxygen at an interaction energy of 5 electron volts (eV). In addition, the interaction of energetic atomic oxygen with materials is believed to be responsible for the "shuttle glow" first observed during the flight of Space Transportation System (STS) 3. The shuttle glow phenomenon has been extensively studied and modeled because of its long-range potential impact on optical communication schemes and its more immediate impact on the Space Telescope. This report summarizes the results of certain material degradation and erosion experiments carried out aboard the STS-8 flight, which occurred between August 30, 1983 and September 5, 1983. Based on these data, a generic degradation model has been developed for common structural polymers.

6.2 STS Flight 8 Hardware and Oxygen Atom Fluence

Details of the STS-8 exposure experiment have been reported elsewhere[1]. In STS-8, two experimental trays were placed on a payload carrier at a forward location in the orbiter bay. These trays held samples of materials in the form of discs as well as strips. Figure 1 illustrates the placement of these two trays with respect to the orbiter. All strip samples were mounted on calibrated heating plates to evaluate the effect of temperature on degradation. Templabels were used to monitor sample temperatures in flight. Temperatures of 75°F, 150°F, and 250°F were planned. Readings from templabels, however, indicated that temperatures of 75°F, 250°F, and 260°F were reached during flight. The total flight duration was 140 hours with four principal attitudes acquired during the mission. Table 1 summarizes the flight attitudes. The principal material exposure attitude was ±XLV, payload bay into the velocity vector, and is illustrated in Figure 1. This attitude was acquired three times during the mission and the total oxygen atom fluence was calculated to be 3.0×10^{-20} atoms/cm^2 over a 42-hour duration. This number was derived from Goddard Space Flight Center (GSFC) atmospheric density models and NOAA solar activity predictions for the actual flight trajectories.

6.3 Experimental

6.3.1 Sample Preparation

Six types of disc samples (1" in diameter) and two types of strip (3"×1") samples were prepared for the STS flight 8 exposure experiment. Polymethylmethacrylate (PMMA) beads were purchased from Polysciences, Inc. at two intrinsic viscosities: 1.4 and 0.4. The samples were compression molded at 177°C between teflon-coated Kapton sheets. A film of 0.007 inch thickness was obtained for the 0.4 viscosity material and a thicker film of 0.044 in. was prepared from the 1.4 intrinsic viscosity PMMA. Polyethylene (PE) with a density of 0.915 and polystyrene (PS) were molded at 150°C and 177°C, respectively, as received from Polysciences, Inc. Film thicknesses of 0.005 in. were made. Polysulfone (Union Carbide Udel 1700) pellets were dried in a vacuum oven at 150°C for 3 days and then compression molded at 293°C to form 0.005 in. thick films. No mold releasing agent which contains silicon was used in any compression molding in order to avoid sample surface contamination. Instead,

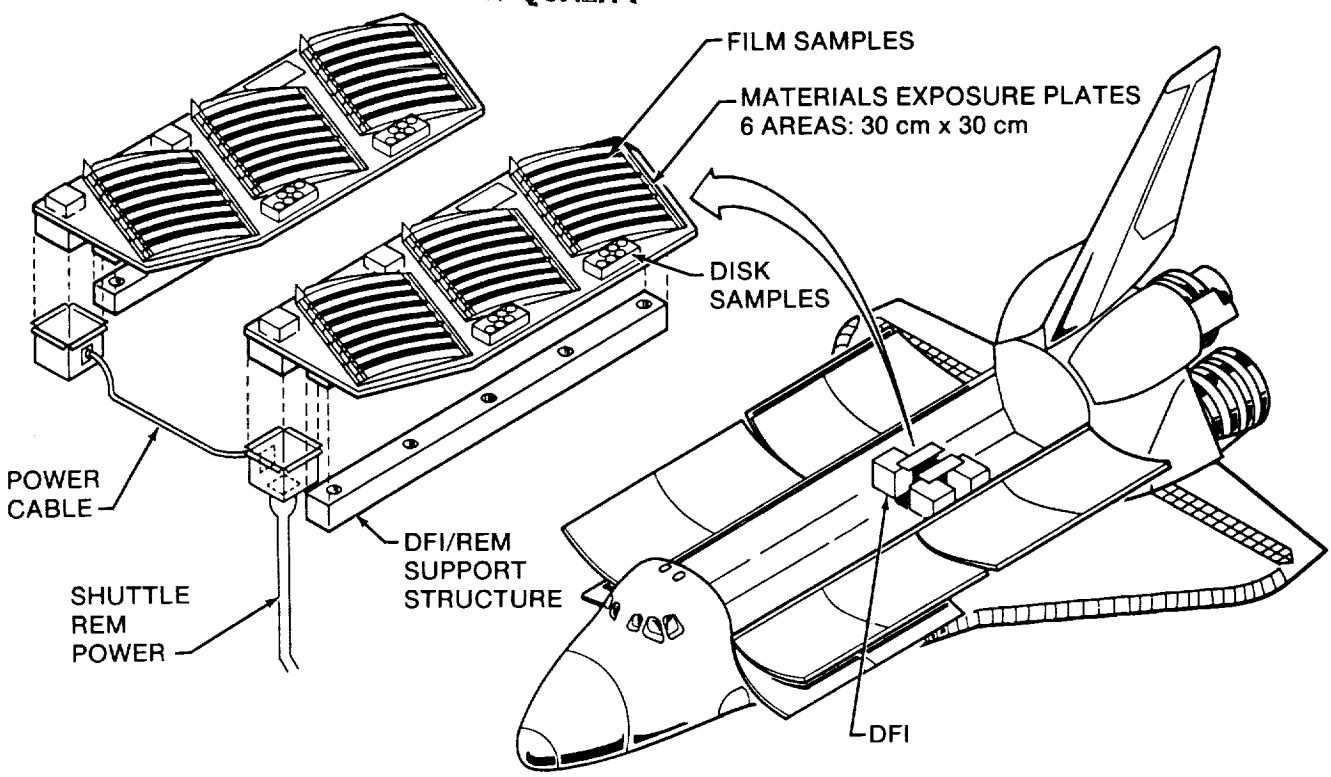

Figure 1.- Material Tray Configuration.

Table 1.- STS Flight 8 Attitude Summary

ATTITUDE	ORBITS	HOURS
–ZLV NOSE FWD	35	52.83
–XSI ORB RATE	10	15.67
–ZLV FREE DRIFT	9	12.92
±XLV PLB FWD	27	41.17
±XLV PLB NORTH	1	1.33
STAR TRACKER TESTS	2	2.75
KuBd/IMU ALIGNMENT	8	12.00
TAIL GLOW	1	1.50
TOTALS	93	140.17

samples were molded between two sheets of teflon-coated Kapton films. Teflon was used for ease of sample release. Kapton (DuPont 500H) and teflon-coated Kapton (Dupont F131) were cut from as-received sheets. The above films were cut into approximately 1-inch diameter discs.

Carbon-filled polyurethane-base Z-306 chemglaze paint samples were also flown on STS-8. This chemglaze paint is of interest to study because of its display of the material glow phenomenon believed to be a consequence of interaction of the surface layer with energetic oxygen atoms in the low-Earth orbit environment. Samples were provided by Marshall Flight Center, Huntsville, Alabama.

Two types of strip samples were prepared for exposure and subsequent mechanical testing: 3" × 1" PMMA (viscosity 0.4) and polysulfone films. Table 2 lists various tests that were performed on the samples. Table 3 shows the weight loss data.

6.3.2 Analysis

The following analyses were carried out on the STS-8 samples:

1. ESCA - Electron Spectroscopy for Chemical Analysis was performed on a Hewlett Packard ESCA photoelectron spectrometer Model 5958. This test provides data on the elemental composition of the surface (approximately the top 50 - 100 A) of each sample. High-resolution spectra were curve-fitted to resolve the presence of multiple atomic components and estimates of concentration in atomic percentage.

2. HPLC - High Pressure Liquid Chromatography was carried out by a Water Associates Model 6000A chromatogram. Four-column (10^5 A, 10^4 A, 10^3 A, and 500 A) microstyrogel separation was performed. Polystyrene was used for molecular weight calibration and chloroform was used as the solvent.

3. Tensile Stress-Strain Tests - Tensile stress-strain tests were carried out by stretching the sample in a tensile mode at a preset crosshead speed in a table Model-TM-Instron machine.

   This Instron was equipped with an environmental chamber with temperature control to ±0.5°C. The load was measured as a function of time in a strip chart recorder. Tests were performed at a strain rate of 0.02 min^{-1}. Test temperature was 25°C.

4. RR - A CW Ar+ and Kr+ ion laser and a CW Ar+ ion pumped dye laser were used as the tunable excitation source for resonance Raman spectroscopy. In order to select the best excitation and minimize the fluorescence background, several excitation wavelengths were used.

5. Weight Loss - Samples were measured using a Mettler Type #15 160g balance with a sensitivity of 0.1 mg.

6. Rheovibron - Dynamic mechanical testing was performed using a Rheovibron Dynamic Viscoelastometer Model DDV-II. Test temperature range was −133 to 240°C, at 11-Hz frequency.

6.4 Results

6.4.1 Polyethlene

Polyethylene (PE) has the simplest possible chemical structure of all polymers and, hence, the fewest possible modes of interaction with energetic oxygen atoms. It was therefore used as a model system. Since PE is known to undergo slow terrestrial oxidation, extreme care was taken when samples of PE were prepared to minimize this oxidation process. The weight loss of disc samples flown aboard STS VIII was found to be 1.3 ± 0.2 mg/cm^2. Erosive weight loss amounted to 7 percent of the total sample weight. Control and exposed surfaces of PE have similar Raman spectra, as shown in Figure 2. There is a hint of the formation of a C-O bond on the exposed surface, as evidenced by the broad peak at 1090 cm^{-1}. Hence, the thickness of the residual oxidized layer was expected to be very small. Both low- and high-resolution ESCA were performed in order to characterize this layer. Figure 3 is the ESCA spectra of control and exposed surfaces of polyethylene.

High-resolution ESCA spectra of the carbon in PE were illustrated in Figure 4. The integrated area under each peak was used to calculate the percent composition and the results are listed in Table 4. It is clear that the chemical composition of the exposed surface layer (50A) includes 9.9 atom percent oxygen, in contrast to 0.8 atom percent on a control surface (backside of the same sample). High-resolution ESCA on the carbon peak also indicated that oxidized carbon atoms were formed on the exposed surface. It is of interest to note that both singly oxidized (C2), as as well doubly oxidized (C3) carbon atoms, including

Table 2.- Tests Performed on Samples Flown on STS -8

MATERIAL	ESCA	HPLC	TENSILE STRESS-STRAIN	WEIGHT LOSS RR	WEIGHT LOSS	RHEOVIBRON
PMMA (Viscosity 1.4)	X	X	X		X	
PMMA (Viscosity 0.4)	X	X	X		X	
POLYETHYLENE	X			X	X	
POLYSULFONE (UDEL 1700)	X	X	X	-	X	
POLYSTYRENE	X				X	
KAPTON (DuPont 500H)	X			X	X	X
KAPTON (DuPont F131)	X			X	X	X
Z-306 CHEMGLAZE PAINT	X					

× = Completed
- = Attempted but unable to obtain data

Table 3.- Weight Loss Data

MATERIAL	WEIGHT LOSS mg/cm^2
POLYETHYLENE	1.3 ± .2
POLYMETHYLMETHACRYLATE:	
(VISCOSITY - 1.4)	1.2
(VISCOSITY - 0.4)	2.1
POLYSULFONE	1.1
KAPTON (DuPont 500H)	1.3
KAPTON (DuPont F131)	<0.2
POLYSTYRENE	0.8

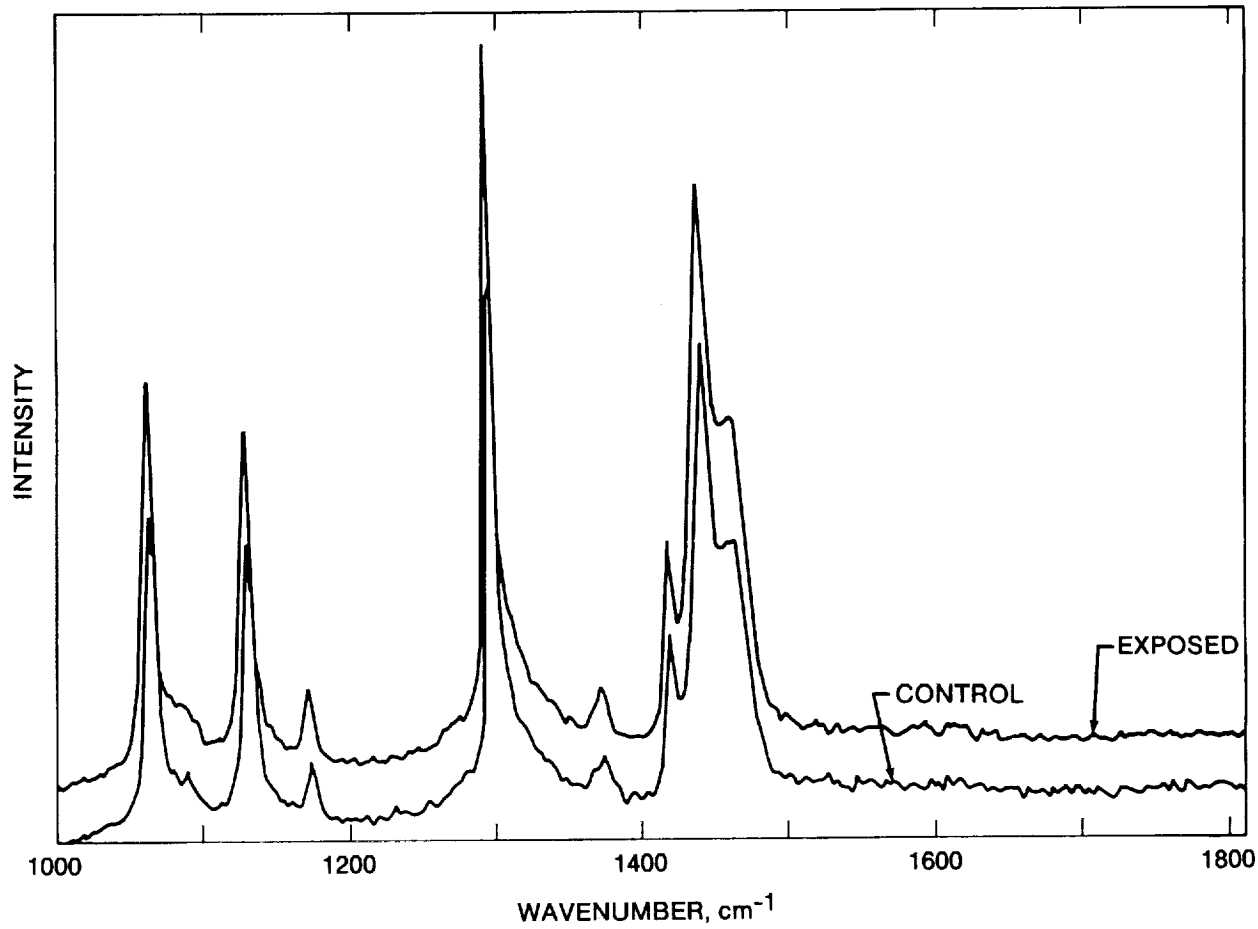

Figure 2.- Raman Spectra of Polyethylene.

carboxylic acid groups were detected on the exposed surface. The ESCA data on the composition of this residual oxidized layer lead to the conclusion that the initial or the primary interaction of the PE surface with atomic oxygen creates a partially oxidized intermediate state which may undergo volatilization or subsequent further oxidation leading to the formulation of carboxyl groups found the ESCA spectroscopy.

The density of PE before and after exposure was measured and is shown in Table 5. Within experimental error, density data showed no detectable differences. This result indicates that crystalline segments erode at the same rate as the amorphous segments, since otherwise an increase in the crystallinity could be expected in the residual film.

6.4.2 Polymethylmethacrylate

Polymethylmethacrylate (PMMA) of two intrinsic viscosities (0.4 and 1.4) were used. While the high-viscosity (1.4) sample showed a weight loss of 1.2 mg/cm^2, the low-viscosity sample (0.4) showed almost twice as much weight loss, i.e. 2.1 mg/cm^2. Results of HPLC analysis are shown in Table 6 and Figure 5. These data indicated the low-viscosity PMMA contained a substantial amount of a low molecular-weight component which would be susceptible to volatilization. This may account for the unusually high weight loss observed for this sample.

ESCA analysis was also carried out on both disc samples. Within experimental error (± 2 percent) both high- and low-viscosity samples exhibit similar results, and are summarized in Table 7.

It is interesting to point out that while PMMA was suffering weight loss due to erosion, the chemical composition of the eroded surface remained unchanged.

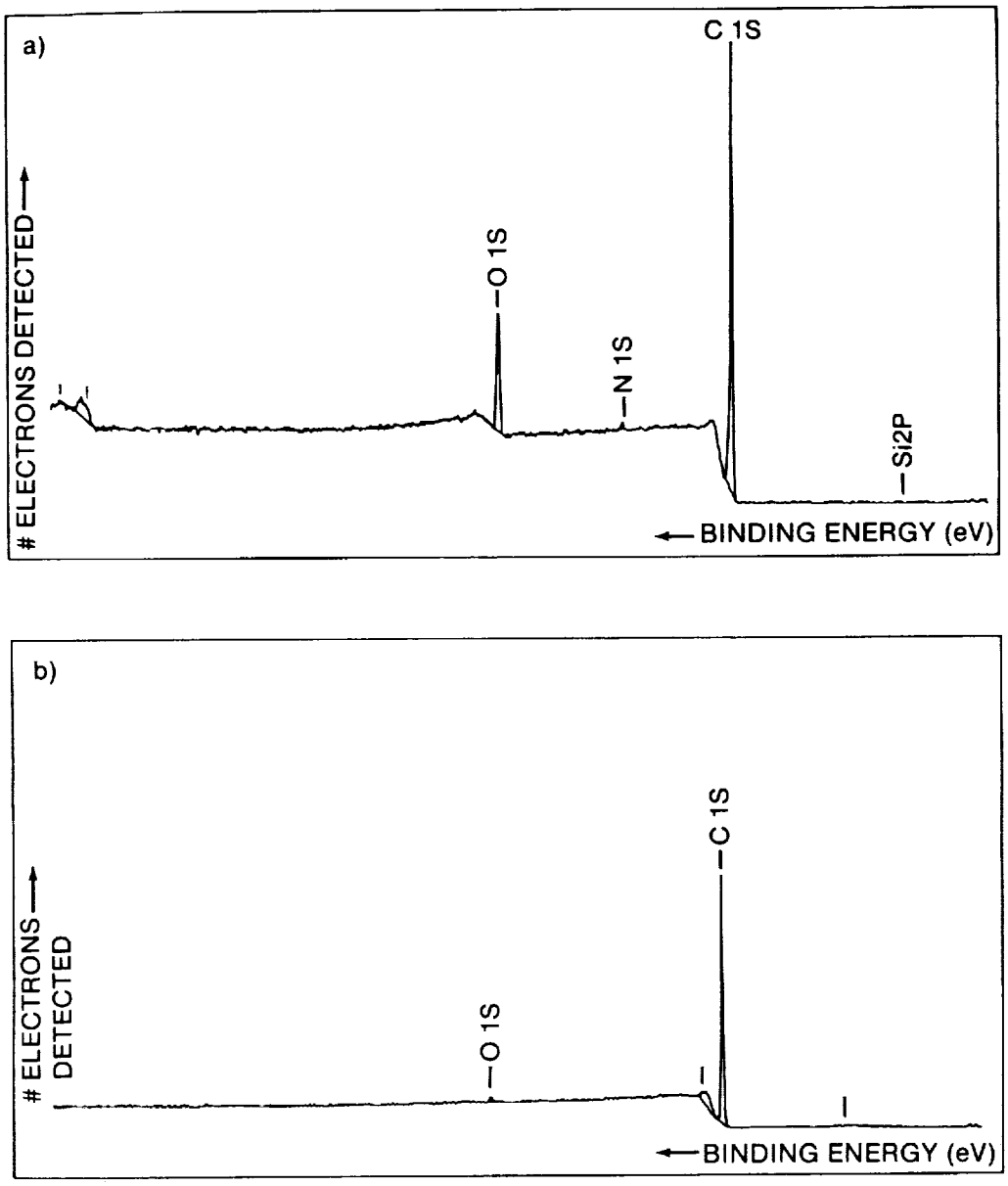

Figure 3.- ESCA Spectra of a) Control and b) Exposed Surfaces of Polyethylene.

Tensile stress-strain tests were also performed on PMMA strips. Stress-strain data were obtained after accounting for changes in the thickness of the specimen due to erosion. Results showed no detectable change in the tensile modulus and are illustrated in Figure 6.

The HPLC data indicate that chain scission and unzipping processes were occurring in PMMA on oxygen atom interaction. Since the oxidized material would be volatilized under these conditions, the eroded surface would retain the chemical composition of this original material. The extent of the molecular weight loss is insufficient to cause a measurable decrease in deformation properties; hence, no change in the tensile modulus is observed.

6.4.3 Polysulfone

The weight loss of a disc sample of polysulfone was found to be 1.1 mg/cm^2, which amounts to 3.5 percent change of the total sample weight. An attempt to obtain a resonance Raman spectrum of polysulfone failed due to the intense fluorescence and photo-instability of the sample at visible wavelengths (600-450 nm). Results of ESCA analysis are shown in

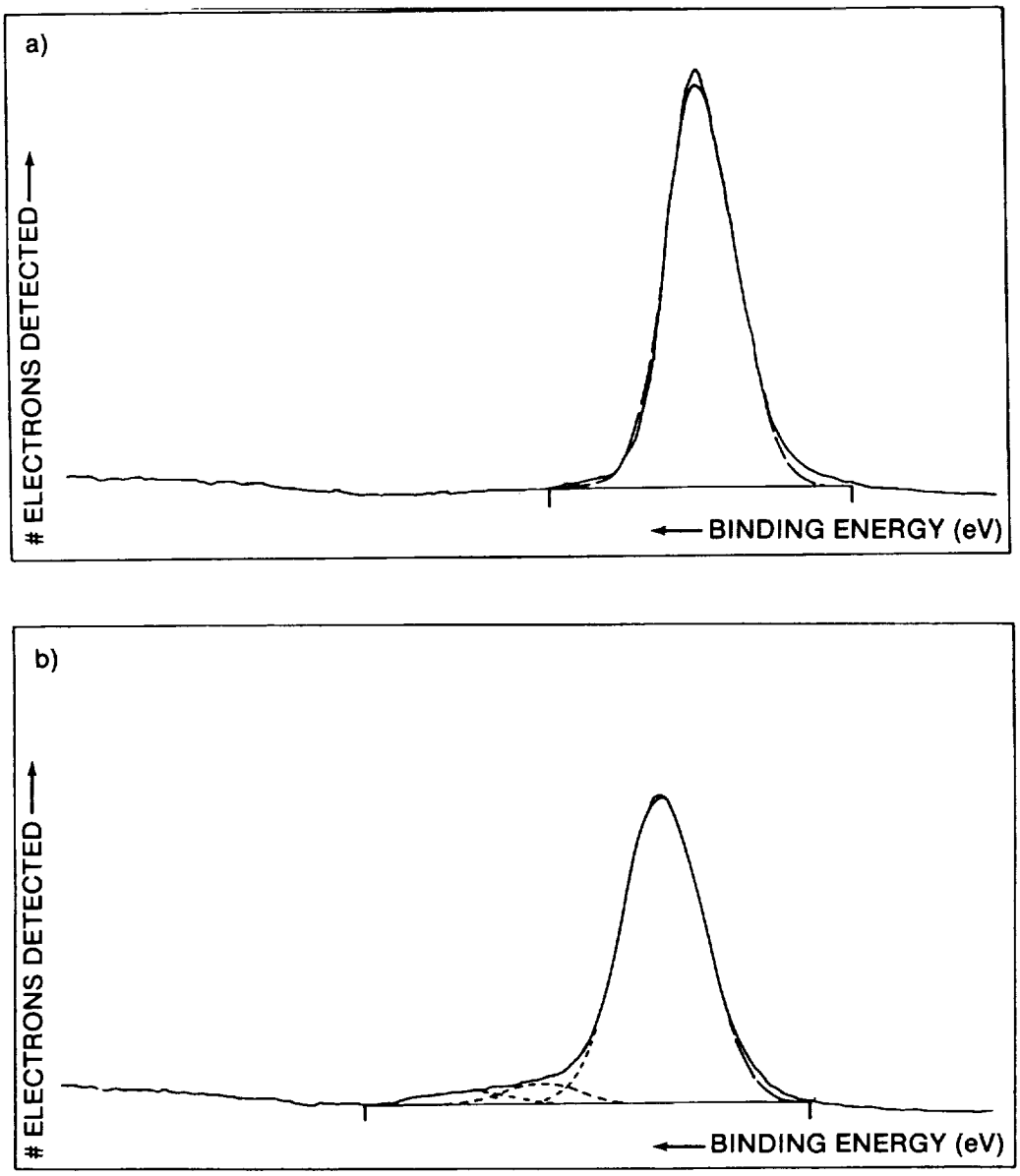

Figure 4.- High-Resolution ESCA Spectra of the Carbon in a) Control and b) Exposed Surfaces of Polyethylene.

Table 8. The control surface matches well with that of a pure polysulfone. The exposed surface, however, showed a 10 percent decrease in hydrocarbon concentration and a 7 percent increase in oxygen content.

Tensile stress-strain measurements were carried out on the strip polysulfone samples and the results are shown in Figure 7. A substantial drop in the tensile modulus was observed as a result of atomic oxygen exposure. The onset of yield is found in the exposed samples at around 3 percent strain.

The HPLC data indicate substantial loss of molecular weight due to chain scission. This decrease in molecular weight causes a decrease in mechanical properties such as the tensile modulus, reflected in the tensile stress-strain in data. Presumably the chain scission is initiated through oxidation of the polysulfone chain, probably at the phenyl nucleus. HPLC results are summarized in Table 9.

Table 4.- Percent Composition of Polyethylene Surfaces from ESCA

	% COMPOSITION				O/C
	C_1	C_2	C_3	O	
THEORETICAL	100	--	--	--	--
CONTROL	99.2	--	--	0.8	0.01
EXPOSED	81.5	4.5	3.1	9.9	0.11

C_1: C–C C_2: C=O, O–C–O C_3: O–C=O

Table 5.- Density Measurement of Polyethylene

CONDITION	DENSITY gm/cm^3
CONTROL	0.916
EXPOSED	0.917

Table 6.- Summary of Results of HPLC on PMMA

	TESTING CONDITION	$\overline{M}_n$	$\overline{M}_w$
1.4 VISCOSITY	CONTROL	192,000	404,000
	EXPOSED	166,000	357,000
0.4 VISCOSITY	CONTROL	143,000	250,000
	EXPOSED	101,000	209,000

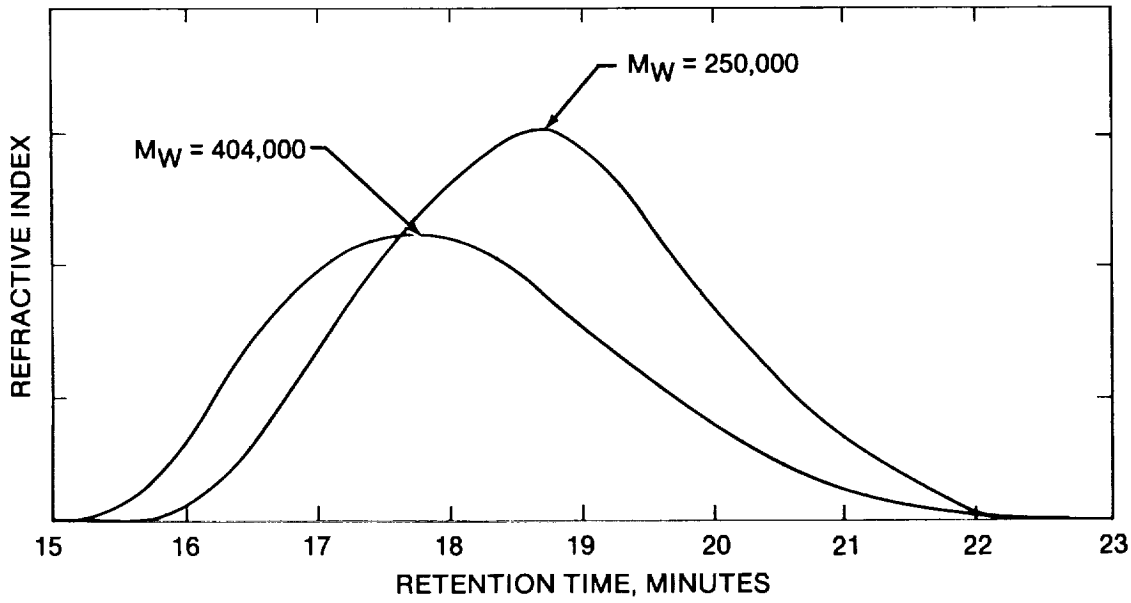

Figure 5.- HPLC of Polymethylmethacrylate.

Table 7.- Percent Composition of Polymethylmethacrylate Surfaces from ESCA

	% COMPOSITION				O/C
	O	C_1	C_2	C_3	
THEORETICAL	29	43	14	14	0.41
CONTROL	24	48	14	13	0.32
EXPOSED	26	45	14	14	0.36

C_1: C–C C_2: C–O, C_3: O–C=O

6.4.4 Kapton and Teflon-Coated Kapton

An average weight loss of 1.3 mg/cm^2 was observed on the exposed DuPont (500H) disc. No detectable weight loss could be determined on the teflon-coated Kapton DuPont (F131) samples. Resonance Raman spectra of Kapton before and after exposure are illustrated in Figure 8. The only notable difference is the disappearance of the 1600 cm^{-1} phenylene peak. This result was reported earlier for the exposed Kapton sample returned from STS-2, -3, and -5 missions. Results of ESCA analysis of Kapton are shown in Table 10. Rheovibron measurements were taken in triplicate at room temperature and are summarized in Table 11.

6.4.5 Polytyrene

Polystyrene has the simplest chemical structure for an aromatic polymer and is therefore used as a model compound. The average weight loss of a disc sample is 0.8 mg/cm^2, which is substantially lower than the other samples exposed. Surface composition from high-resolution ESCA analysis is listed in Table 12.

The exposed surface was contaminated, as evidenced by the detection of phosphaste salts, calcium, and zinc (P_1, p_2, Ca, and Zn). The additional weight of these contaminants may be partially responsible for the low erosion rate of the polystyrene

observed. Note that the hydrocarbon (C_1) content was reduced from 97 percent to 28 percent, while the oxygen content rose from 2.2 percent to 34 percent as a result of exposure. This rise in oxygen content on the exposure surface is substantial, in spite of the contribution from PO_4^{3-} and P_2O_5.

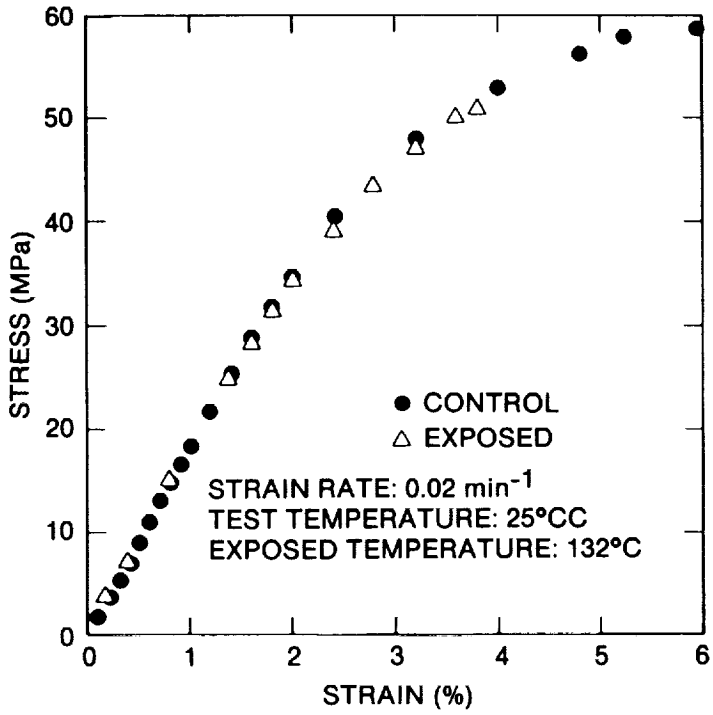

Figure 6.- Stress-Strain Curves of PMMA Returned from STS Flight 8.

Table 8.- Percent Composition of Polysulfone Surfaces by ESCA

	% COMPOSITION							O/C
	C_1	C_2	C_3	S	O_1	O_2	N	
THEORETICAL	72	13	-	3.1	6.3	6.3	-	0.15
CONTROL	72	7.4	2.2	2.6	8.3	5.8	1.5	0.16
EXPOSED	62	8.8	2.6	3.4	10.5	10.5	-	0.29

C_1: C–C C_2: C–O, C_3: shake-up S:SO2 O1: S=O, C=O O2: C-O

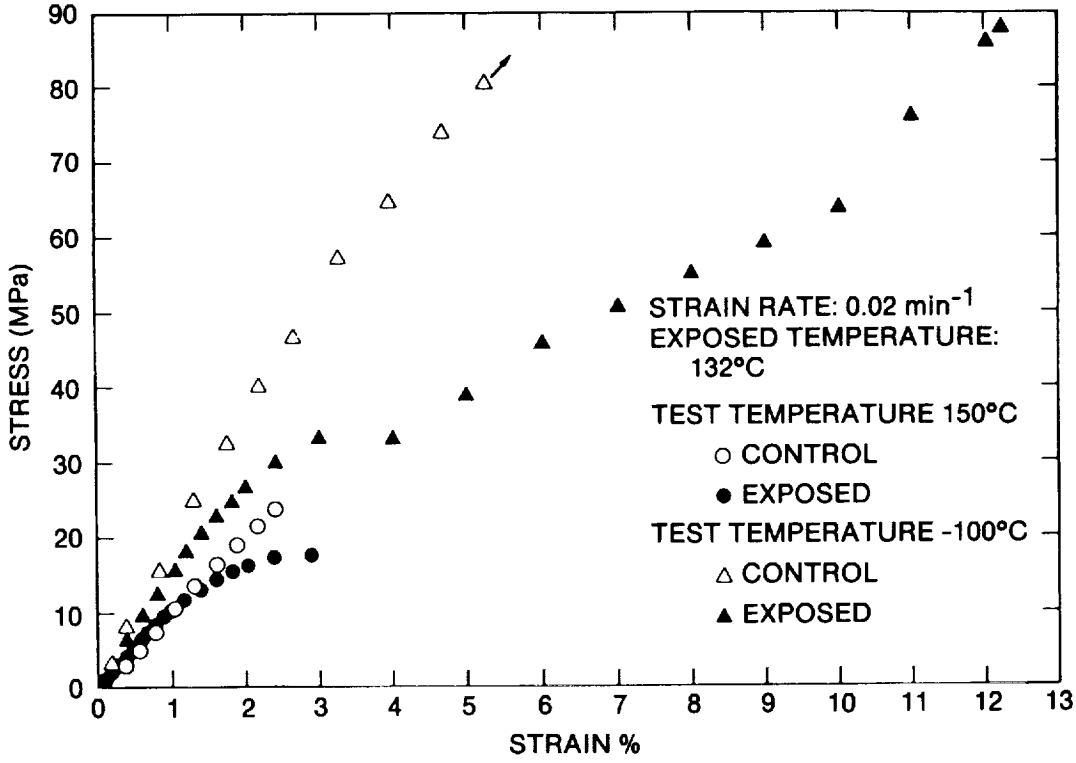

Figure 7.- Stress-Strain Curves of Polysulfone Returned from STS Flight 8.

Table 9.- Summary of HPLC Results on Polysulfone

	TESTING CONDITION	$\overline{M}_n$	$\overline{M}_w$
DISC	CONTROL	57,400	86,700
	EXPOSED	25,700	73,400
STRIP	CONTROL	51,700	94,700
	EXPOSED	35,600	74,600

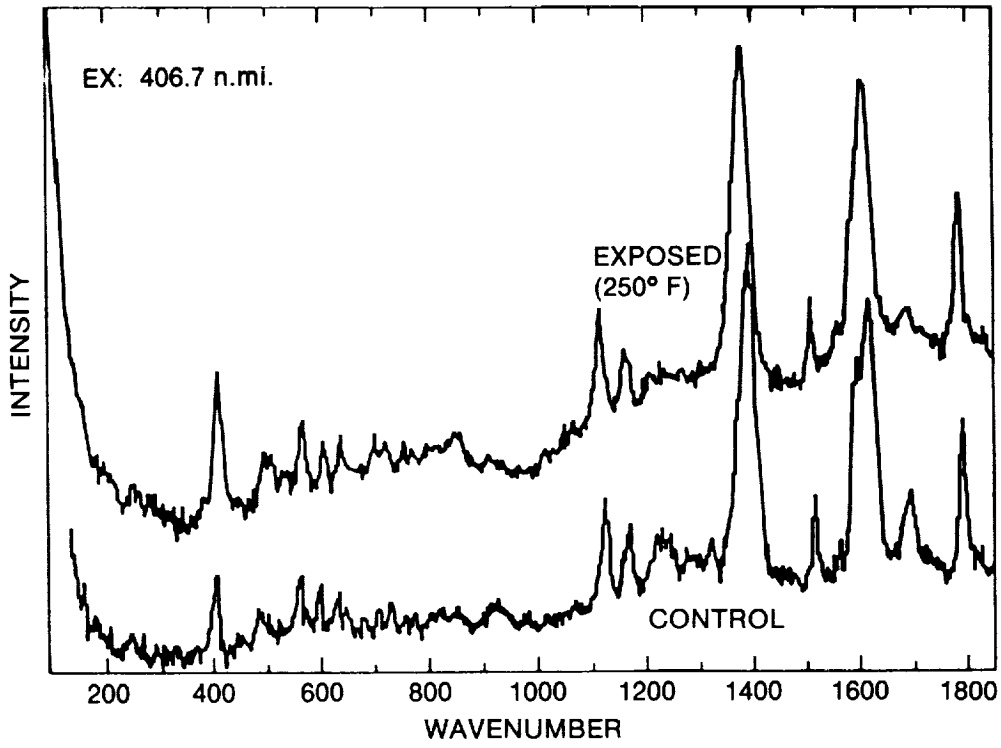

Figure 8.- Resonance Raman Spectra of Kapton Before and After Exposure.

Table 10.- Percent Composition of Kapton Surfaces from High-Resolution ESCA

	% COMPOSITION						
	C_1	C_2	C_3	O_1	O_2	N	O/C
CONTROL	48	14	14	14	3.4	6.9	0.23
EXPOSED	29	30	14	15	4.1	7.1	0.26

C_1: C-C C_2: C-O,C-N C_3: N−C=0 O_1: C=O, O_2: C-O

Table 11.- Dynamic Modulus Data for Kapton Flown on STS -8

MATERIAL	TESTING CONDITION	E, 10^5 psi
KAPTON	CONTROL	26.4 ± 0.2
	EXPOSED	26.1 ± 0.6
TEFLON-COATED KAPTON	CONTROL	26.8 ± 0.2
	EXPOSED	23.5 ± 0.3

Table 12.- ESCA Summary of Results on Polystyrene

	% COMPOSITION									
	C_1	C_2	C_3	C_4	P_1	P_2	Ca	Zn	O	O/C
THEORETICAL	100	-	-	-	-	-	-	-	-	-
CONTROL	97	-	-	-	-	-	-	-	2.2	0.02
EXPOSED	28	14	3.7	2.0	1.4	4.1	11	1.7	34	0.71

C_1: C–C C_2: C–O C_3: O–C=O C4: shake-up P_1: PO_4^{3-} P_2: P_2O_5

6.4.6 Z-306 Chemglaze Paint

Surface composition of the chemglaze paint was also tested by ESCA Figures 9 and 10 are the high-resolution carbon and oxygen ESCA spectra of Z-306, respectively. The percent composition of the surface is summarized in Table 13.

16.5 Discussion

The following generic model of interaction of organic materials with energetic oxygen atoms has been developed, based on the results of the physichemical characterization of samples flown on STS -8 (see Figure 11):

$$P + O \xrightarrow{k_1} PO$$

$$PO + O \xrightarrow{k_2} PO_2$$

$$PO + O \xrightarrow{k_3} V_1 + P$$

$$PO_2 + O \xrightarrow{k_4} V_2 + P$$

When the polymer surface (P) is exposed to an energetic oxygen atom (O), a polymeric intermediate such as an oxide (PO or PO_2) is formed. The intermediate may then encounter another oxygen to form either PO2 or a volatile product (V1) plus the original polymer (P). PO_2 may also react further

with oxygen to form a different volatile product occurs, it results in mass loss and contributes to the weight loss experienced by most of the samples flown (see Table 3). Therefore, the extent of degradation of samples is controlled by the amount of oxide formed. The mode of degradation, however, depends on the rate of depletion of oxides (PO and PO_2). If the rate of depletion is relatively fast, the oxygen concentration accumulating on the polymer surface will be low and the sample will undergo weight loss, but with no apparent changes in bulk properties. This appears to be the case for Kapton (DuPont 500H).

The longer the oxides remain on the surface, the higher the oxygen concentration and the lower the weight loss. Bulk properties may change, however, if the oxides remain long enough to react chemically with the polymer. ESCA data indicate there are chemical changes occurring on the surface (50 Å) of the polyethylene film. A 10 percent oxygen composition was found on the sample surface versus 0.8 percent on the unexposed side. Density measurements, however, failed to indicate any change in the bulk between the control and exposed films.

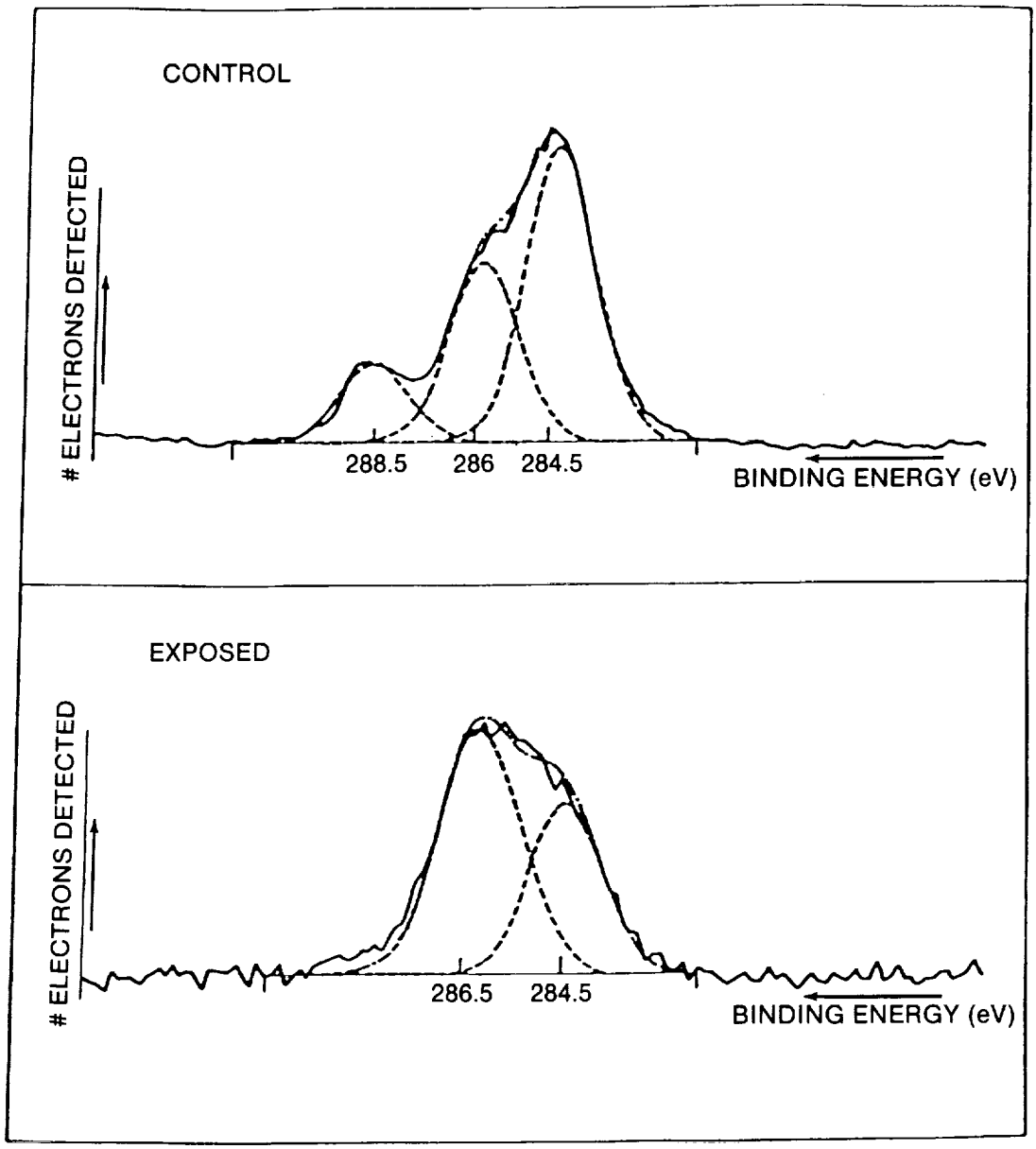

Figure 9.- High-Resolution ESCA Spectra of Carbon on Z-306 Surfaces.

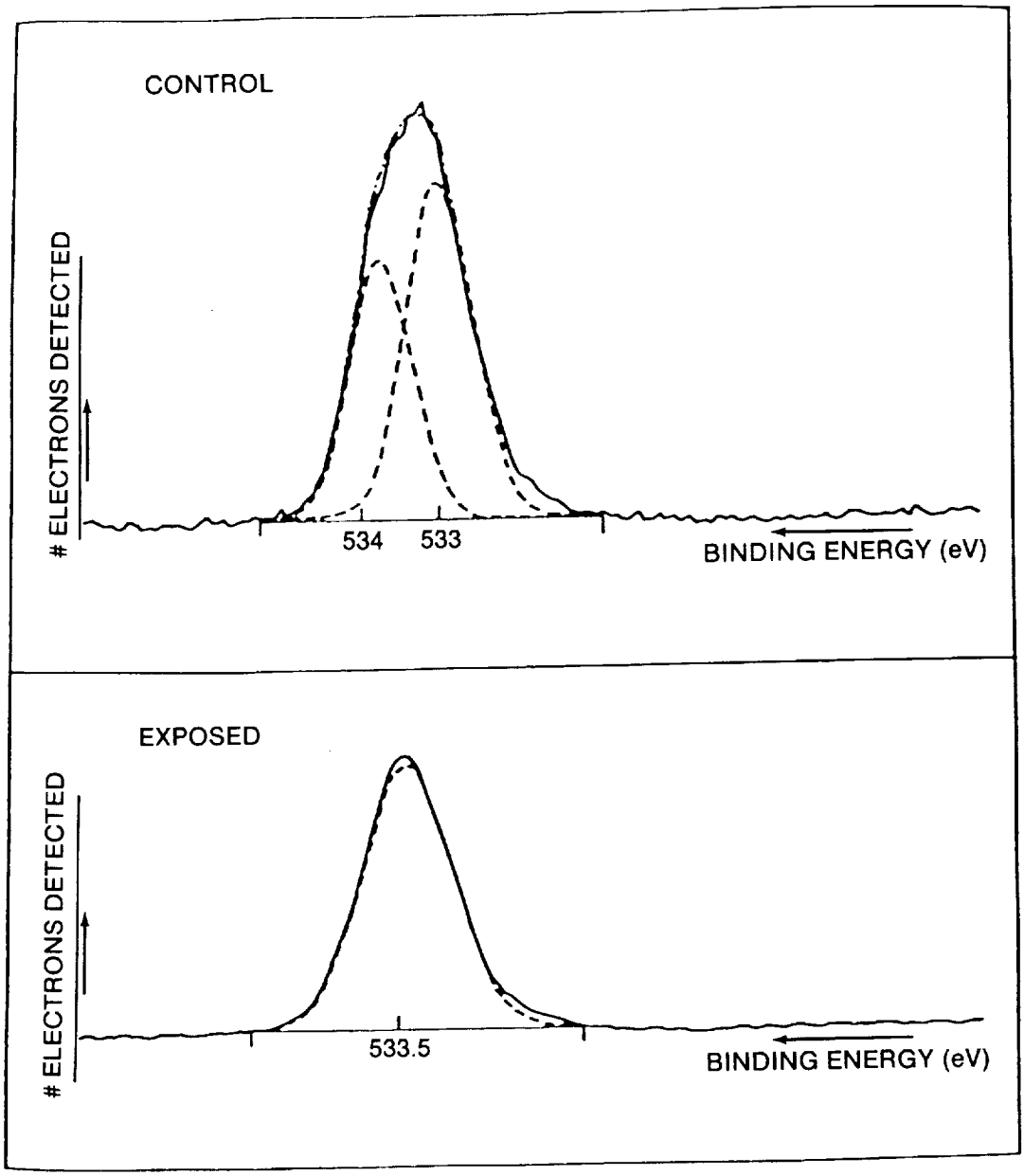

Figure 10.- High-Resolution ESCA Spectra of Oxygen on Z-306 Surfaces.

Oxide concentrations were also calculated from ESCA data for polysulfone and used as indicators of the oxygen buildup on the sample surface. The surface of the polysulfone sample displayed a 7 percent increase in oxygen content There is also a significant change in bulk properties indicated by tensile stress-strain data. Teflon-coated Kapton (Dupont F131), on the other hand, experienced no detectable loss of weight, which may correspond to a slow buildup of oxides on the surface. Rheovibron measurements showed a decrease in the dynamic modulus of 3.3×10^5 psi between control and exposed samples.

When analyzing oxide concentration measurements obtained from ESCA data, all exposed samples (with the exception of PMMA) showed an oxygen concentration buildup. PMMA also experienced a large weight loss, but with little chemical changes. Tensile stress-strain data indicate no appreciable difference between the control and exposed samples.

Table 13.- Surface Composition of the Z-306 Paint Aboard STS-8

	% COMPOSITION						
	C_1	C_2	C_3	O	Si	F	N
CONTROL	39	23	10	26	-	-	1.7
EXPOSED	6.5	11	-	57	24	1.6	-

C_1: C-C C_2: C–O C_3: O–C=O Si = SiO_2

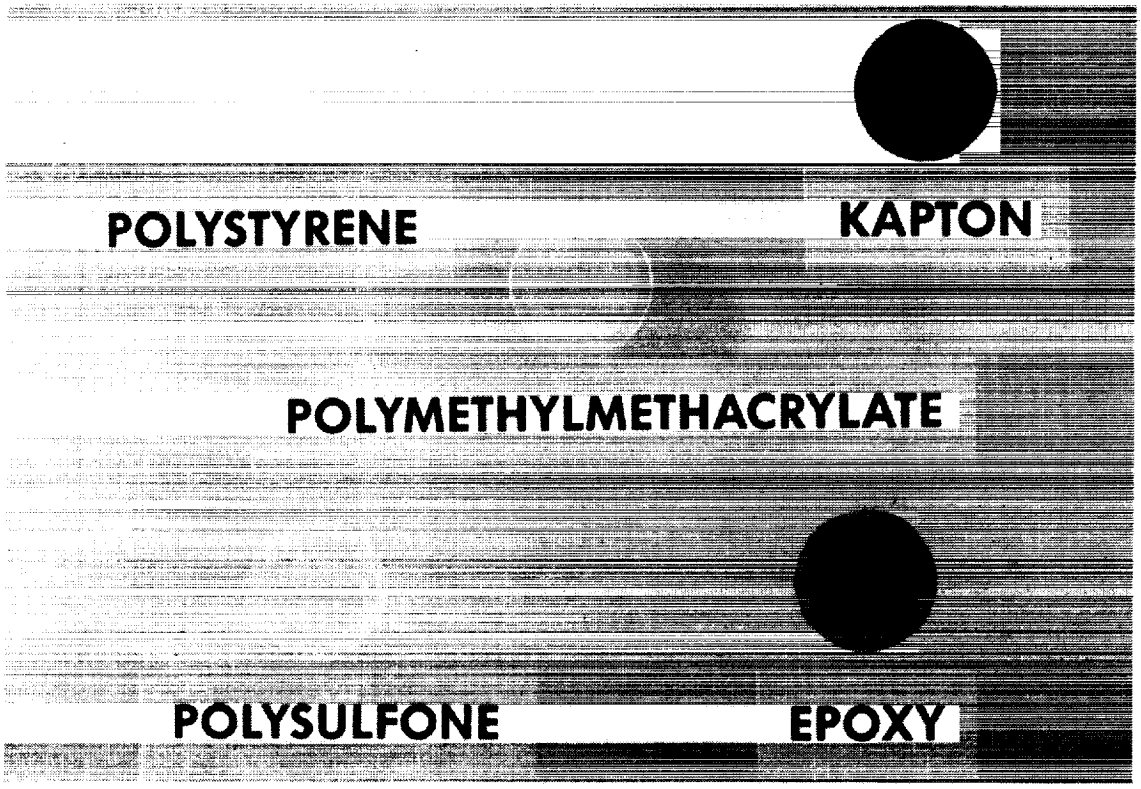

Figure 11.- Polymer Samples Eroded by Atomic Oxygen During STS-8.

One theory to explain these data is that PMMA is known to unzip under certain circumstances once degradation is initiated. This would give rise to weight loss, but with no apparent chemical change on the surface since fresh PMMA chains are always brought to the surface as these oxidized chains undergo depolymerization and subsequent removal through evaporation. The mechanism at play here seems to be the unzipping of the polymer chain.

The chemical composition of the Z-306 chemglaze control surface is what one would expect of the paint. This paint is a carbon-filled polyurethane embedded with silica. Further analysis of the oxygen sites in the control surface indicates that both carbonyls and C-O (esters, ethers) are present. The eroded surface, in contrast, is 70 to 80 percent SiOx. It also contains minor amounts of carbonyl groups and some fluoride. These data indicate that the erosion proceeds until a continuous layer of SiOx is left on the surface, thus, providing protection from further attack by the energetic oxygen atoms.

6.6 Conclusion

A set of polymeric films were exposed to the low-earth orbital environment aboard STS-8. Pre- and post-flight characterization studies were performed on each sample. These studies indicated that:

1. A residual oxidized layer was found on most, but not all, samples. The composition of this layer and its thickness reflected the overall mechanism of interaction of these materials with atomic oxygen, leading to erosion.

2. Certain samples, such as polysulfone, showed changes in bulk properties, while other samples, such as PMMA, showed no change in bulk properties, despite suffering considerable erosion.

3. There was evidence of secondary oxidation in some samples, caused by interaction of atomic oxygen with the oxidized layer.

More detailed studies, especially including in-situ monitoring of volatile degradation products, are needed to further elucidate the mechanism of the erosion process.

16.7 Reference

1. Leger, L. J., Visentine, J. T., and Kuminecz, J. F., "Low Earth Orbit Atomic Oxygen Effects on Surfaces," AIAA Paper 84-0548, January, 1984.

1. Report No.	2. Government Accession No.	3. Recipient's Catalog No.
NASA TM 100459		

4. Title and Subtitle	5. Report Date
Atomic Oxygen Effects Measurements for Shuttle Missions STS-8 and 41-G (3 volumes)	September 1988
	6. Performing Organization Code
7. Author(s)	8. Performing Organization Report N
James T. Visentine, Compiler	10. Work Unit No. 992-15-00-00-72
9. Performing Organization Name and Address	11. Contract or Grant No.
Lyndon B. Johnson Space Center Houston, Texas 77058	13. Type of Report and Period Covere
12. Sponsoring Agency Name and Address	Technical Memorandum
National Aeronautics and Space Administration Washington, D. C. 20546	14. Sponsoring Agency Code

15. Supplementary Notes

16. Abstract

This technical memorandum represents a compilation of 15 technical papers and is organized by subject matter into three separate volumes. Volume 1 of this document summarizes the effects of atomic oxygen exposure upon typical spacecraft materials, such as polyimide films, thermal control paints, epoxies, silicones, and fluorocarbons. Volume 2 summarizes the effects of these interactions upon optical coatings, thin metallized films, and advanced spacecraft materials, such as high-temperature coatings and new coatings for infrared optical systems. In addition to these results, Volume 2 includes a description of a generic model proposed by the NASA Jet Propulsion Laboratory, which may explain the atomic oxygen interaction mechanisms that lead to surface recession and weight loss. Volume 3 presents a futuristic look into the atomic oxygen program and outlines requirements for follow-on studies to produce an accurate reaction rate data base for Space Station design. It also identifies Shuttle flight experiments and ongoing activities underway at research laboratories in the United States to evaluate materials in a neutral, 5 eV O-atom environment and to develop a more thorough understanding of the chemical mechanisms leading to surface recession and space glow. This volume, entitled Atomic Oxygen Effects Experiments: Current Status and Future Directions includes a detailed discussion of atomic oxygen simulation techniques now under development in the United States. In light of these discussions, it is limited in its distribution to U. S. Government agencies and contractors only.

17. Key Words (Suggested by Author(s))	18. Distribution Statement
Atomic oxygen Environmental exposure Space environmental effects Space durable materials STS material exposure studies	Volume I: Unlimited Volume II: Unlimited Volume III: U.S. Government agencies and contractors only Subject category: 27

19. Security Classif. (of this report)	20. Security Classif. (of this page)	21. No. of pages	22. Price*
Unclassified	Unclassified	Volume II: 88 pages	

*For sale by the National Technical Information Service, Springfield, Virginia 22161